Peterhead CCS Project

Doc Title: Geochemical Reactivity Report

Doc No. **PCCS-05-PT-ZR-3323-00001**
Date of issue: **19/03/2015**
Revision: **K03**
DECC Ref No: **11.116**
Knowledge Cat: **KKD-Subsurface**

KEYWORDS
Goldeneye, CO_2, Geochemistry, Reactive Transport Modelling, RTM.

Produced by Shell U.K. Limited
ECCN: EAR 99 Deminimus

IMPORTANT NOTICE

Information provided further to UK CCS Commercialisation Programme (the **Competition**)

The information set out herein (the **Information**) has been prepared by Shell U.K. Limited and its sub-contractors (the **Consortium**) solely for the Department for Energy and Climate Change in connection with the Competition. The Information does not amount to advice on CCS technology or any CCS engineering, commercial, financial, regulatory, legal or other solutions on which any reliance should be placed. Accordingly, no member of the Consortium makes (and the UK Government does not make) any representation, warranty or undertaking, express or implied as to the accuracy, adequacy or completeness of any of the Information and no reliance may be placed on the Information. In so far as permitted by law, no member of the Consortium or any company in the same group as any member of the Consortium or their respective officers, employees or agents accepts (and the UK Government does not accept) any responsibility or liability of any kind, whether for negligence or any other reason, for any damage or loss arising from any use of or any reliance placed on the Information or any subsequent communication of the Information. Each person to whom the Information is made available must make their own independent assessment of the Information after making such investigation and taking professional technical, engineering, commercial, regulatory, financial, legal or other advice, as they deem necessary.

Table of Contents

Table of Figures

List of Tables

Executive Summary

CO_2 storage in an aquifer or hydrocarbon reservoir changes the composition of the formation brine due to dissolution of CO_2. The bicarbonate (HCO_3^-) concentration increases and the pH decreases. This brings the brine out of equilibrium with respect to the various minerals that make up the reservoir rock, leading to dissolution of some minerals and precipitation of other minerals. For Goldeneye some of these changes may have occurred already, due to the presence of 0.4% CO_2 in the hydrocarbon gas, nevertheless also for Goldeneye the storage leads to much higher CO_2 concentrations than that to which the reservoir has been exposed before. Therefore also in Goldeneye dissolution and precipitation processes should be expected to occur.

In general the mineralogical changes could impact each of the three key subsurface CO_2 storage selection criteria: capacity, injectivity and containment. To qualify and quantify this impact a reactive transport study was performed. The results of this study are described in this report. The main results are summarised in Table 0-1.

Note that this report does not cover well integrity risks such as the reactivity of the CO_2 with well cement. This is covered in a separate report (Conceptual CWI design report, Key Knowledge Deliverable 11.093 (1)).

This report has been update since the Longannet Carbon Capture and Storage (CCS) Project version to include a new section on calcite dissolution in response to a query from the U.K. Regulator.

Table 0-1: Overview of the main results. The numbers in the graph refer to key regions of the reservoir and cap rock exposed to CO_2

	Region	Description	Conclusion
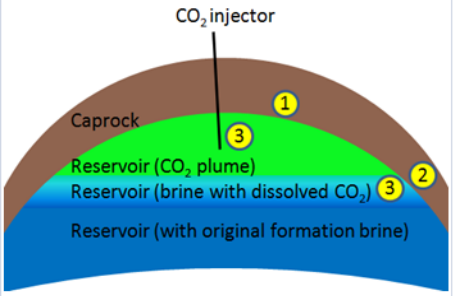	1	Caprock exposed to CO_2 plume	CO_2 diffuses over a distance of 50-75 m in 10,000 years. Caprock alterations possible within this distance. Alterations tend to decrease porosity. Therefore low risk of induced leakage.
	2	Caprock exposed to formation brine with dissolved CO_2	Mostly same as above. The main difference is that in this region (unlike in region 1) potential calcite rich features running through the caprock might be exposed to a slow dissolution process. It would take more than 200,000 years to create a leak path even under worst case assumptions. If this were to happen only brine (with some CO_2 dissolved) could leak because this region is below the gas water contact.
	3	Reservoir within and close to CO_2 plume	Permeability decrease possible during injection period but unlikely to have significant impact on injectivity. Potential for a large CO_2 mineralisation in optimistic scenario. Dissolution storage relatively low (14% of injected CO_2 after 10,000 years).

1. Introduction

The Peterhead CCS Project aims to capture around one million tonnes of CO_2 per annum, over a period of 10 to 15 years, from an existing combined cycle gas turbine (CCGT) located at SSE's Peterhead Power Station in Aberdeenshire, Scotland. This would be the world's first commercial scale demonstration of CO_2 capture, transport and offshore geological storage from a (post combustion) gas-fired power station.

Post cessation of production, the Goldeneye gas-condensate production facility will be modified to allow the injection of dense phase CO_2 captured from the post-combustion gases of Peterhead Power Station into the depleted Goldeneye reservoir.

The CO_2 will be captured from the flue gas produced by one of the gas turbines at Peterhead Power Station (GT-13) using amine based technology provided by CanSolv (a wholly owned subsidiary of Shell). After capture the CO_2 will be routed to a compression facility, where it will be compressed, cooled and conditioned for water and oxygen removal to meet suitable transportation and storage specifications. The resulting dense phase CO_2 stream will be transported direct offshore to the wellhead platform via a new offshore pipeline which will tie-in subsea to the existing Goldeneye pipeline.

Once at the platform the CO_2 will be injected into the Goldeneye CO_2 Store (a depleted hydrocarbon gas reservoir), more than 2 km under the seabed of the North Sea. The project layout is depicted in Figure 1-1 below:

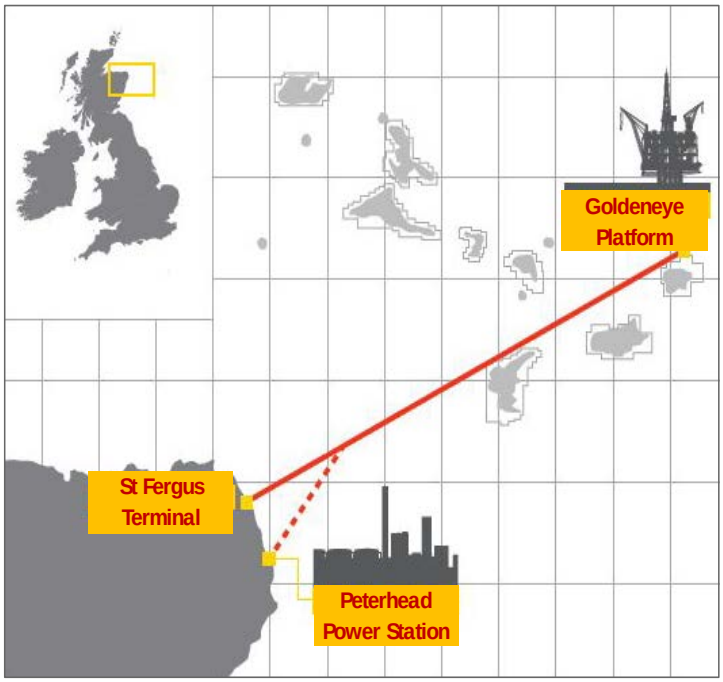

Figure 1-1: Project Location

1.1. Summary

The key subsurface selection criteria for a CO_2 storage reservoir are capacity (how much CO_2 can it store), injectivity (how many wells are required for storage, affecting the cost of storage) and containment (will the CO_2 stay underground). There are many factors that influence these selection criteria. The factor addressed in this report is the geochemical interactions between the (dissolved) CO_2 and the rock minerals. Each of the key criteria can be affected by these interactions:

- CO_2 can mineralise to form carbonate minerals, thus increasing the storage capacity and security of containment (Figure 1-2).
- It can change (increase or decrease) the injectivity due to rock alterations around the well.
- It can change (increase or decrease) the sealing capacity of the cap rock.

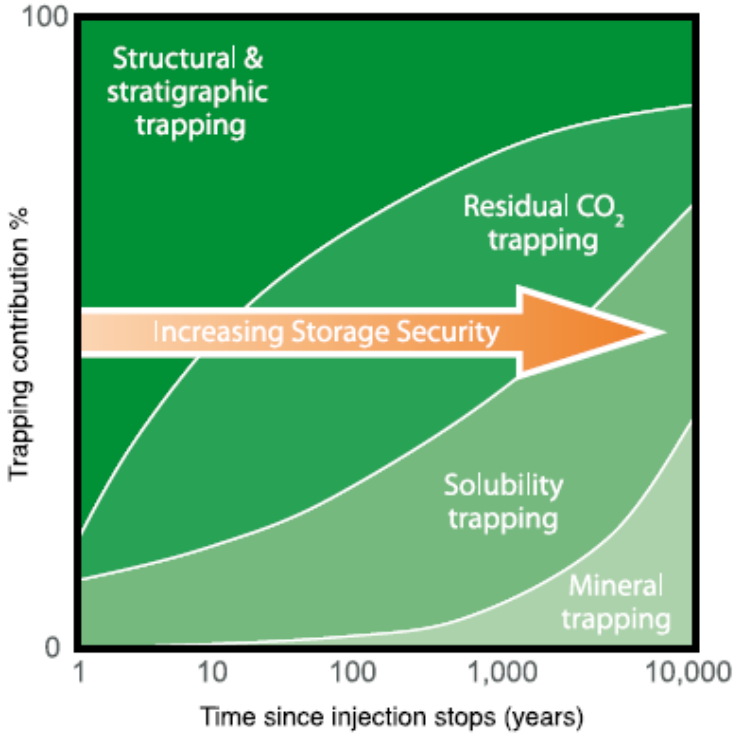

Figure 1-2: Schematic of CO_2 trapping mechanisms through time (from IPCC special report (2))

The interplay between the CO_2-rock geochemical interactions and the CO_2 movement through the reservoir (and cap rock) is the domain of reactive transport modelling. This report covers the reactive transport modelling that was performed specifically for Goldeneye.

The objective of this report is to qualify and where possible quantify the effect of the geochemical interactions on cap rock sealing capacity, injectivity and CO_2 trapping (mineralisation).

2. Modelling approach

2.1. Geological setting

The Goldeneye geology is described in another report (3). In this section we provide a short summary of the relevant elements for the reactive transport modelling, namely what rock formations the injected CO_2 will encounter.

Figure 2-1 illustrates the generalised stratigraphy (up to the Chalk Group) of the Goldeneye area, and Figure 2-2 shows the cross-sections of the reservoir stratigraphy. The CO_2 will be injected in the Captain Sandstone Formation. In terms of reservoir quality and storage capacity the Captain D zone is the dominant formation within the reservoir, but the CO_2 is also likely to flow into the other Captain zones. From a mineralogical point of view, all Captain sandstones are similar and no distinction has been made between them in the reactive transport modelling. The Captain zones also contain some mudstone intervals. These are assumed impermeable and have been ignored in the reactive transport modelling within the reservoir. Their mineralogy is similar to that of the primary seal.

The CO_2 will also contact the primary seal which is formed from a combination of upper Valhall Formation and Rødby Formation shales (in the remainder of the report simply referred to as Rødby). These two units combined comprise a 60 m to 85 m thick succession of laminated, calcareous mudstones. Above the Rødby the calcite contents increases further (marl formations and then Chalk), with the Lista Shale (secondary seal) above that. The reservoir itself contains localised calcite rich features (Well 14/29a-3, Figure 2-3), which have been interpreted as calcite cemented faults and/or fractures. These features can have very high calcite contents, but with low porosity. The locations of Well 14/29a-3 and the other exploration/appraisal and development wells are shown in Figure 2-4.

This report assesses the reactivity of the injected CO_2 with the reservoir itself as well as with the Rødby. The reactivity with shallower formations has not been studied; however the reactivity with calcite rich fault zones has been studied.

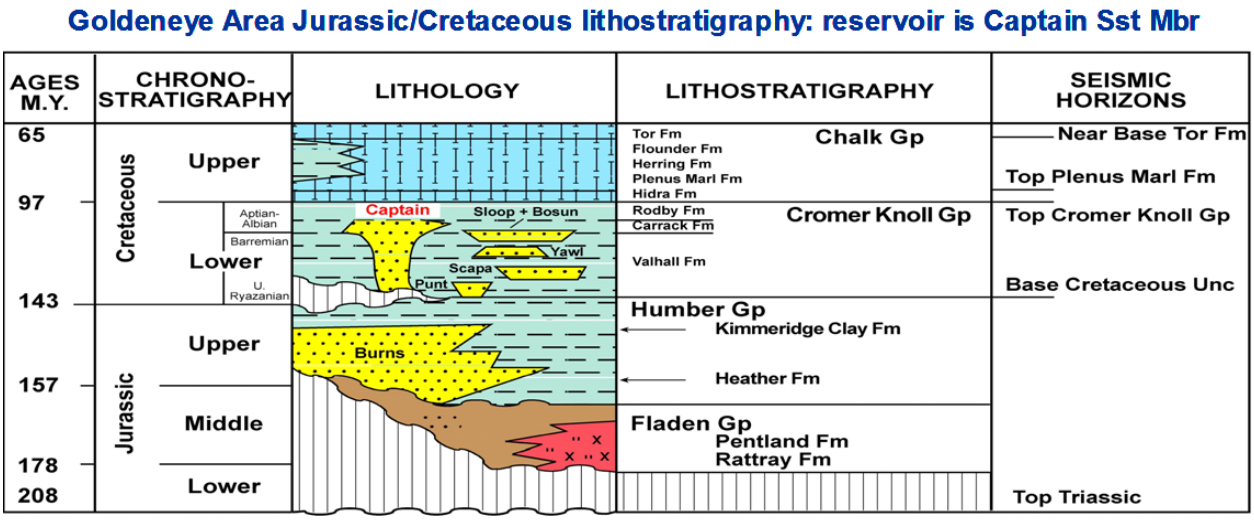

Figure 2-1: Generalised stratigraphy of the Goldeneye area (from: Goldeneye Static Model (Field) report (3)).

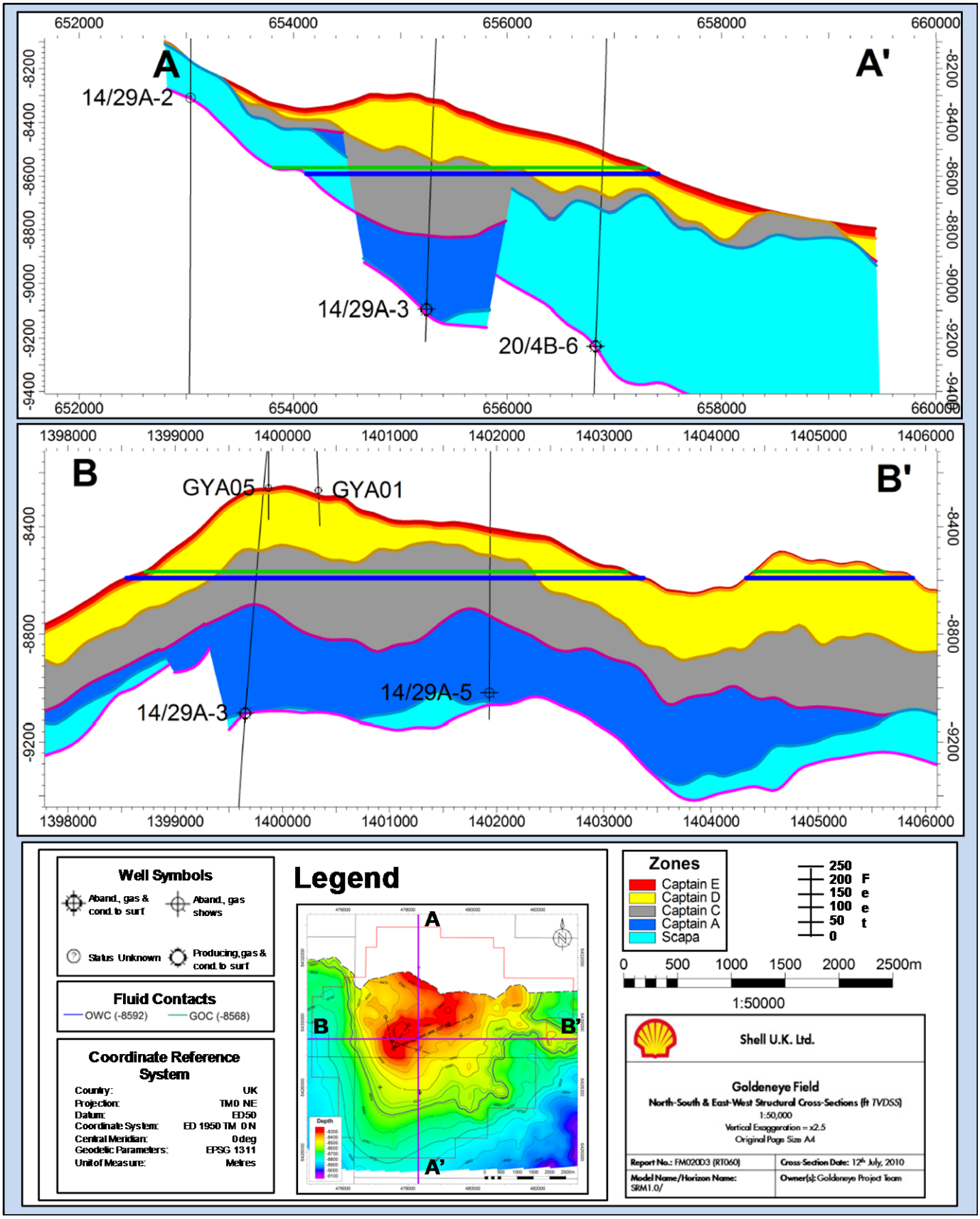

Figure 2-2: Representative structural cross-sections through Goldeneye field (from: Goldeneye static model (field) report (3)). Vertical scale in ft.

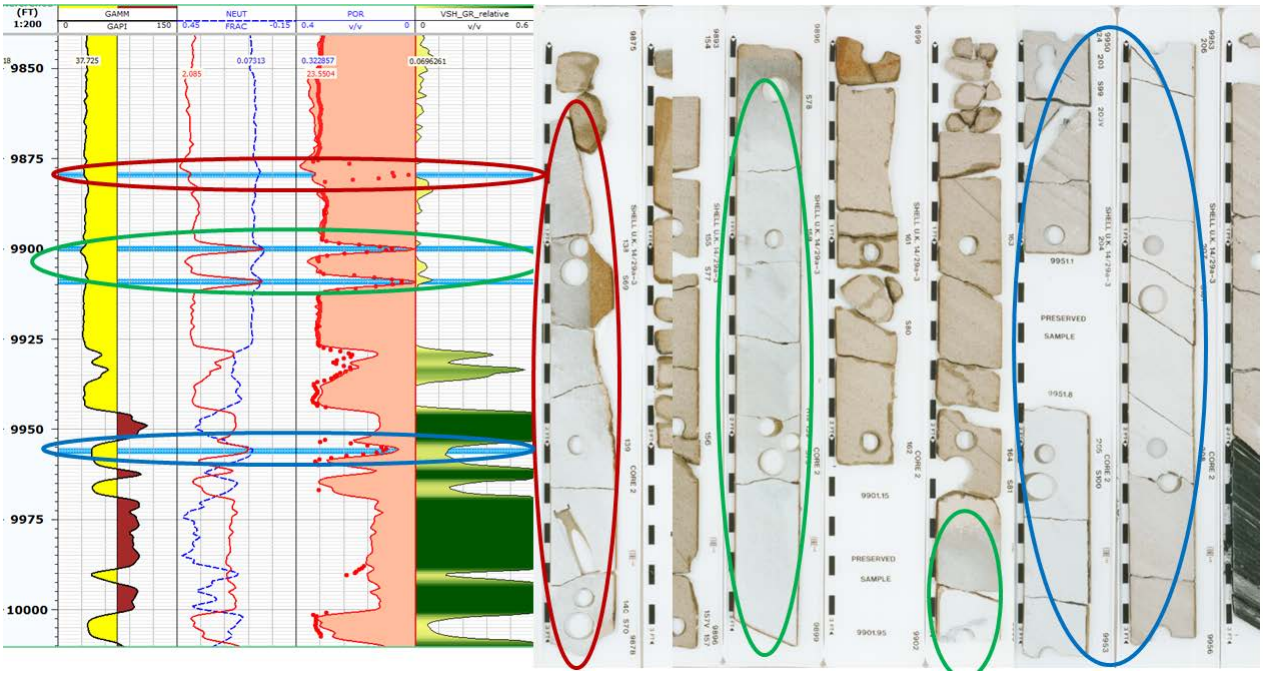

Figure 2-3: Log and core from well 14/29a-3, showing low porosity calcite rich intervals (approximately 1 m thick).

Note: This is interpreted as local calcite cementation in a fault zone.

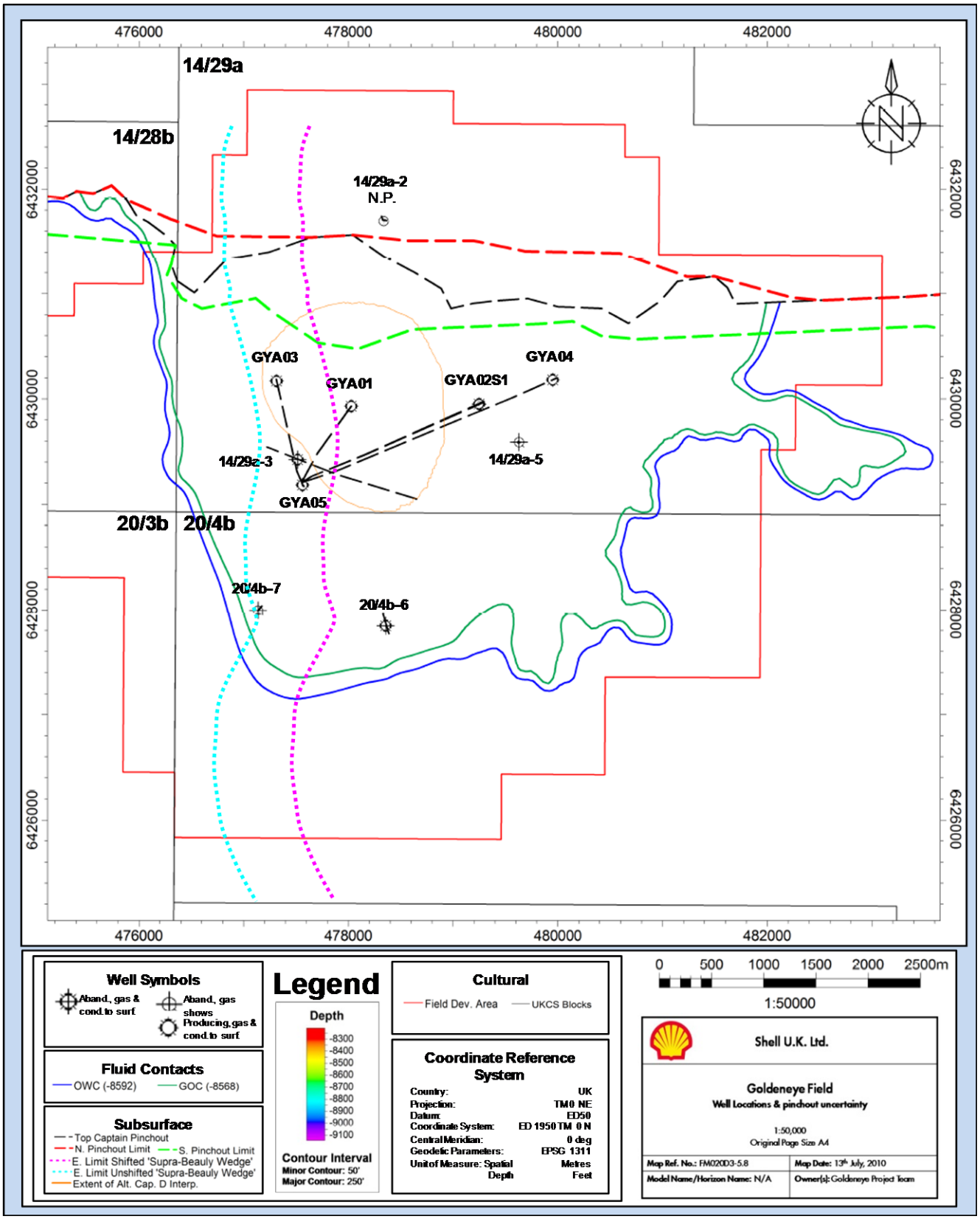

Figure 2-4: Goldeneye well locations

2.2. Modelling tools

In this study the interactions between the injected CO_2 and the rock formations were modelled using a standard geochemical simulator, PHREEQC (4), both in stand-alone mode and coupled to the Shell state-of-the-art multi-phase reservoir simulator MoReS.

The following types of simulation were performed:

- PHREEQC stand-alone batch runs (zero-dimensional - 0D) on the reservoir and cap rock. The objective was to understand the reactivity of the system and the sensitivity to key subsurface parameters.
- PHREEQC stand-alone one-dimensional (1D) diffusion runs on the cap rock and on any calcite-filled faults through the cap rock. The objective was to study whether the diffusive transport of CO_2 into the cap rock (or within a calcite-filled fault zone through the cap rock) might increase porosity in the cap rock. Increased porosity would be a risk for containment as it could open leak paths for convective transport of CO_2 through the cap rock.
- Coupled PHREEQC-MoReS runs on the reservoir. The objective was to check the assumptions underlying the PHREEQC stand-alone batch runs on the reservoir, check the conclusions derived from these stand-alone runs, analyse spatial trends, and check assumptions (boundary conditions) on the PHREEQC stand-alone 1D diffusion runs on the cap rock and faults.

Suitability of these modelling tools has been demonstrated in the CO_2 store best practice report (5) and simulator benchmarking for CO_2 storage (6). Because of the presence of hydrocarbons in the reservoir, simulators without gas and oil phases (such as TOUGHREACT) are not suitable for this project.

2.3. Geochemical database

Key in any geochemical modelling is the use of an appropriate thermodynamic database for the chemical reactions within the brine and between the brine, CO_2 and minerals. This is especially important for CO_2 storage projects because many existing databases are dedicated to groundwater modelling and are often only valid for low temperatures (below Goldeneye temperature of approximately 83°C). They are biased towards nuclear waste disposal, or are lacking common reservoir minerals. For the Goldeneye project a dedicated database was constructed in the following way:

- Based on Lawrence Livermore National Laboratory (llnl).dat (7) (i.e. EQ3/6) (distributed with PHREEQC). This gives valid thermodynamic constants over a wide temperature range (from 0°C to 100-200°C)
- Removal of reactions and minerals not relevant for CO_2 storage in siliclastic and carbonate reservoirs, based on geological inputs from geologists
- Add -dw (diffusion constants) and -millero (density parameters) from phreeqc.dat
- Add common reservoir minerals that are absent from llnl.dat but included in the TOUGHREACT (8) database (such as glauconite, ankerite)
- Add kinetics based on Palandri & Kharaka (9), plus some information from TOUGHREACT papers (10). The precise kinetic rate formula used is given in Appendix 1.

Since Goldeneye is a NaCl dominated brine with ionic strength of 0.95 and low sulphate concentration, the Extended Debije-Hückel activity model (as present in llnl.dat) was used.

To check the robustness of the database choice, sensitivity runs using the Bureau de Recherches Géologiques et Minières (BRGM) Thermoddem (11) database were done in the standalone PHREEQC batch model for the reservoir.

3. Goldeneye specific data input

3.1. Mineralogy

Core is available for the Captain reservoir as well as the Rødby seal. A new core petrographic study (12) was commissioned from CoreLab for the purpose of the CO_2 storage project. Rock samples were studied by scanning electron microscopy (SEM) supplemented by energy dispersive X-ray (EDX) analysis, whole rock and clay X-ray diffraction (XRD) analysis, and (for 10 samples out of 34 total) Thin Section (TS) analysis.

Typical images for the reservoir, top seal, and calcite feature in the reservoir are presented in Figure 3-2, Figure 3-3 and Figure 3-4. Mineralogy based on XRD is presented in Table 3-1. From this it can be seen that the mineralogy in the Captain sandstones are similar for all zones (Captain A-E). Also the mineralogy in the Captain Mudstones is similar to that of the Rødby Mudstones, and is actually also similar to the Captain Sandstones except for the much higher clay contents and differences in relative fractions for other minerals. It can also be seen that the calcite feature has a very high calcite content (76%). This could be even higher in other places in the fault zones.

Within the reservoir, the calcite is mainly present as cement, only a small fraction of it is present as skeletal fragments.

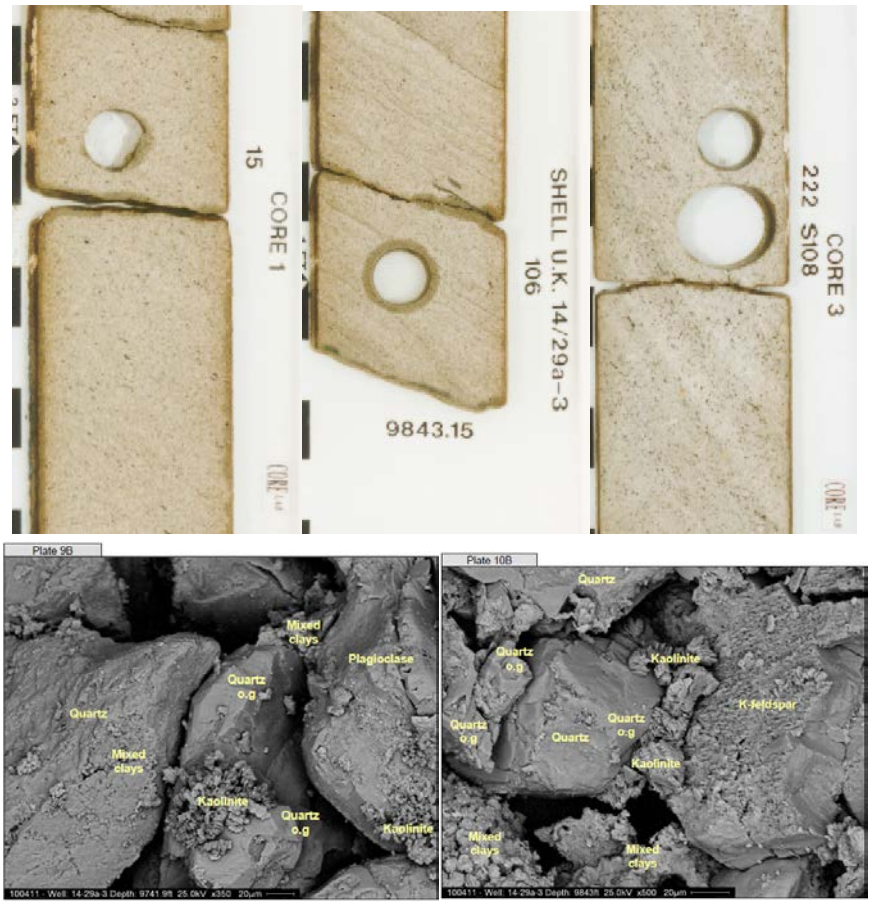

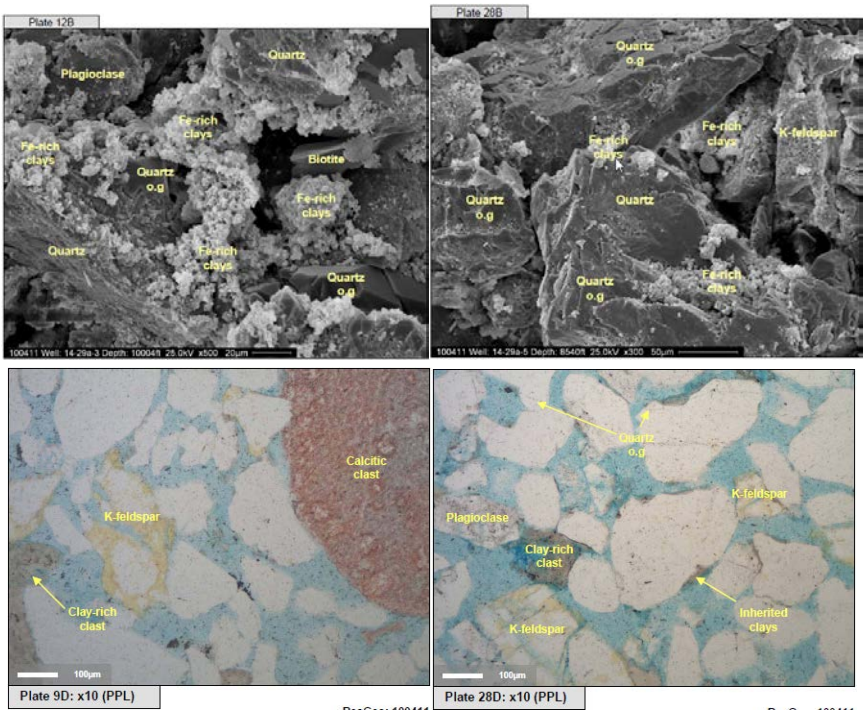

Figure 3-1: Images of Captain Sandstone (13)

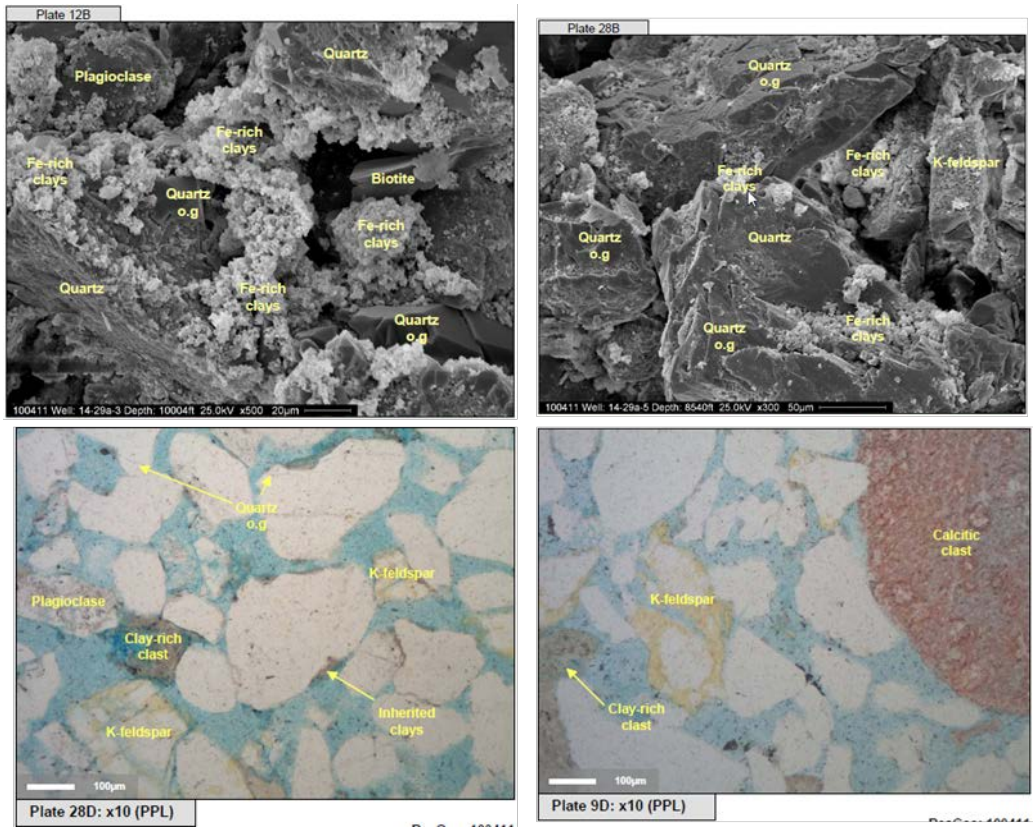

Figure 3-2: **Core (top row), SEM (middle two rows) and thin sections (bottom row) images of Captain Sandstone (13)**

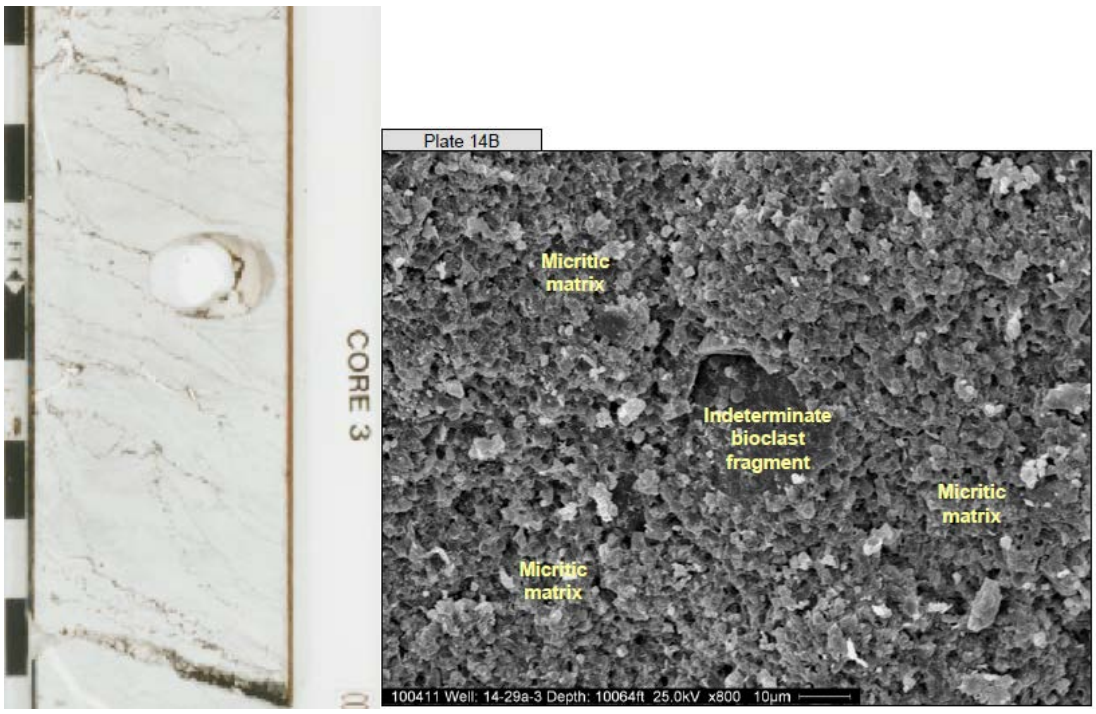

Figure 3-3: **Core (left) and SEM (right) images of calcite rich feature in Captain C (interpreted as part of a fault zone) (13)**

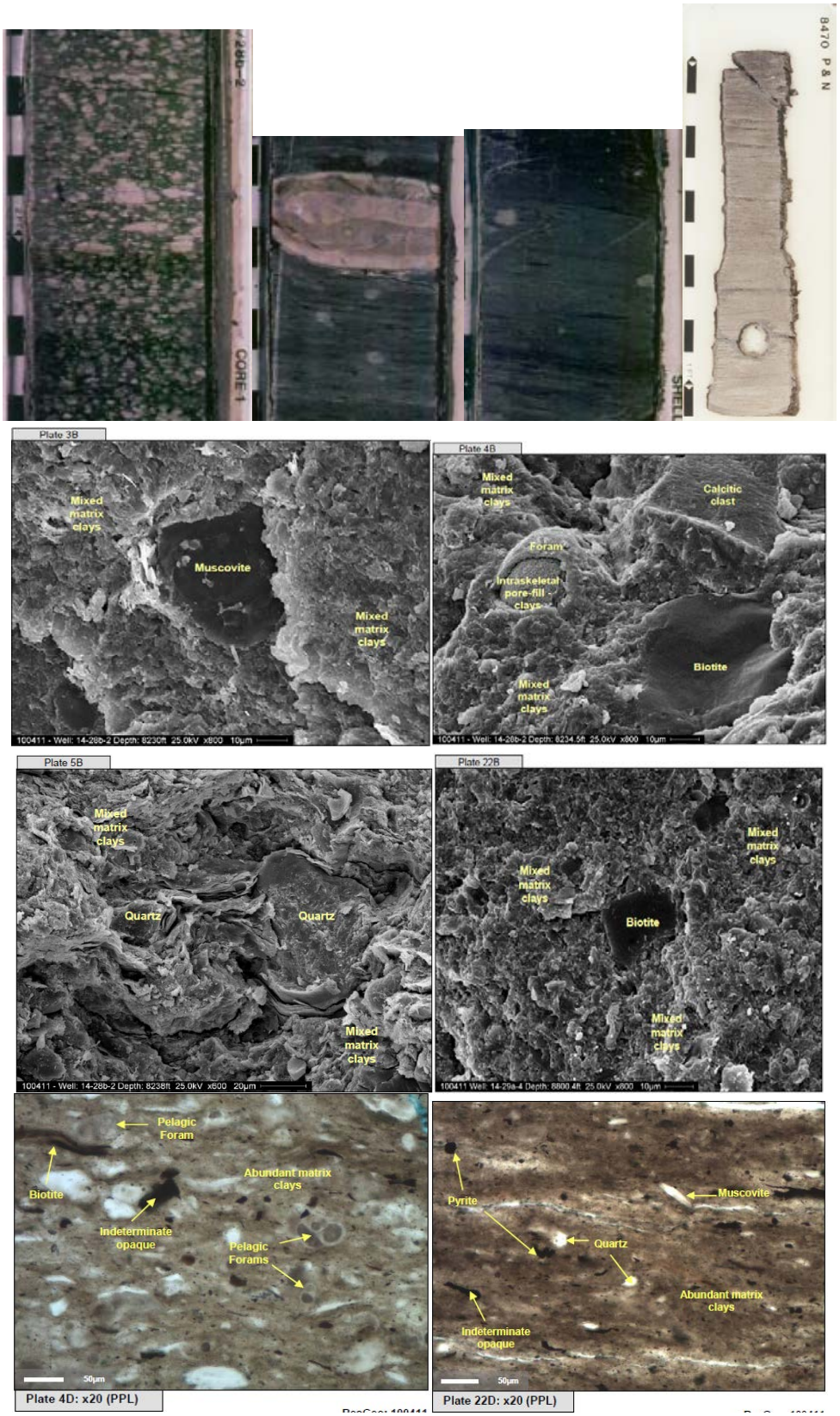

Figure 3-4: **Core (top row), SEM (middle two rows) and thin sections (bottom row) images of Rødby seal (13)**

The XRD results are shown in Table 3-1, with mineral content calculated from thin section analysis in Table 3-2. The sample summary (including sample locations) is presented in Table 3-3.

Table 3-1: Bulk and clay XRD data (13)

Sample No.	Plug No	Depth (ft)	CALCULATED WHOLE ROCK COMPOSITION (Weight %)												RELATIVE CLAY ABUNDANCE Normalized to 100%					
			Quartz	K-Feldspar	Plagioclase	Gypsum	Calcite	Dolomite/ Fe-Dolomite	Siderite	Barite	Pyrite	Smectite	Illite/Smect.	Illite + Mica	Kaolinite	Chlorite	Total Clay	Illite + Mica	Kaolinite	Chlorite	Smectite	Mixed Layer Illite/Smectite*	Smectite in Illite/Smectite
14/28a-1																							
1	N/A	6154	18.0	1.6	1.8	0.7	15.1	0.0	0.0	0.0	4.8	0.0	44.4	11.8	1.8	0.0	58.0	20.4	3.2	0.0	0.0	76.4	85-95%
2	N/A	6160.5	16.8	1.9	3.1	0.9	11.3	0.0	0.0	0.0	7.3	0.0	44.1	13.3	1.3	0.0	58.7	22.7	2.2	0.0	0.0	75.1	85-95%
14/28b-2																							
3	N/A	8230	13.1	1.4	3.6	0.0	3.4	0.0	0.0	0.0	0.0	0.0	63.4	9.7	2.6	2.9	78.6	12.4	3.3	3.6	0.0	80.6	85-95%
4	N/A	8234.5	14.2	2.7	3.2	0.0	8.1	0.0	0.0	0.0	0.0	48.3	0.0	5.7	15.9	2.0	71.9	7.9	22.1	2.9	67.1	0.0	-
5	N/A	8238	15.2	1.2	3.4	0.0	6.8	0.0	0.0	0.0	0.0	0.0	55.9	5.4	2.5	9.6	73.4	7.4	3.4	13.0	0.0	76.1	85-95%
6	N/A	8242.5	9.4	1.2	2.7	0.0	0.8	0.0	0.0	0.0	0.0	0.0	63.4	4.3	15.7	2.5	85.9	5.0	18.3	2.9	0.0	73.8	85-95%
14/29a-2																							
7	N/A	8267-8270	63.8	6.2	4.4	0.0	8.6	3.7	0.0	0.0	0.0	0.0	3.7	6.1	3.1	0.4	13.3	46.0	22.9	3.4	0.0	27.7	45-65%
8	N/A	8321-8324	39.8	4.0	3.1	0.0	26.4	0.5	0.0	0.0	0.0	0.0	17.4	4.8	2.0	2.0	26.2	18.4	7.8	7.4	0.0	66.4	55-65%
14/29a-3																							
9	16	9741.9	83.3	6.9	5.4	0.1	0.3	0.0	0.0	0.0	0.0	0.0	0.0	0.8	2.5	0.5	3.8	21.8	65.1	13.1	0.0	0.0	-
10	106	9843	80.7	6.1	7.0	0.0	0.5	0.1	0.0	0.0	0.1	0.0	0.0	0.9	3.5	1.0	5.4	17.2	64.4	18.4	0.0	0.0	-
11	N/A	9947.5	15.8	2.1	4.1	0.0	0.5	0.0	0.0	0.0	1.7	0.0	43.6	8.8	28.6	2.7	75.7	11.6	27.3	3.6	0.0	57.5	55-65%
12	222	10004	76.7	9.0	6.6	0.0	0.5	0.0	0.0	0.0	0.0	0.0	0.0	1.4	1.0	4.9	7.3	19.5	12.9	67.6	0.0	0.0	-
13	232	10043	83.5	4.8	8.2	0.0	0.5	0.2	0.0	0.0	0.0	0.0	0.0	0.5	1.5	0.7	2.7	17.7	56.6	25.7	0.0	0.0	-
14	N/A	10064	1.9	1.0	1.2	0.1	75.7	1.2	0.0	0.0	2.2	0.0	7.9	2.7	5.1	1.2	16.9	15.8	30.4	6.8	0.0	47.0	20-30%
15	259	10079	80.8	4.7	5.1	0.0	0.5	0.0	0.0	0.0	5.1	0.0	0.0	0.5	2.1	1.2	3.8	12.8	55.8	31.4	0.0	0.0	-
16	N/A	10124	18.0	1.2	0.9	0.6	14.4	0.0	0.0	0.0	14.6	0.0	6.3	9.1	32.4	2.6	50.4	18.1	64.3	5.2	0.0	12.4	50-65%
17	N/A	10126.5	12.6	2.7	5.6	0.0	5.5	0.0	0.0	0.0	3.1	0.0	35.2	6.4	25.5	3.4	70.5	9.0	36.3	4.8	0.0	49.9	25-35%
18	N/A	10148	16.9	4.0	5.4	0.5	4.7	0.5	0.0	0.0	4.1	0.0	29.6	5.3	24.9	4.2	64.0	8.3	38.9	6.6	0.0	46.2	30-40%
19	N/A	10176	57.5	5.8	4.8	0.1	8.6	0.0	0.0	0.0	0.6	0.0	7.3	2.6	11.1	1.6	22.6	11.6	48.9	7.1	0.0	32.4	30-40%
20	267	10184.9	86.6	4.4	4.1	0.0	0.6	0.3	0.0	0.0	0.0	0.0	0.0	0.5	3.1	0.3	3.9	13.6	79.2	7.2	0.0	0.0	-
* The mixed-layered illite/smectite phase appears to be either regularly ordered (R1) containing ca. 25-40% smectite or randomly ordered (R0) containing ca. 50-90% smectite.																							
14/29a-4																							
21	N/A	8775.3	10.7	1.3	3.8	0.0	6.4	0.0	0.0	0.0	1.5	0.0	52.6	10.5	8.7	4.6	76.4	13.7	11.5	6.0	0.0	68.8	85-95%
22	N/A	8800.4	18.1	0.7	2.5	0.0	8.1	0.0	0.0	0.0	0.2	55.2	0.0	8.2	5.2	1.8	70.4	11.7	7.3	2.6	78.4	0.0	-
23	N/A	8831	10.8	1.9	3.3	0.0	0.4	0.0	0.0	0.0	1.0	61.1	0.0	6.1	13.1	2.4	82.7	7.4	15.8	3.0	73.8	0.0	-
24	N/A	8894	84.5	3.2	5.4	0.0	0.2	0.1	0.0	0.0	0.1	0.0	0.0	1.0	3.8	1.7	6.5	15.0	59.3	25.7	0.0	0.0	-
25	N/A	8983.3	9.8	1.8	3.4	0.2	11.4	0.0	0.0	0.0	3.2	21.7	17.6	11.3	16.5	3.1	70.2	16.0	23.6	4.4	30.9	25.1	55-65%
14/29a-5																							
26	6	8478	78.2	4.8	5.1	0.0	0.7	0.0	0.0	0.0	0.0	0.0	0.0	1.0	5.6	4.7	11.3	8.9	49.9	41.2	0.0	0.0	-
27	N/A	8490.5	9.1	1.7	3.6	0.0	0.6	0.0	0.0	0.0	1.3	0.0	36.2	6.2	37.6	3.7	83.7	7.4	44.9	4.4	0.0	43.3	55-65%
28	65	8540	78.4	6.0	5.9	0.0	0.6	0.0	0.2	0.0	0.2	0.0	0.0	1.5	4.1	3.1	8.7	17.6	47.4	35.0	0.0	0.0	-
29	N/A	8587.5	24.1	4.8	7.9	0.0	4.9	0.5	0.0	0.0	0.6	0.0	32.6	6.0	13.8	4.7	57.1	10.6	24.1	8.2	0.0	57.1	55-65%
30	N/A	8603	77.9	3.8	5.1	0.0	8.0	0.0	0.0	0.0	0.0	0.0	1.3	1.0	0.6	2.3	5.2	18.0	12.1	44.8	0.0	25.1	50-65%
31	N/A	8642.5	15.8	2.3	5.2	0.0	0.8	0.3	0.0	0.0	3.9	0.0	45.4	6.1	15.5	4.6	71.6	8.5	21.7	6.5	0.0	63.3	55-65%
32	142	8674	78.9	7.0	7.9	0.0	1.3	0.2	0.0	0.0	0.0	0.0	0.0	0.8	3.5	0.4	4.7	17.0	73.9	9.1	0.0	0.0	-
33	N/A	8690	19.8	1.3	5.7	0.0	2.6	0.9	0.0	0.0	6.6	0.0	28.4	18.6	13.3	2.8	63.1	29.6	21.0	4.4	0.0	45.0	55-65%
34	N/A	8699.5	19.0	2.3	3.7	0.0	3.5	1.0	0.0	0.0	8.5	0.0	32.7	14.6	13.0	1.6	61.9	23.6	21.0	2.6	0.0	52.8	60-70%
* The mixed-layered illite/smectite phase appears to be randomly ordered (R0) containing ca. 50-95% smectite.																							

Table 3-2: Mineral abundances from modal analysis on thin sections (13) ("Tr" = only traces observed)

Plate No.	4	9	12	16	19	22	26	28	30	32
Well	14/28b-2	14/29a-3	14/29a-3	14/29a-3	14/29a-3	14/29a-4	14/29a-5	14/29a-5	14/29a-5	14/29a-5
Sample No.	4	9	12	16	19	22	26	28	30	32
Plug No.		16	222				6	65		142
Depth (ft)	8234.5	9741.9	10004	10124	10176	8800.4	8478	8540	8603	8674
Classification (Nagtegaal, 1978)	Silty Mudstone	Arkosic Arenite	Arkosic Arenite	Silty Mudstone	Arkosic Arenite	Silty Mudstone	Arkosic Arenite	Arkosic Arenite	Quartz Psammite	Arkosic Arenite
Dominant Lithology	Silty Mudstone	Sandstone	Sandstone	Silty Mudstone	Sandstone	Silty Mudstone	Sandstone	Sandstone	Silicified Calcitic Sandstone	Sandstone
DETRITAL MINERALS %	98.6	94.4	89.3	91.0	79.3	97.0	87.3	89.6	68.5	85.3
Quartz	7.3	76.3	73.0	7.0	55.0	2.0	74.0	67.6	60.3	68.7
Monocrystalline	7.0	72.3	65.7	7.0	50.7	2.0	70.0	61.3	55.0	64.7
Polycrystalline	0.3	4.0	7.3		4.3	Tr	4.0	6.3	5.0	3.7
Microcrystalline (Chert)									0.3	0.3
Feldspar	1.3	11.3	11.0	1.3	10.0	0.0	9.0	10.6	6.3	13.6
Potassium	0.3	8.3	6.7		6.3		5.3	6.3	4.3	5.3
Plagioclase	1.0	3.0	4.3	1.3	3.7		3.7	4.3	2.0	8.3
Lithic Fragments	1.3	4.3	2.7	1.7	4.4	Tr	2.3	4.0	1.3	1.3
Sedimentary	1.0	3.0	2.0	1.7	3.7	Tr	2.0	4.0	1.0	1.0
Igneous										
Metamorphic										
Volcanic										
Undifferentiated	0.3	1.3	0.7		0.7		0.3		0.3	0.3
Mica	2.3	0.6	Tr	Tr	1.3	0.3	1.0	1.7	Tr	0.7
Muscovite	1.0	0.3	Tr	Tr	1.0	0.3	0.3	0.7	Tr	Tr
Biotite	1.0	0.3	Tr	Tr	0.3		0.7	1.0	Tr	0.7
Chlorite	0.3		Tr							
Detrital Matrix/Intergranular Clays	81.0	0.7		72.3	6.3	93.3		4.7		0.7
Inherited clays								Tr		Tr
Bioclast	4.7	0.3		7.0	0.3	0.7	0.3	Tr	0.3	Tr
Glauconite		0.3	2.3		0.3		0.7	0.3	0.3	Tr
Phosphatic grains		0.3				Tr				
Carbonaceous Material	0.7			1.7	1.7	0.7		0.7	Tr	Tr
Detrital Opaques					Tr		Tr			
Heavy Minerals		0.3	0.3				Tr	Tr	Tr	0.3
DIAGENETIC MINERALS %	1.3	5.6	10.7	9.0	20.7	3.0	12.6	10.3	31.3	14.7
Quartz Overgrowths		2.0	5.7		4.3		3.3	6.3	1.0	6.7
Feldspar (Overgrowths and Laths)										
Chert									19.0	
Barite										
Hydrocarbons (?Bitumen)										
Carbonates	0.0	Tr	0.7	1.0	4.4	Tr	0.3	Tr	11.0	3.7
Non-Ferroan Calcite (Pore-Filling)			0.7	1.0	0.7	Tr	0.3	Tr	0.3	0.7
Non-Ferroan Calcite (Replacive)			Tr		Tr			Tr		
Ferroan Calcite (Pore-Filling)		Tr	Tr		3.7			Tr	10.7	3.0
Ferroan Calcite (Replacive)		Tr	Tr		Tr					
Non-Ferroan Dolomite (Pore-Filling)										
Non-Ferroan Dolomite (Replacive)										
Ferroan Dolomite (Pore-Filling)										
Ferroan Dolomite (Replacive)										
Siderite (Pore-Filling)								Tr		
Siderite (Replacive)										
Authigenic Clay Minerals	0.3	3.3	4.3	Tr	10.3	0.0	9.0	3.7	0.3	4.0
Kaolinite (Pore-Filling)		2.0	1.3		8.7		4.0	0.7		1.3
Kaolinite (Replacive)		0.3	Tr		1.3		0.3			Tr
Grain-Coating Clays		0.3	2.0				3.7	1.0		2.0
Grain-Replacive Clays	0.3	0.7	0.3	Tr	0.3		0.3	0.7	0.3	0.7
Other Pore-Filling Clays			0.7				0.7	1.3		
Evaporites	0.0	0.0	0.0	0.0	0.0	0.0	0.0	0.0	0.0	0.0
Anhydrite (Pore-Filling)										
Anhydrite (Replacive)										
Halite/Gypsum										
Opaques	1.0	0.3	Tr	8.0	1.7	3.0	Tr	0.3	Tr	0.3
Pyrite (Pore-Filling & Replacive)	0.7	Tr		8.0	1.7	2.0	Tr	0.3	Tr	0.3
Non-Resolvable	0.3	0.3	Tr		Tr	1.0	Tr	Tr	Tr	Tr
TOTAL POROSITY %	0.0	18.2	17.8	0.0	3.2	0.0	21.9	21.5	Tr	18.7
PRIMARY POROSITY	0.0	16.0	15.9	0.0	2.9	0.0	20.1	19.5	0.0	16.5
SECONDARY POROSITY	0.0	2.2	1.9	0.0	0.3	0.0	1.8	2.0	Tr	2.2

Table 3-3: List of samples used for petrographical analysis (13)

	Well	CoreLab Sample No.	Plug No.	Depth (ft)	Plate No.	TS	SEM	XRD
Kimmeridge	14/28a-1	1		6154	1		X	X
Kimmeridge	14/28a-1	2		6160.5	2		X	X
Rodby	14/28b-2	3		8230	3		X	X
Rodby	14/28b-2	4		8234.5	4	X	X	X
Rodby	14/28b-2	5		8238	5		X	X
Rodby	14/28b-2	6		8242.5	6		X	X
Scapa	14/29a-2	7		8267-8270	7		X	X
Scapa	14/29a-2	8		8321-8324	8		X	X
Captain D	14/29a-3	9	16	9741.9	9	X	X	X
Captain D	14/29a-3	10	106	9843	10		X	X
Captain D	14/29a-3	11		9947.5	11		X	X
Captain C	14/29a-3	12	222	10004	12	X	X	X
Captain C	14/29a-3	13	232	10043	13		X	X
Captain C	14/29a-3	14		10064	14		X	X
Captain C	14/29a-3	15	259	10079	15		X	X
Captain C	14/29a-3	16		10124	16	X	X	X
Captain C	14/29a-3	17		10126.5	17		X	X
Captain C	14/29a-3	18		10148	18		X	X
Captain C	14/29a-3	19		10176	19	X	X	X
Captain A	14/29a-3	20	267	10184.9	20		X	X
Rodby	14/29a-4	21		8775.3	21		X	X
Rodby	14/29a-4	22		8800.4	22	X	X	X
Captain E	14/29a-4	23		8831	23		X	X
Captain D	14/29a-4	24		8894	24		X	X
Captain C	14/29a-4	25		8983.3	25		X	X
Captain E	14/29a-5	26	6	8478	26	X	X	X
Captain E	14/29a-5	27		8490.5	27		X	X
Captain D	14/29a-5	28	65	8540	28	X	X	X
Captain E	14/29a-5	29		8587.5	29		X	X
Captain C	14/29a-5	30		8603	30	X	X	X
Captain C	14/29a-5	31		8642.5	31		X	X
Captain C	14/29a-5	32	142	8674	32	X	X	X
Captain C	14/29a-5	33		8690	33		X	X
Captain C	14/29a-5	34		8699.5	34		X	X

3.2. Formation brine and gas compositions

Five downhole brine samples are available from the reservoir, acquired from wells 14/29a-3 and 14/29a-5 (Table 3-4). These samples were taken somewhat below the oil water contact. There is little variation between the samples, and each sample withstands a simple quality check (charge balance within a couple of percentage points). The second sample (a3_2) is considered the most representative one within this set and it is closest to the average. Therefore this sample has been used as starting point for the brine composition in the modelling. No brine samples (nor reliable interpreted salinity from petrophysical logs) are available from the cap rock and the other geological layers above.

As shown in Table 3-5 the Goldeneye hydrocarbon gas contains some CO_2 (0.4 mole %). Therefore the brine in the original gas cap will have higher bicarbonate concentrations and lower pH than measured in any of the samples. Although in the water leg the amount of dissolved CO_2 may be lower than in the hydrocarbon leg, it is likely that the samples degassed prior to the pH measurement and compositional analysis. The measured pH on sample a3_2 was 7.32 under ambient conditions.

The measured brine density for a3_2 was 1.042 mg/l at surface conditions and the total dissolved solids (TDS), from the compositional analysis, is approximately 56,000 mg/l (54,000 ppm in terms of mass).

The injected CO_2 stream will be nearly pure (design specifications are shown in Table 3-6). In the modelling a 100% CO_2 stream was assumed.

Table 3-4: Measured reservoir brine compositions, with some basic statistics (average and deviations from the average)

		Concentration (mg/l)												
		a3_1	a3_2	a3_3	a3_4	a5	avg	d a3_1	d a3_2	d a3_3	d a3_4	d a5	stdev	stdev/avg
Sodium	Na +	19180.00	19990.00	20370.00	20751.00	19885.00	20035.20	-4.3%	-0.2%	1.7%	3.6%	-0.7%	587.46	2.9%
Magnesium	Mg 2+	230.00	235.00	245.00	243.50	264.50	243.60	-5.6%	-3.5%	0.6%	0.0%	8.6%	13.21	5.4%
Potassium	K +	225.00	255.00	260.00	253.50	210.00	240.70	-6.5%	5.9%	8.0%	5.3%	-12.8%	21.96	9.1%
Calcium	Ca 2+	1020.00	1050.00	1060.00	1309.00	1372.00	1162.20	-12.2%	-9.7%	-8.8%	12.6%	18.1%	164.94	14.2%
Iron	Fe 2+	3.30	0.72	0.05		1.58	1.41	133.6%	-49.0%	-96.5%	-100.0%	11.9%	1.41	99.5%
Strontium	Sr 2+	245.00	250.00	250.00	314.50	264.00	264.70	-7.4%	-5.6%	-5.6%	18.8%	-0.3%	28.73	10.9%
Barium	Ba 2+	79.00	83.00	83.00	52.00	50.12	69.42	13.8%	19.6%	19.6%	-25.1%	-27.8%	16.86	24.3%
Boron	B 3+	95.00	97.00			95.65	95.88	-0.9%	1.2%	-100.0%	-100.0%	-0.2%	1.02	1.1%
Aluminium	Al 3+	0.50	0.50			0.35	0.45	11.1%	11.1%	-100.0%	-100.0%	-22.2%	0.09	19.2%
Silicon	Si 4+	18.00	20.00			17.45	18.48	-2.6%	8.2%	-100.0%	-100.0%	-5.6%	1.34	7.3%
Phosphorus	P 5+	0.36	0.68			1.97	1.00	-64.1%	-32.2%	-100.0%	-100.0%	96.3%	0.85	84.9%
Lithium	Li +	5.30	5.80			6.17	5.76	-7.9%	0.8%	-100.0%	-100.0%	7.2%	0.44	7.6%
Chloride	Cl -	33420.00	33680.00	33470.00	33448.50	32920.00	33387.70	0.1%	0.9%	0.2%	0.2%	-1.4%	280.93	0.8%
Bicarbonate	HCO3 -	710.00	805.00	1010.00	738.50		815.88	-13.0%	-1.3%	23.8%	-9.5%	-100.0%	135.40	16.6%
Sulphate	SO4 2-	15.00	13.00	28.00	11.60	15.35	16.59	-9.6%	-21.6%	68.8%	-30.1%	-7.5%	6.56	39.5%

Table 3-5: Hydrocarbon gas composition (13)

Component	Sep. Gas Mol.%	Separator Liquid Wt.%	Separator Liquid Mol.%	Calculated Fluid Wt.%	Calculated Fluid Mol.%
N_2	1.024	0.039	0.109	1.107	0.949
H_2S	0.000	0.000	0.000	0.000	0.000
CO_2	0.408	0.113	0.201	0.717	0.391
nC1	86.592	4.359	21.359	54.302	81.266
nC2	6.964	2.757	7.207	8.748	6.984
nC3	2.844	4.093	7.297	5.893	3.208
iC4	0.408	1.480	2.001	1.302	0.538
nC4	0.897	4.384	5.930	3.167	1.308
neo-C5	0.003	0.019	0.021	0.014	0.005
iC5	0.218	2.610	2.844	1.299	0.432
nC5	0.281	4.143	4.515	1.884	0.627
Cyclopentane	0.012	0.290	0.325	0.110	0.038
iC6	0.098	3.299	3.009	1.205	0.336
nC6	0.086	3.959	3.611	1.343	0.374
Methylcyclopentane	0.022	1.322	1.234	0.423	0.121
Benzene	0.014	1.061	1.068	0.326	0.100
Cyclohexane	0.022	1.878	1.754	0.573	0.164
iC7	0.039	4.145	3.252	1.256	0.301
nC7	0.023	3.679	2.886	1.071	0.257
Methylcyclohexane	0.015	3.117	2.495	0.890	0.217
Toluene	0.006	2.487	2.122	0.688	0.179
iC8	0.013	5.506	3.789	1.529	0.321
nC8	0.004	2.968	2.043	0.811	0.171
Ethylcyclohexane	0.001	0.866	0.606	0.235	0.050
Ethylbenzene	0.000	0.341	0.252	0.092	0.021
Meta and Para Xylenes	0.001	1.911	1.415	0.517	0.117
Ortho Xylene	0.000	0.684	0.507	0.184	0.042
iC9	0.003	4.077	2.499	1.103	0.206
nC9	0.001	2.390	1.465	0.642	0.120
C10	0.001	7.739	4.324	2.076	0.354
C11	0.000	5.423	2.727	1.451	0.223
C12	0.000	3.947	1.822	1.056	0.149
C13	0.000	3.535	1.507	0.945	0.123
C14	0.000	2.719	1.077	0.727	0.088
C15	0.000	2.075	0.768	0.555	0.063
C16	0.000	1.496	0.519	0.400	0.042
C17	0.000	1.334	0.436	0.357	0.036
C18	0.000	0.925	0.286	0.247	0.023
C19	0.000	0.591	0.173	0.158	0.014
C20	0.000	0.506	0.141	0.135	0.011
C21	0.000	0.381	0.101	0.102	0.008
C22	0.000	0.299	0.076	0.080	0.006
C23	0.000	0.231	0.056	0.062	0.005
C24	0.000	0.178	0.041	0.047	0.003
C25	0.000	0.138	0.031	0.037	0.003
C26	0.000	0.110	0.024	0.029	0.002
C27	0.000	0.087	0.018	0.023	0.001
C28	0.000	0.068	0.014	0.018	0.001
C29	0.000	0.054	0.010	0.014	0.001
C30	0.000	0.043	0.008	0.012	0.001
C31	0.000	0.034	0.006	0.009	<0.001
C32	0.000	0.026	0.005	0.007	<0.001
C33	0.000	0.021	0.004	0.006	<0.001
C34	0.000	0.017	0.003	0.004	<0.001
C35	0.000	0.012	0.002	0.003	<0.001
C36+	0.000	0.034	0.005	0.009	<0.001
Total	100.000	100.000	100.000	100.000	100.000

Table 3-6: CO_2 injection stream (maximum load process condition) (14)

		OUT
		CO_2 product gas
	From	REFLUX ACCUMULATOR
	To	OSBL
Component Molar Fraction		
H_2O		50 ppmv
Amine		<0.1 ppmv
CO_2		0.9999
N_2		60 ppmv
O_2		1 ppmv
SO_2		0.000
NO_2		0.000
NH_3		<0.1 ppmv
Nitrosamine		<0.1 ppmv
Deg-L (amine)		0.000
NDMA		0.000
DMA		2.0 ppmv
NaOH		0.000
H_2SO_4		0.000
Na_2SO_3		0.000
Na_2SO_4		0.000
NaCOOH		0.000
$NaNO_3$		0.000
Total		1.000

4. Reservoir (Captain) Reactivity

The reactivity in the reservoir caused by the injected CO_2 is addressed using batch models first (Section 4.1) using standalone PHREEQC; and then the coupled geochemical reactions and fluid transport are modelled (Section 4.2) using the MoReS-PHREEQC reactive transport simulator.

A potential geochemical risk not discussed in this chapter is that of reservoir souring (H_2S generation). Reservoir souring is a known health, safety, environment (HSE) risk for e.g. water injection projects, and therefore the question may be asked if it could be a risk for CO_2 injection. The Goldeneye reservoir souring potential is analysed in Appendix 3. The conclusion is that the probability of reservoir souring is negligible.

4.1. Batch models

4.1.1. Assumptions and initial conditions

The batch model is (by definition) a zero dimensional (0D) model where fluid transport is ignored. The model assumptions require some discussion. In general all assumptions/input parameters are geared towards the high-reactivity end of their uncertainty range. In this way the maximum expected effects of the geochemical reactivity on injectivity and mineralisation are investigated (and in Section 5 on containment).

4.1.1.1. Petrophysical parameters

For the porosity a reservoir averaged porosity was used (24%). The water saturation requires more thought. Pre-production the connate water saturation in the gas cap was low (approximately 7% in the crest), however since Goldeneye has experienced aquifer influx during production, the average water saturation (in the required CO_2 storage space) is much higher prior to CO_2 injection. Based on the history matched Goldeneye full field model (15) this is roughly 50%. Therefore in the batch model a saturation of 50% was used. However it should be stressed that upon CO_2 injection much of this water will be swept away, and during injection and post injection the water saturation will be lower than 50%. Based on the full field model long term prediction, this is approximately 20% on average. Therefore in the batch model a sensitivity run was done at a lower water saturation of 20% (close to residual water saturation: at which the water is immobile).

4.1.1.2. Open or closed system

Another question is whether to assume an open or closed system for the batch runs. Since even during the injection period most of the water exposed to injected CO_2 (i.e. in the CO_2 plume) is nearly immobile (due to the low water saturation), a closed system is assumed, i.e. water transport is not taken into account (the 2D coupled models, described in Section 4.2, will take transport into account). Furthermore since not all injected CO_2 is expected to dissolve in water, and the reservoir pressure is in rough approximation constant through time, a constant CO_2 fugacity was assumed in the batch runs, namely corresponding to 100% CO_2 and a pressure of 250 bara. Using the Shell in-house equation of state (EOS) model STFlash the fugacity was calculated to be 123 bara, corresponding to a log fugacity of 2.09, with the log fugacity defined as log(fugacity[bar]). Note that in reality there will be a mixing between the CO_2 and the remaining hydrocarbon gas further away from the well, so this fugacity is somewhat on the high side (resulting in a somewhat too low pH and a somewhat too large reactivity). The original fugacity, with 0.4 mol% CO_2 in the hydrocarbon gas at

263 bara, has been calculated as 0.65 bara from the EOS model, corresponding to a log fugacity of -0.19.

The Goldeneye reservoir temperature is approximately 83°C. Upon CO_2 injection there will be a lower temperature near the injectors. However the extent of this cooling zone is limited in spatial extent during injection, and disappears post injection. Therefore this temporary cooling effect has not been taken into account in the reactive transport modelling.

4.1.1.3. Initial mineral assemblage (primary minerals)

The mineral assemblage was based on reservoir-averaged values from the petrography (Table 4-1). It is assumed that the observed minerals from the chlorite group is chamosite rather than clinochlore, based on geological considerations. The heavy minerals were left out of the modelling as they are expected to be unreactive. The list of primary minerals was further simplified in order to obtain a less complex system while capturing all the important reactions. This is described in the next section.

Table 4-1: Base mineralogical assemblage and parameters used in the reservoir modelling

				Based on Goldeneye petrography	Xu et al., Chem Geol 2010
Mineral Name	**Chemical Formula**	**specific gravity**	**Volume %**	**specific surface area (cm2/g)**	**specific surface area (cm2/g)**
Quartz	SiO2	2.65	65.41	20.53	9.80
Albite_low	NaAlSi3O8	2.62	5.81	247.67	9.80
K-Feldspar	KAlSi3O8	2.56	5.81	139.51	9.80
Kaolinite	Al2Si2O5(OH)4	2.60	2.08	38461.54	151.60
Illite	K0.6Mg0.25Al1.8Al0.5Si3.5O10(OH)2	2.90	5.33	538461.54	151.60
Smectite-high-Fe-Mg	Ca.025Na.1K.2Fe.5Fe.2Mg1.15Al1.25Si3.5H2O12	2.41	0.56	538461.54	151.60
Montmor-Ca	Ca.165Mg.33Al1.67Si4O10(OH)2	2.15	0.56	538461.54	
Muscovite	KAl3Si3O10(OH)2	2.88	0.63	2207.00	
Phlogopite (for Biotite)	KAlMg3Si3O10(OH)2	2.90	1.50	2207.00	
Glauconite-2	Mg0.5K1.5Fe3AlSi7.5O20(OH)4	2.68	0.63	2207.00	9.80
Chamosite-7A	Fe2Al2SiO5(OH)4	3.13	2.91	10000.00	151.60
Calcite	CaCO3	2.71	2.96	738.01	9.80
Siderite	FeCO3	3.80	0.97	526.32	9.80
Barite	BaSO4	4.65	0.19	526.32	
Pyrite	FeS2	5.00	0.44	1197.60	12.90

4.1.1.4. Initial brine composition

An important consideration is what initial brine composition to use in the modelling. The challenge is that the measured brine composition is not in thermodynamic equilibrium with the identified primary minerals and the 0.4% CO_2 in the hydrocarbon gas. This is a well-known problem in geochemical modelling. There can be multiple reasons for this lack of consistency:

1) the formation water in the reservoir may not be completely static (hydrodynamic aquifer) in combination with the long times required to equilibrate with some of the minerals;
2) not all primary minerals are present in each sample i.e. that there is spatial variation in the mineralogy. Therefore it is likely that there is also some spatial variation in the brine composition;
3) the geochemical database may be inaccurate;
4) the measured brine composition may be inaccurate (e.g. some solutes may have degassed or precipitated from subsurface to the wellhead and between sampling locations and lab measurements).

Usually in geochemical modelling consistency of the initial conditions is enforced by equilibrating the measured brine composition to the mineral assemblage (and any initial CO_2), thus changing the brine composition. To a large extent this is for practical considerations, namely to ensure that the model is stable if it is run without any CO_2 injection (and more importantly in the case of a 1D/2D/3D model with CO_2 injection, to ensure that those regions in the model that are not contacted by injected CO_2

are stable). As long as there are a small number of primary minerals the equilibration step works well without changing the brine composition too much. However with a larger set of primary minerals, as in Table 4-1, it is typically not possible because the equilibrium step mathematically imposes too many constraints (a larger number of constraints than the number of degrees of freedom, violating Gibbs phase rule). This creates a dilemma. Usually it is resolved by adapting (reducing) the number of primary minerals in the model.

In the Goldeneye case, and presumably in many other cases, it turns out that for the batch (0D) runs with CO_2 injection it is actually not so important to resolve the dilemma. The reason is that with CO_2 injection the results (in terms of mineral evolution over time) are nearly the same for the simulation starting from the measured brine composition and the simulation starting from the equilibrated brine composition (to be specific, this was checked for the case with a reduced number of minerals, Case 2 in Table 4-3 in the next section). Presumably this is because the injected CO_2 has much higher fugacity than the CO_2 originally present in the hydrocarbon gas, so that the geochemical system is brought so far out of equilibrium by the CO_2 injection that variations in the initial composition have very little impact. For completeness, the composition of the equilibrated brine (for the reduced number of minerals case, Case 2 in Table 4-3) is presented in Table 4-2.

Table 4-2: Brine compostions under surface conditions (measured) and reservoir conditions (equilibrated)

	measured	equilibrated	unit
temperature	15.56	83	(°C)
pH	7.32	6.43	-
Al	0.000019	0.0000002	mol/kgW
B	0.0091	0.0091	mol/kgW
Ba	0.00061	0.00061	mol/kgW
C	0.0134	0.0260	mol/kgW
Ca	0.0266	0.00218	mol/kgW
Cl	0.964	0.957	mol/kgW
Fe	0.000013	0.00028	mol/kgW
K	0.0066	0.0052	mol/kgW
Li	0.00085	0.00085	mol/kgW
Mg	0.0098	0.0055	mol/kgW
Na	0.8823	0.9482	mol/kgW
P	0.000022	0.000022	mol/kgW
S	0.00014	0.00014	mol/kgW
Si	0.00034	0.00062	mol/kgW
Sr	0.0029	0.0029	mol/kgW

4.1.1.5. Mineral reaction rates and secondary minerals

Table 4-1 also gives the mineral specific gravity used in the modelling (used for the calculation of porosity changes) and the specific surface areas controlling the speed of the reactions (kinetic rate formula). In general the specific surface areas are very reservoir specific since they depend on the mineral crystal sizes (which can be determined from TS or SEM if resolution is high enough) as well as on pore geometry (some crystals may be poorly accessible by the brine, leading to the concept of effective surface area). In Table 4-1 two columns of specific surface areas are presented, the first column based on the Goldeneye petrography plus for those minerals with one of the crystal

dimensions below SEM resolution (clay minerals, chlorite and micas) typical values for their dimensions. In this column no reduction factor was incorporated, because the porespace seems well connected (in line with the high Goldeneye permeability of approximately 1 Darcy) and there is only limited coating on the minerals. Unfortunately there is no BET data available on the Goldeneye samples (this would give the total surface area).

The second column represents generic parameters derived from the literature (e.g. used by the TOUGHREACT modelling/development group (10)). It can be seen that for most minerals the second column has much lower specific surface areas. In the absence of Goldeneye specific measurements on reaction times the model was run with both sets of specific surface areas. This leads to a significant spread in reaction times, as will be clear in the model results. For the base model the first column kinetics were used, i.e. the high (or at least fast) reactivity case. This is in line with the 'high reactivity' mindset explained at the start of this section. Moreover it has the advantage that the system reaches a full stability within the simulated period (10,000 years), so that the complete reaction path can be analysed.

Based on geological (diagenetic) experience the following secondary minerals (i.e. potential minerals that may form upon CO_2 injection) were allowed in the model: anhydrite, ankerite, celestite, dawsonite, dolomite-ordered, goethite, halite, fluorite, hematite, magnesite, montmorrilionite-K, pyrrhotite, and SiO_2 (amorphous). Most of these will not form according to the model, and these were left out in the simplified model.

Since the rate of mineral reactions is determined by the slowest reacting minerals involved, the faster reacting minerals were assumed to be in instantaneous equilibrium with the brine. This avoids numerical problems and speeds up the PHREEQC (and MoReS-PHREEQC) simulations. In most runs the following minerals were assumed to be in instantaneous equilibrium: barite, calcite, glauconite, illite, kaolinite, siderite, anhydrite, ankerite, celestite, dawsonite, dolomite, goethite, and halite. For some of these minerals it may be questioned if the assumption is valid. For kaolinite, which plays a key role in the mineral reactions, it was verified that the assumption is valid by doing a sensitivity run with kaolinite in the kinetics.

Rate constants and other parameters for the adopted rate laws are the same as in Palandri & Kharaka9.

4.1.2. Results

A number of different cases were simulated; the overview is presented in Table 4-3.

Table 4-3: Overview of simulated cases

Case	Water saturation	Number of minerals	Specific surface area	Comments
1	50%	**25 (full set)**	high	
2	50%	9 (reduced set)	high	
3	**20%**	9 (reduced set)	high	
4	50%	9 (reduced set)	**low**	Specific surface areas from Xu at al.
5	50%	**8**	high	Dawsonite absent
6	50%	**24**	high	Dawsonite absent
7	50%	**25 (full set)**	high	Clinochlore instead of Chamosite
8	50%	9 (reduced set)	high	Using initial brine composition equilibrated with the primary minerals. Very small impact. Not presented in report
9	50%	9 (reduced set)	high	Kaolinite in kinetics. Very small impact. Not presented in report

The mineralogical and brine evolution of the full system (Case 1 - all primary and secondary minerals considered) is shown in Figure 4-1 and Figure 4-2. It was checked in PHREEQC that at the end of the simulation (10,000 years) all saturation indices are smaller or equal to zero, so that the system is at equilibrium at this stage, i.e. the full reaction path has been completed.

Based on the observations from Figure 4-1 a simplified system (Case 2) was modelled, in which only the primary and secondary minerals undergoing the largest alterations in Figure 4-1 were kept, namely calcite, kaolinite, albite, chamosite, phlogopite, quartz, ankerite, dolomite and dawsonite. Siderite was removed because in the full system there is a competition between siderite, dolomite and ankerite, with (according to the model) ankerite plus some dolomite eventually being the stable phases. The results are shown in Figure 4-3 and Figure 4-4. From this it can be verified that the final mineralogical state of the system is nearly identical to that of the full system. The main difference is that the reactions in the time period up to approximately 150 years are less complex and start later. This is mainly because siderite was removed from the system.

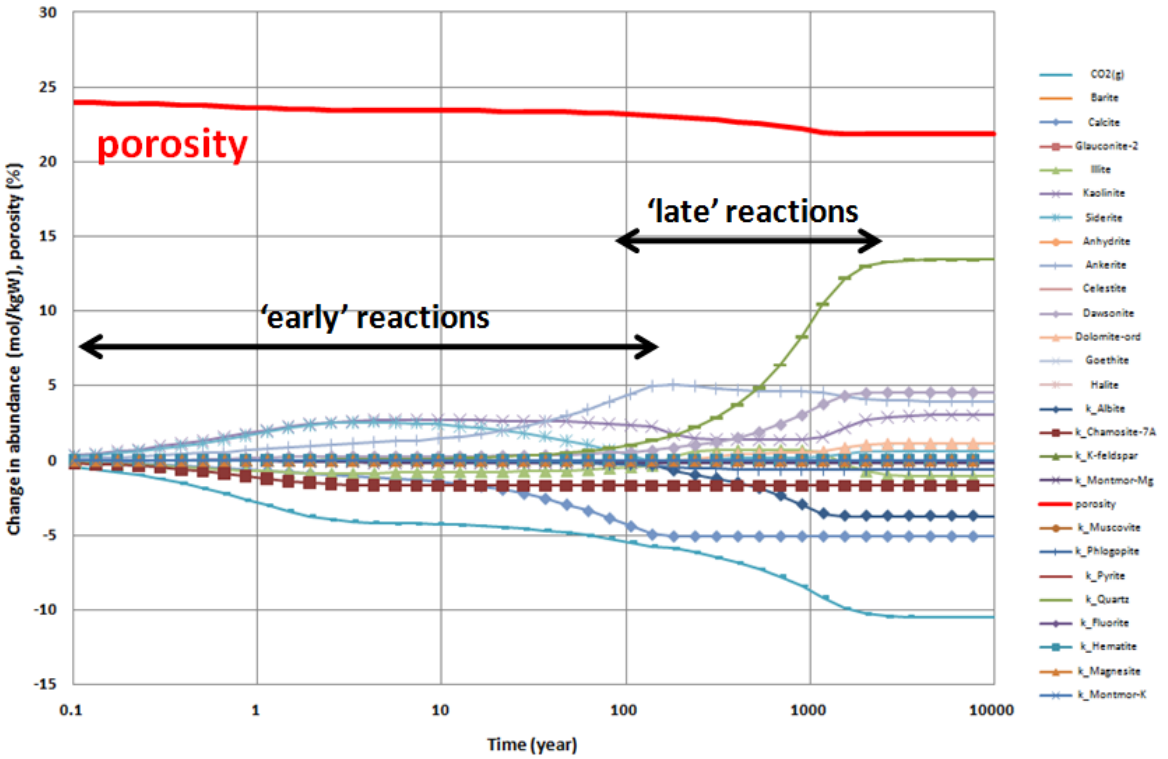

Figure 4-1: **Mineralogical changes with the full range of minerals (Case 1)**

Note: also porosity and amount of CO_2 used from the gaseous phase are plotted. The amounts are expressed in mol/kgW. 1 mol/kgW corresponds to 118 mol/m^3 gross rock volume (for the assumed porosity, water saturation, brine density and total dissolved solids (TDS). Two sets of reactions can be distinguished ('early' and 'late').

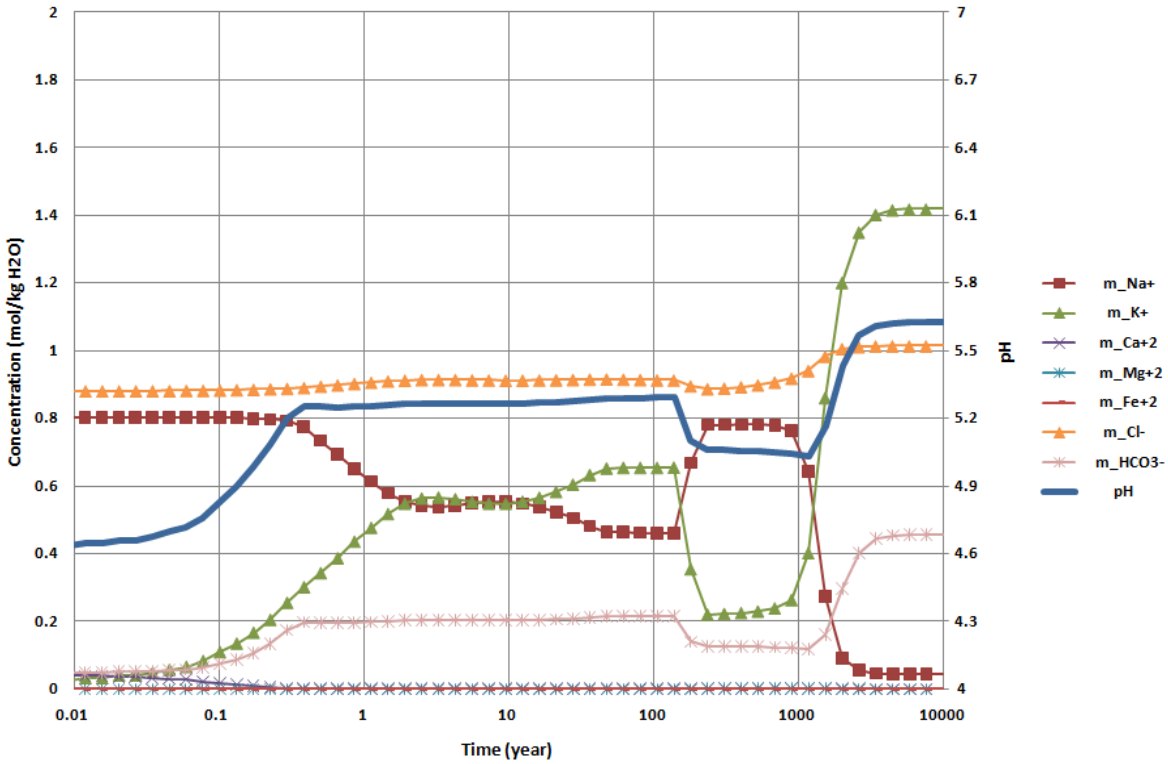

Figure 4-2: **Brine composition and pH evolution with the full range of minerals (Case 1)**

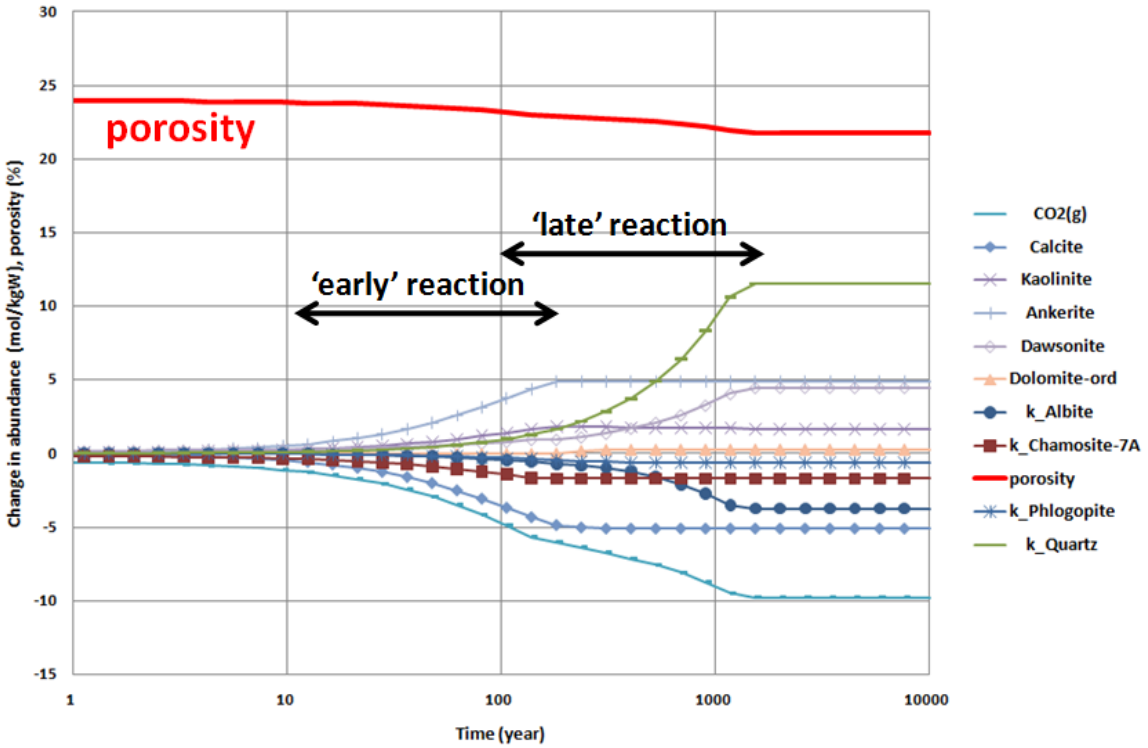

Figure 4-3: Mineralogical changes with the full range of minerals in the simplified model (Case 2)

Note: the amounts are expressed in mol/kgW. 1 mol/kgW corresponds to 118 mol/m³ gross rock volume (for the assumed porosity, water saturation, brine density and TDS). Two sets of reactions can be distinguished ('early' and 'late').

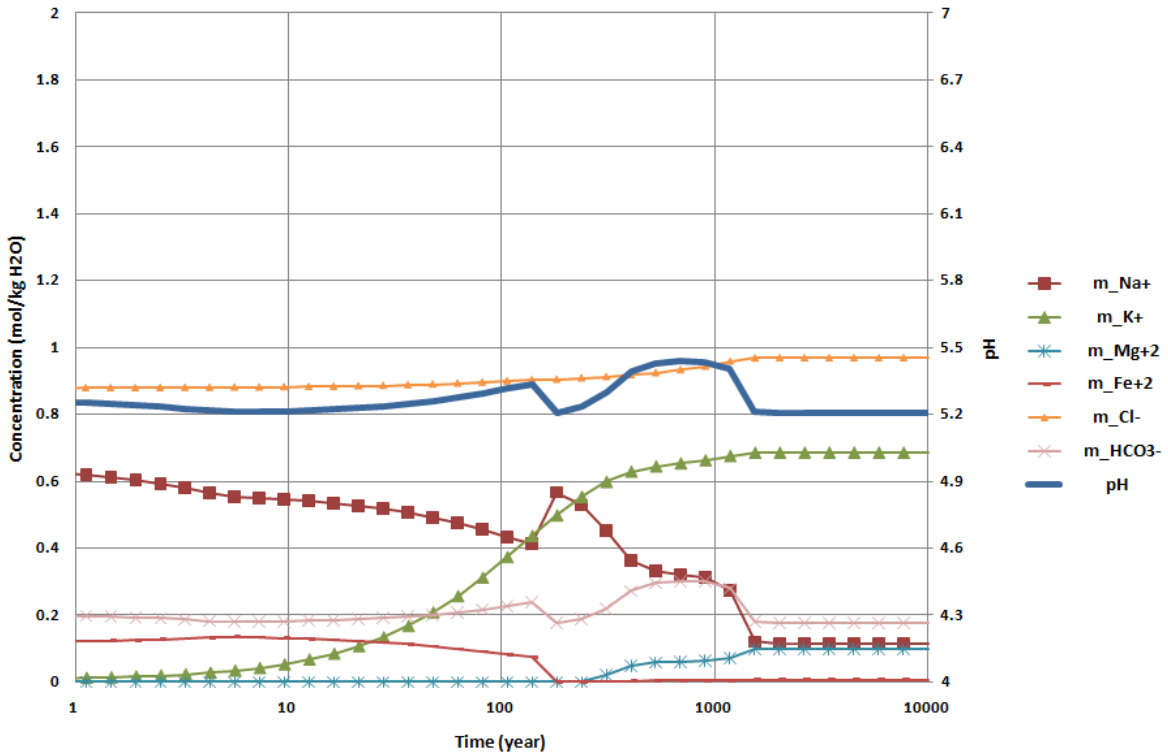

Figure 4-4: Composition evolution in the simplified model (Case 2)

In the following paragraphs the Case 2 results are analysed.

An 'early' and a 'late' reaction can be distinguished. In the early reaction (~10 - ~150 year) calcite is altered into ankerite and some dolomite, with chamosite acting as an iron source, phlogopite as a magnesium source, and kaolinite as a byproduct (sink for aluminum and silicon). This reaction consumes approximately 6 mol CO_2/kgW. Also there is a surplus of K+, leading to increased brine salinity. In the 'late' reaction (~100 - ~1500 year) albite is altered into dawsonite, consuming another approximately 4 mol CO_2/kgW and having quartz as a by-product.

The total CO_2 mineralisation is about 10 mol/kgW. Using the porosity of 24%, water saturation of 50%, and a water density of 1.04 g/cm^3 with salinity 54,000 mg/l)) this corresponds to 1,170 mol (51.5 kg) of CO_2 per m^3 gross rock volume. Given the assumed porosity (24%) and water saturation (50%), and assuming a CO_2 density of 0.65 g/cm^3 (pure CO_2 at reservoir temperature and 250 bara) this would imply that 66% of the gaseous (supercritical) CO_2 is mineralised within 10,000 years. This is a high figure; however it should be stressed again that the model is geared towards high reactivity (in order to investigate the maximum geochemical effects), because all input parameters were selected at the high reactivity end of their uncertainty range. In reality the reactivity could be lower due to lower specific surface areas and/or lower CO_2 fugacity (due to mixing with hydrocarbon gas) and/or a less homogeneous mix of primary minerals, CO_2 and brine.

The porosity at the end of the injection period (10 years) is 23.85% i.e. only a relative reduction of 0.006 of the original porosity. In the simulation with the full mineral set this is a stronger reduction (23.42% i.e. relative reduction by 0.02) due to the earlier onset of siderite reactions. Again, it should be stressed that this is under high reactivity assumptions. Further discussion on injectivity impact is postponed to Section 4.3. By the end of the early reaction, the porosity is reduced from to 23.0%, and by the end of the late reaction, i.e. at the end of the reaction path, the porosity is reduced to 21.8%.

The 'early' reaction is supported by observations in natural CO_2 systems, e.g. in the Otway Basin (16), although in some cases siderite precipitation may be favoured over iron rich dolomite/ankerite due to easier nucleation. The 'late' reaction is only weakly supported by analogues (17). A sensitivity run without allowing dawsonite precipitation is presented below.

In the geochemical database used, the stoichiometric coefficients do not exactly match up in the early reaction. This leads to buffering in the brine (for some ions, notably Fe^{++}, this effect is too strong compared to the buffering in the model with all minerals included), plus some interference with the late reaction. The increased Cl^- concentrations in the brine are due to H_2O consumption in the late reaction. The decrease in Na^+ concentration is due to the brine acting as another source of sodium in the formation of dawsonite (albite being the main source).

A number of sensitivities are presented below. Figure 4-5 and Figure 4-6 show the impact of lower water saturation (Case 3 - using a water saturation of 0.2, i.e. the typical water saturation within most of the gas plume). Expressed as mol/kgW the changes in mineral abundances are approximately a factor 2.5 larger than in Figure 4-3. This is simply because the amount of water per m^3 of gross rock volume is a factor 2.5 smaller (water saturation of 20% instead of 50%). Only in the late reaction the amount of CO_2 consumed is slightly less than in the base run, because there is slightly less Na+ available in the system for the formation of dawsonite. In the brine evolution the differences are somewhat larger. In this case the amount of CO_2 mineralised is 48.7 kg per cubic metre of rock, corresponding to 'only' 39% of the injected CO_2, because 80% (instead of 50%) of the pore space is now assumed filled with gaseous (supercritical) CO_2. The porosity change is nearly identical as with 50% water saturation.

Figure 4-7 and Figure 4-8 show the impact of the alternative (lower) specific surface area assumption (Case 4). In this case the 'early' reaction occurs later than with the high specific surface area assumption (Figure 4-3), while the 'late' reaction shows a less significant delay. As a consequence,

with the low specific surface area assumption the two reactions overlap. The reactions have not fully reached equilibrium after 10,000 years.

Since the precipitation of dawsonite is only found to a limited extent in natural CO_2 reservoirs, Figure 4-9 and Figure 4-10 (case 5, for the reduced number of minerals), and Figure 4-11 and Figure 4-12 (case 6, for the full set of minerals), present the model results when dawsonite is not allowed to precipitate. In both cases the reactions stop after the early (calcite) reaction, i.e. even with the full set of minerals the system does not find an alternative reaction path. A limited amount of albite and CO_2 dissolves, with kaolinite and quartz precipitating and Na+ (and HCO_3^-) concentration in the brine increasing until the brine becomes saturated with respect to albite. Consequently the final amount of CO_2 consumed after 10,000 years is only slightly higher than that of the 'early' reaction in Figure 4-3 and Figure 4-1 , i.e. approximately 6 mol/kgW.

Figure 4-13 and Figure 4-14 show the impact of using a different assumption on Chlorite (Case 7), namely that it is present as clinochlore instead of chamosite. This gives a better stoichiometric fit of the 'early' reaction leading to much smaller changes in the brine composition. Nevertheless in terms of mineralogical changes, porosity reduction and total CO_2 consumption the impact is small.

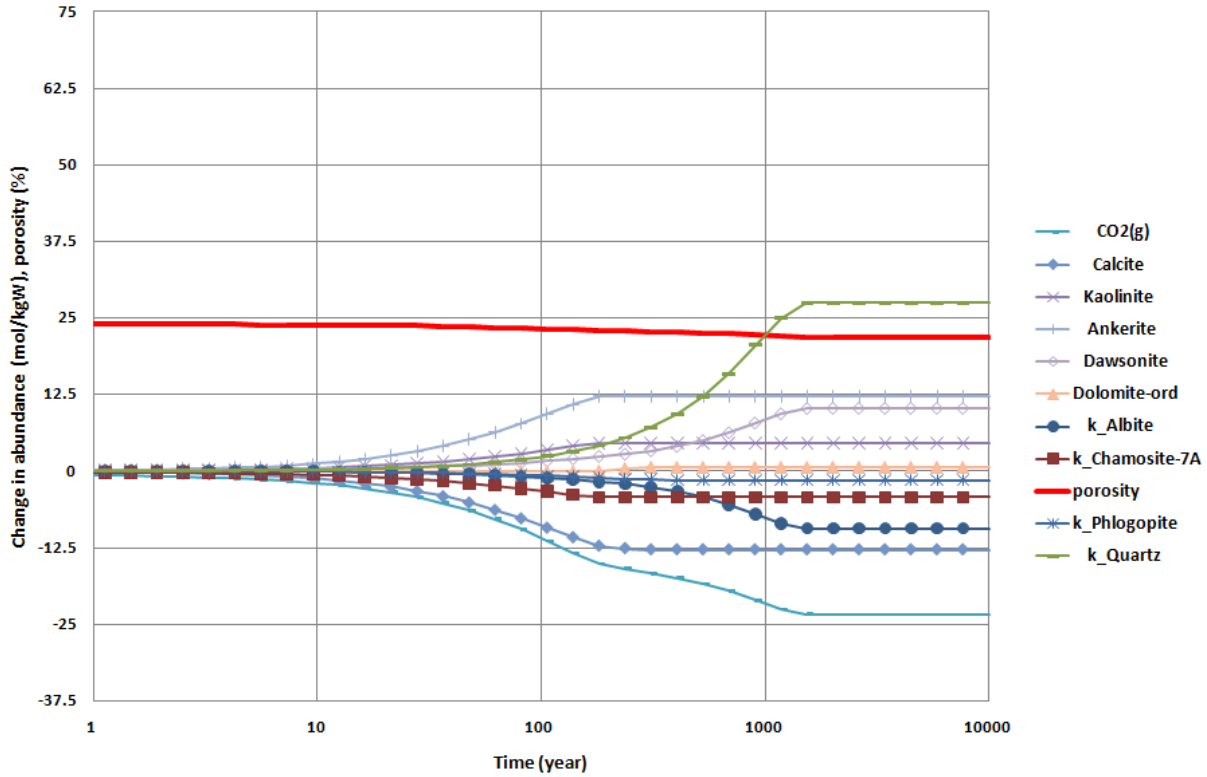

Figure 4-5: Mineralogical changes in the simplified model run for water saturation 0.2 instead of 0.5 (Case 3)

Note: The amounts are expressed in mol/kgW. 1 mol/kgW corresponds to 47 mol/m³ gross rock volume (for the assumed porosity, water saturation of 0.2, brine density and TDS).

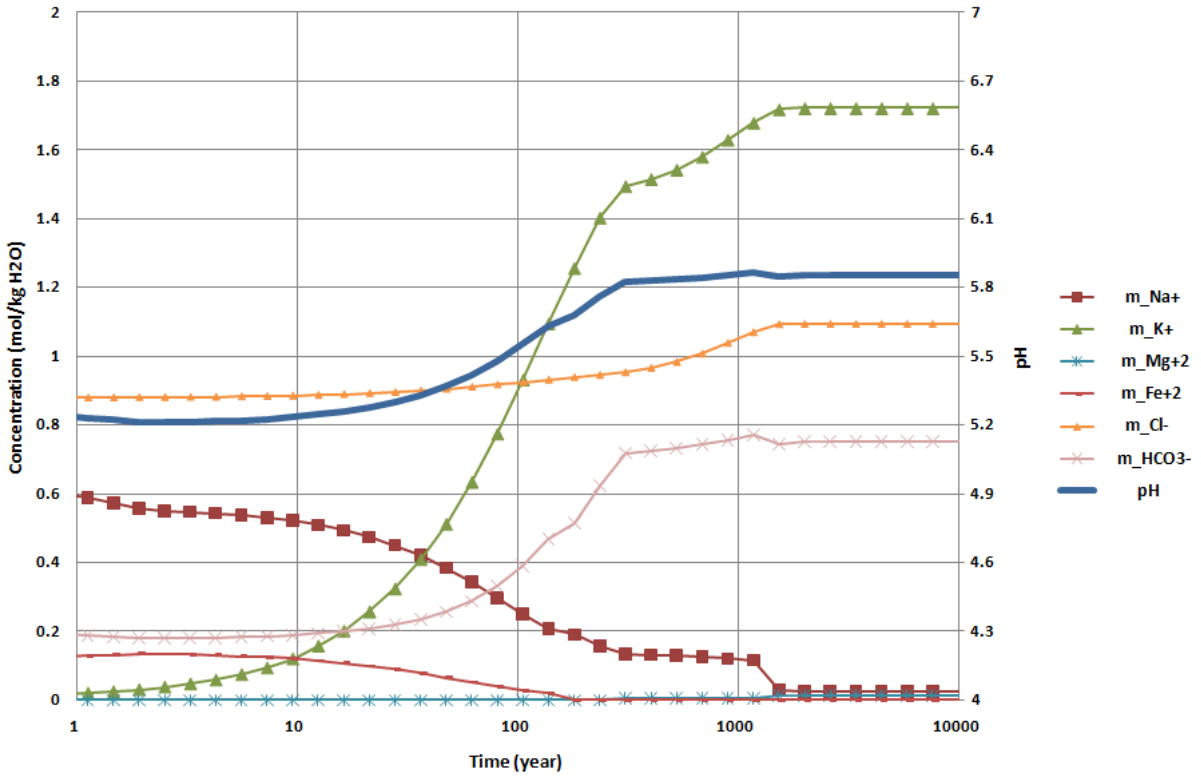

Figure 4-6: Composition evolution in the simplified model run for water saturation 0.2 (Case 3)

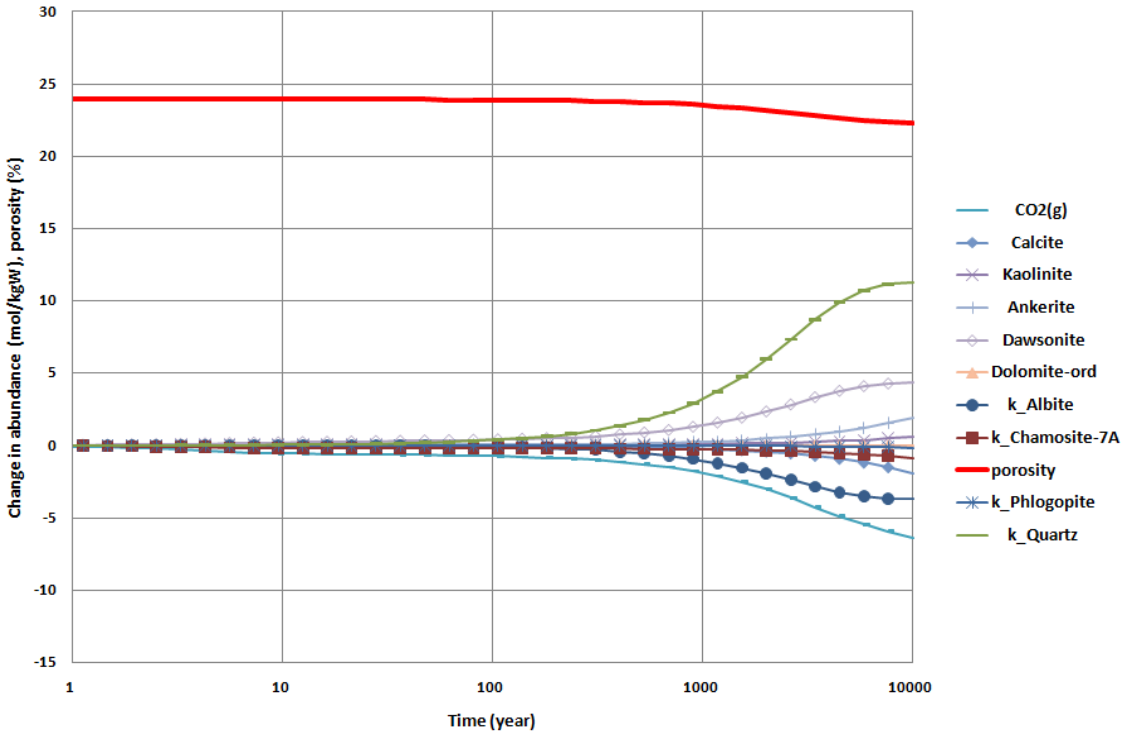

Figure 4-7: Mineralogical changes in the simplified model with specific surface area from Xu et al. (Case 4)

Note: The amounts are expressed in mol/kgW. 1 mol/kgW corresponds to 118 mol/m^3 gross rock volume (for the assumed porosity, water saturation, brine density and TDS).

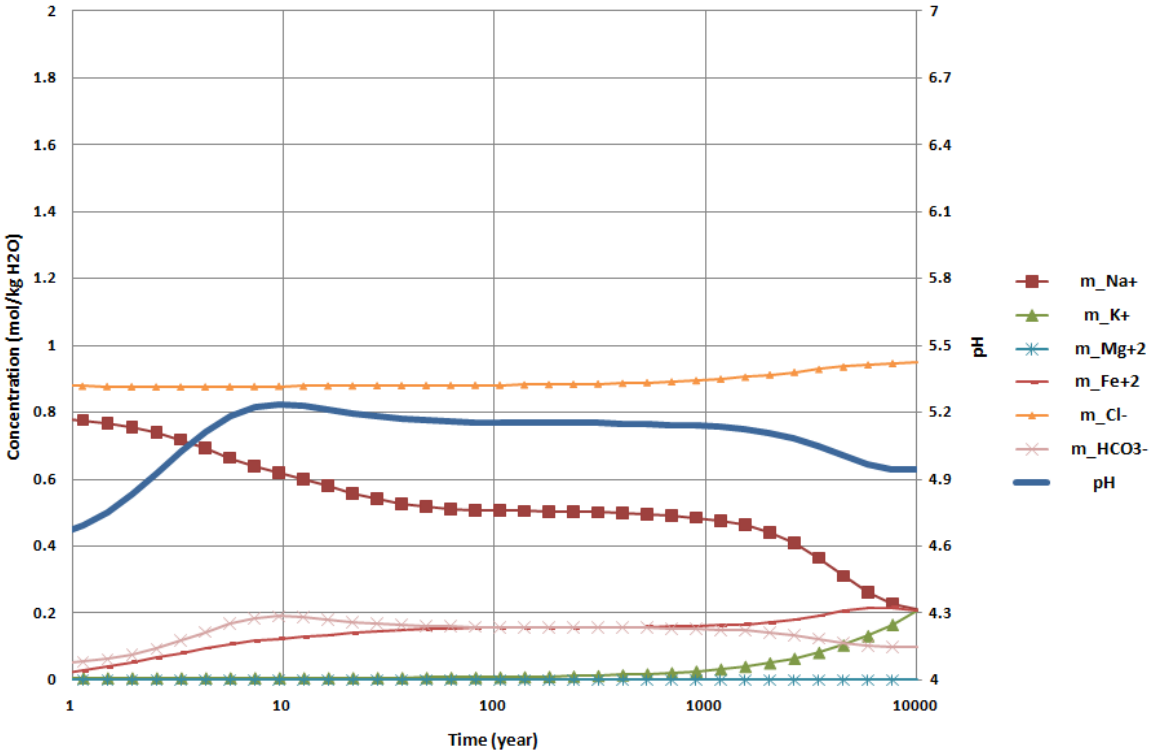

Figure 4-8: Composition evolution in the simplified model with specific surface area from Xu et al. (Case 4)

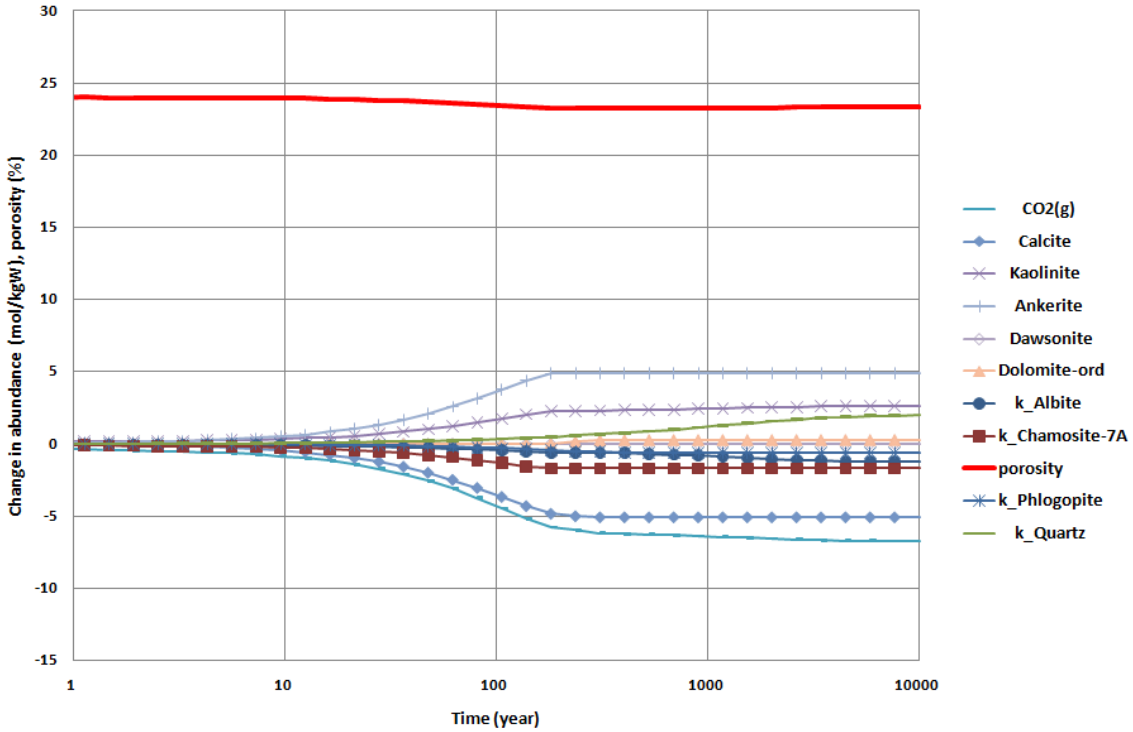

Figure 4-9: Mineralogical changes with no dawsonite precipitation allowed (Case 5 - simplified model)

Note: The amounts are expressed in mol/kgW. 1 mol/kgW corresponds to 118 mol/m^3 gross rock volume (for the assumed porosity, water saturation, brine density and TDS).

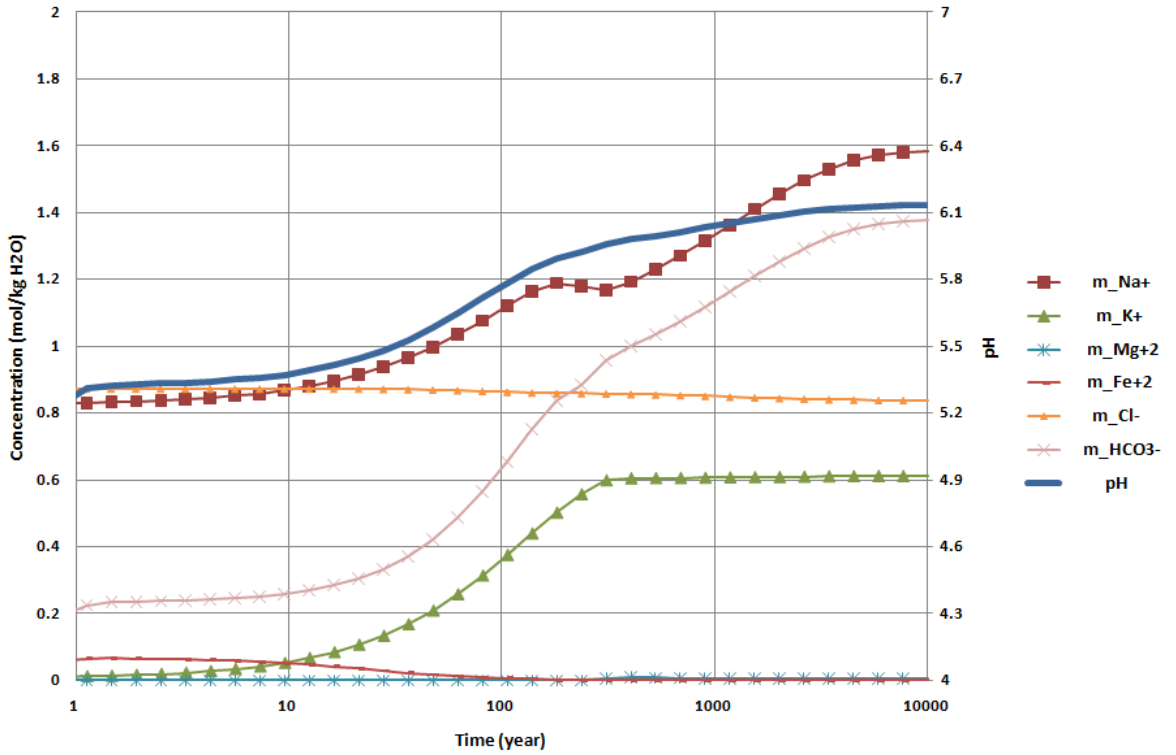

Figure 4-10: Composition evolution with no dawsonite precipitation allowed (Case 5 - simplified model)

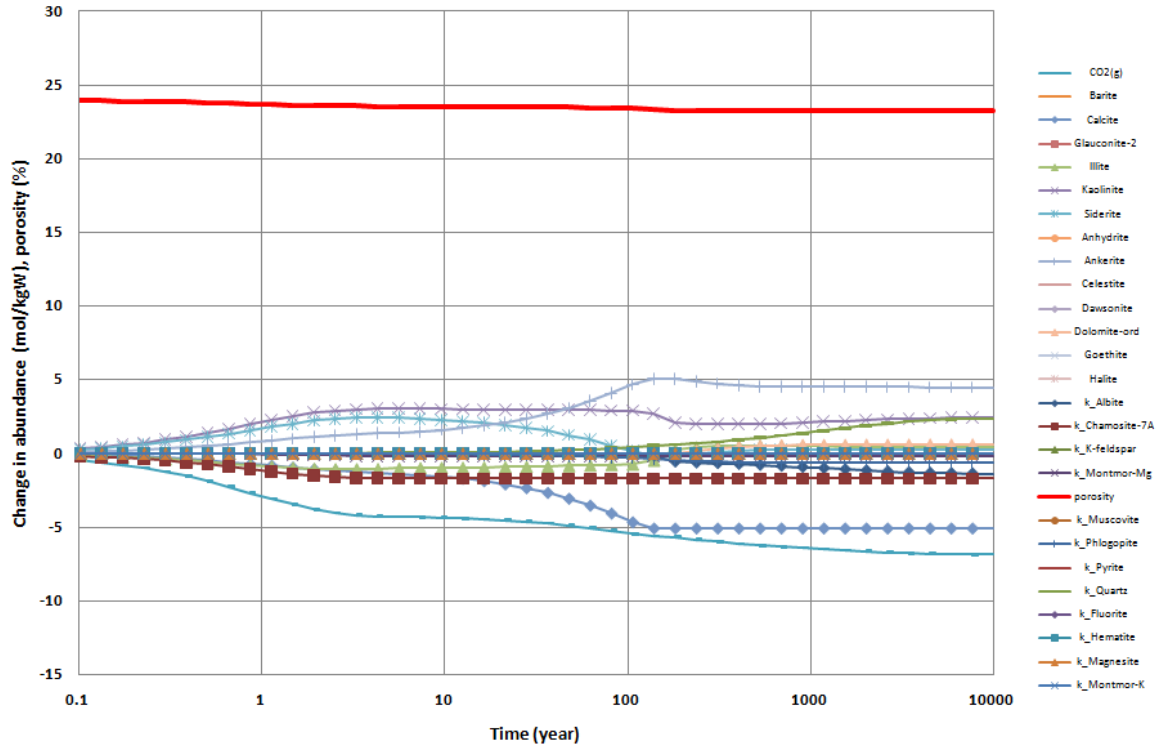

Figure 4-11: Mineralogical changes with no dawsonite precipitation allowed (Case 6 - full range of minerals).

Note: The amounts are expressed in mol/kgW. 1 mol/kgW corresponds to 118 mol/m^3 gross rock volume (for the assumed porosity, water saturation, brine density and TDS).

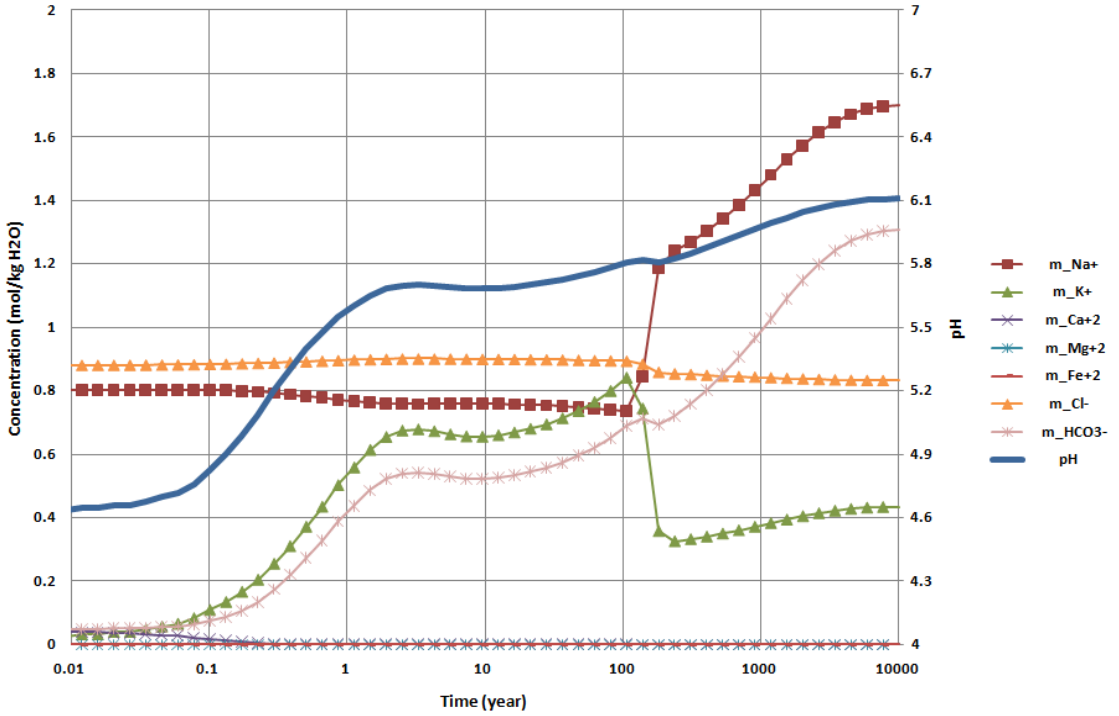

Figure 4-12: Composition evolution with no dawsonite precipitation allowed (Case 6 - full range of minerals)

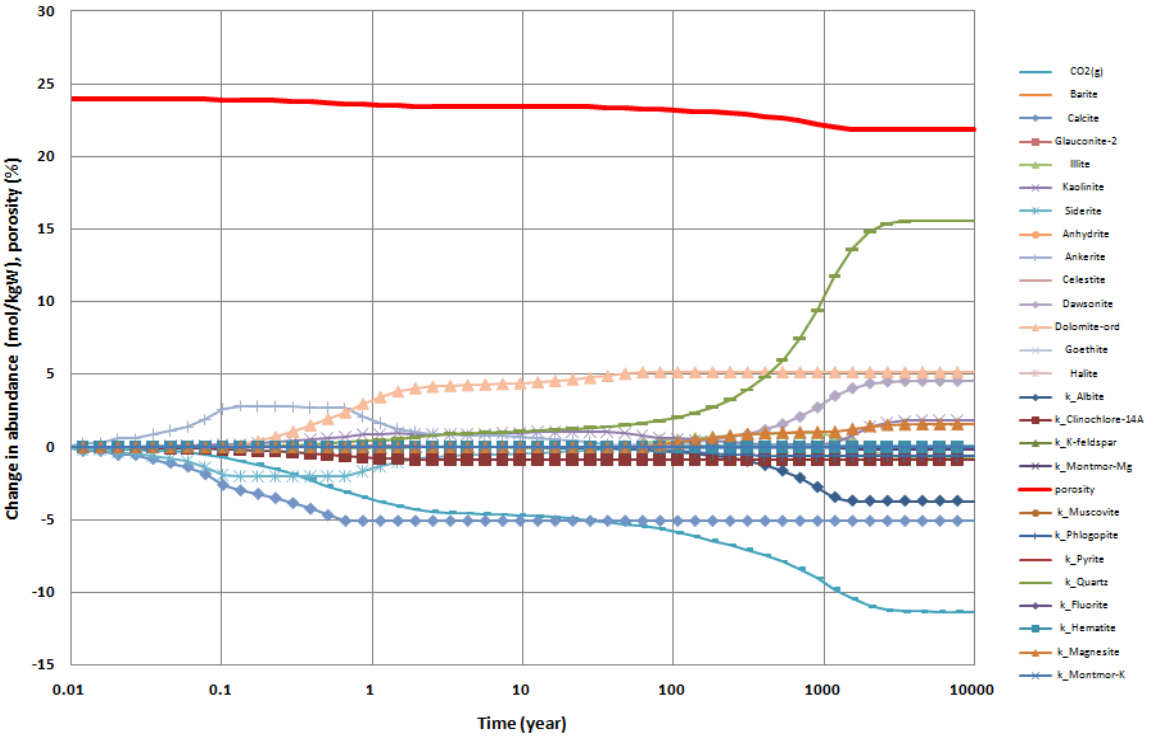

Figure 4-13: Mineralogical changes with clinochlore instead of chamosite (Case 7).

Note: The amounts are expressed in mol/kgW. 1 mol/kgW corresponds to 118 mol/m^3 gross rock volume (for the assumed porosity, water saturation, brine density and TDS).

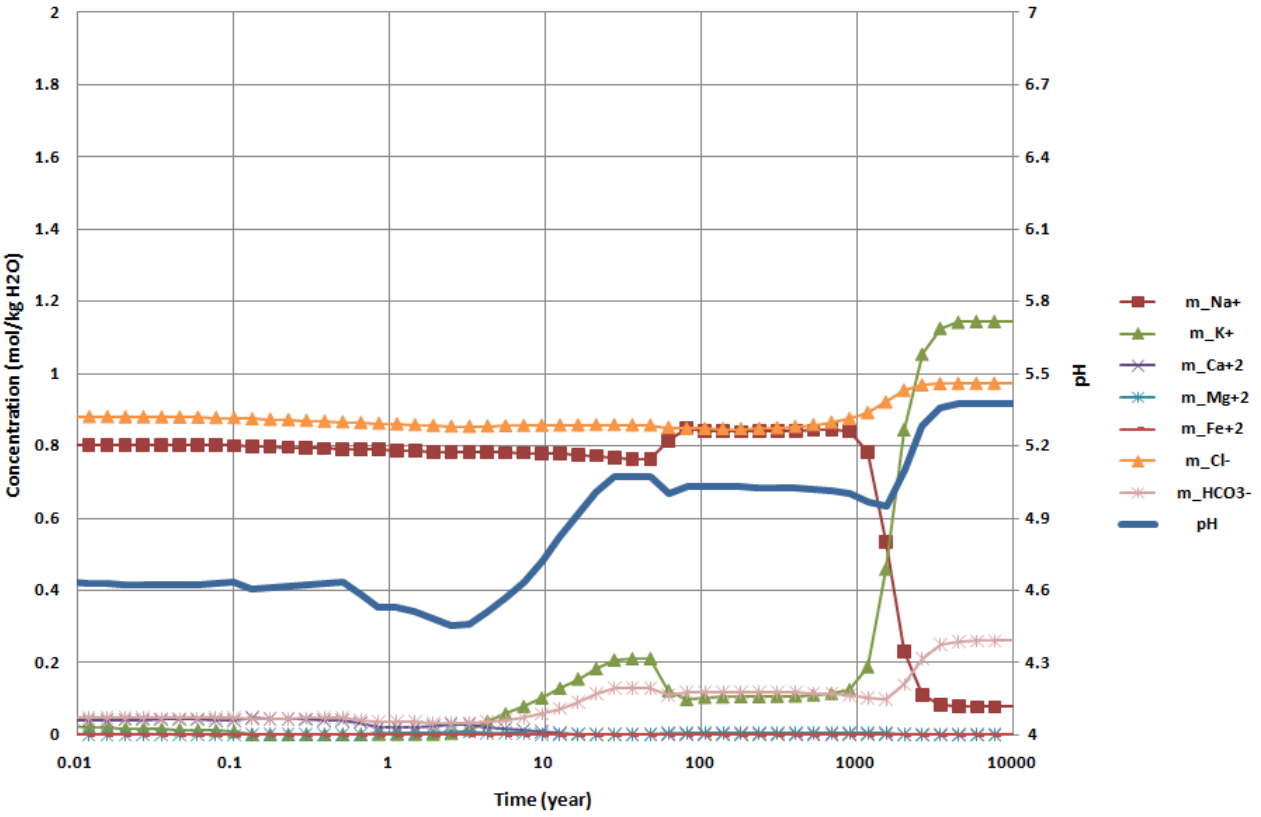

Figure 4-14: Composition evolution with clinochlore instead of chamosite (Case 7).

4.2. Spatial transport effects

A simple 2D geometry was used to investigate the transport effects on the geochemical reactions. The 2D box model represents a slice through the Goldeneye reservoir, rather than a radial model as used in similar reactive transport modelling by Audigane et al. on Sleipner (18). Although the 2D slice is less suitable for studying near wellbore effects, it allows a more representative representation of the reservoir, with a dip angle (2.25 degrees), a crestal structure and an aquifer leg. Also it is more suitable for modelling post-injection gravitational convective mixing (see e.g. Riaz et al (19)) arising from brine density differences, since unlike in a radial model the spatial grid resolution is the same throughout the model (both near wellbore and further away). The 3D version of the box model, referred to as the *Anatis simplified structure model*, has been used for other Goldeneye modelling work as well (during initial phases of the CCS study work, as well as for studying e.g. thermal effects (15)). For the reactive transport modelling the grid resolution along the dip direction was increased in order to better represent the convective mixing. As can be observed in the various figures presented in this section, with the selected grid resolution the convective fingers that develop have a width of approximately one grid cell, suggesting that the grid resolution may be too coarse. However a finer grid simulation (not presented in this report) showed similar spacing between convection fingers, and nearly identical amounts of CO_2 dissolved through time. Therefore the selected grid resolution is considered sufficient. Furthermore a 3D model was run (not presented in this report) to analyse the effect on the convective patterns of reducing from three to two spatial dimensions. It was found that a 2D slice through the 3D model shows a similar convective pattern as observed in the 2D model. CO_2 dissolution rates through time in the 3D model are nearly the same as in the 2D model. This justifies using the 2D model instead of the 3D model.

The model is a 3-phase EOS model (gas and oil phases having CO_2 and hydrocarbon components), with the CO_2 behaviour within the hydrocarbon phase (notably calculation of the fugacity) handled by the internal MoReS EOS model (extended with Henry's law to model CO_2 solubility in the brine). The brine chemistry and mineral interaction are modelled by coupling to PHREEQC (using the CO_2 fugacity calculated from the EOS). The model initialises from the pre-production state, and simulates the production phase, a shut-in period, then the CO_2 injection period (10 years), and finally a post injection period for 600 to 10,000 years post injection. The CO_2 injection period and post injection period were simulated under three different modelling assumptions:

1. No geochemistry, i.e. only taking into account the CO_2 solubility in the brine. Since from natural analogue isotope analysis it has been argued that there is very little CO_2 mineralisation (20), this non-reactivity assumption, although an extreme case, might be a possibility (no mineral trapping within 1000s of years). This model was simulated for 10,000 years, and was used to investigate grid resolution effects to ensure that the grid used is fine enough and that the 2D approximation still gives a reasonable approximation of the convective flow.
2. Geochemistry with kinetics, as in the simplified model (reduced number of primary minerals) in the previous section. This model was simulated for 600 years post injection. With the kinetics as used in the base model (i.e. the fast kinetics) all early (calcite) reactions should have occurred at this stage, and the late (albite) reactions should be well underway. For this reason the model was not run with the slow kinetic assumptions (which from the batch modelling would require a > 10000 year simulation to reach geochemical stability), but this case can be seen as an intermediate case between the fast kinetics case and the no geochemistry case.
3. Geochemistry with all minerals assumed in instantaneous equilibrium. Although this is an unrealistic assumption it makes the model run much faster and still gives insights in some of the coupled chemistry-transport mechanisms, as well as in the final chemical equilibrium state. However this case is mostly of academic interest, and is not described further in this report.

Figure 4-15 shows the saturation through time in the non-reactive Anatis model. 20 years post cessation of injection the gas water contact has stabilised (due to the excellent permeability), after that there are very limited changes in the saturations. There is a small amount of gas cap shrinkage due to continued CO_2 dissolution in the brine. This is also reflected in the average field pressure plot in Figure 4-16. It should be remarked that the Anatis model was only qualitatively history matched to the field production pressure history (15). Quantitatively the pressures are too low, due to a too weak aquifer in the model.

In the Anatis model the well perforations are below top reservoir, therefore initially the CO_2 moves up vertically in a 'chimney'. Compared to the 3D model during injection the CO_2 plume from the injector upwards is too narrow, because there is too much pore volume available close to the wellbore (for the amount of CO_2 injected in the 2D cross-section model). However further away from the injector the saturation profile is close to the 3D one, and post injection the gas saturations are nearly the same. Figure 4-17 shows the mass fraction of dissolved CO_2 through time. This continues evolving beyond the 20 years post injection due to convective flow in the water leg. Approximately 300 years post shut-in the convective fingers hit base reservoir, after which a very slowly moving increased density tongue along the base reservoir develops. Even after 10,000 years the tip of this tongue is only 3 km away from the original hydrocarbon water contact. The total CO_2 dissolution after 10,000 years is 14% of the total amount of CO_2 injected, i.e. 86% is still in the gas phase. This is in contrast with the Sleipner modelling (18) where all CO_2 is dissolved after 6,000 years. This is mainly due to the fact that Goldeneye, unlike Sleipner, has a structural trap leading to a significant difference in the thickness of the gas phase (100 m in the Anatis model versus 10 m in the Sleipner

model). Moreover in Goldeneye the original oil (condensate) rim spreads out vertically due to the hydrocarbon production followed by CO_2 injection. In this rim the total fluid mobility is reduced and therefore it acts as a baffle for the convective flow. The other convective dissolution parameters (such as vertical permeability and density differences) are similar between Sleipner and Goldeneye.

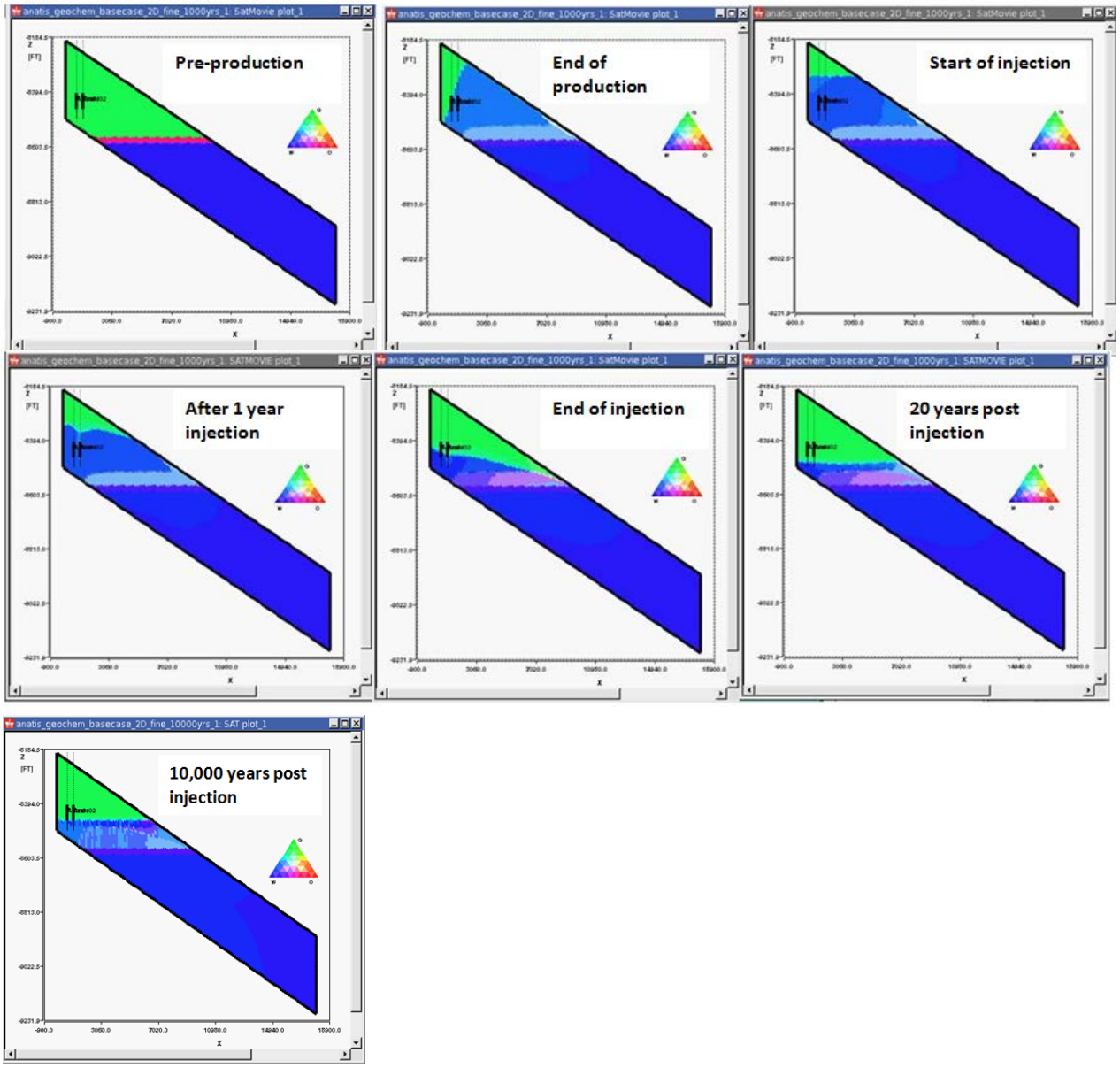

Figure 4-15: Saturation through time in the 2D Anatis model.

Note: No geochemical reaction case. Ternary colour scale with endpoints red (100% oil), blue (100% water) and green (100% gas).

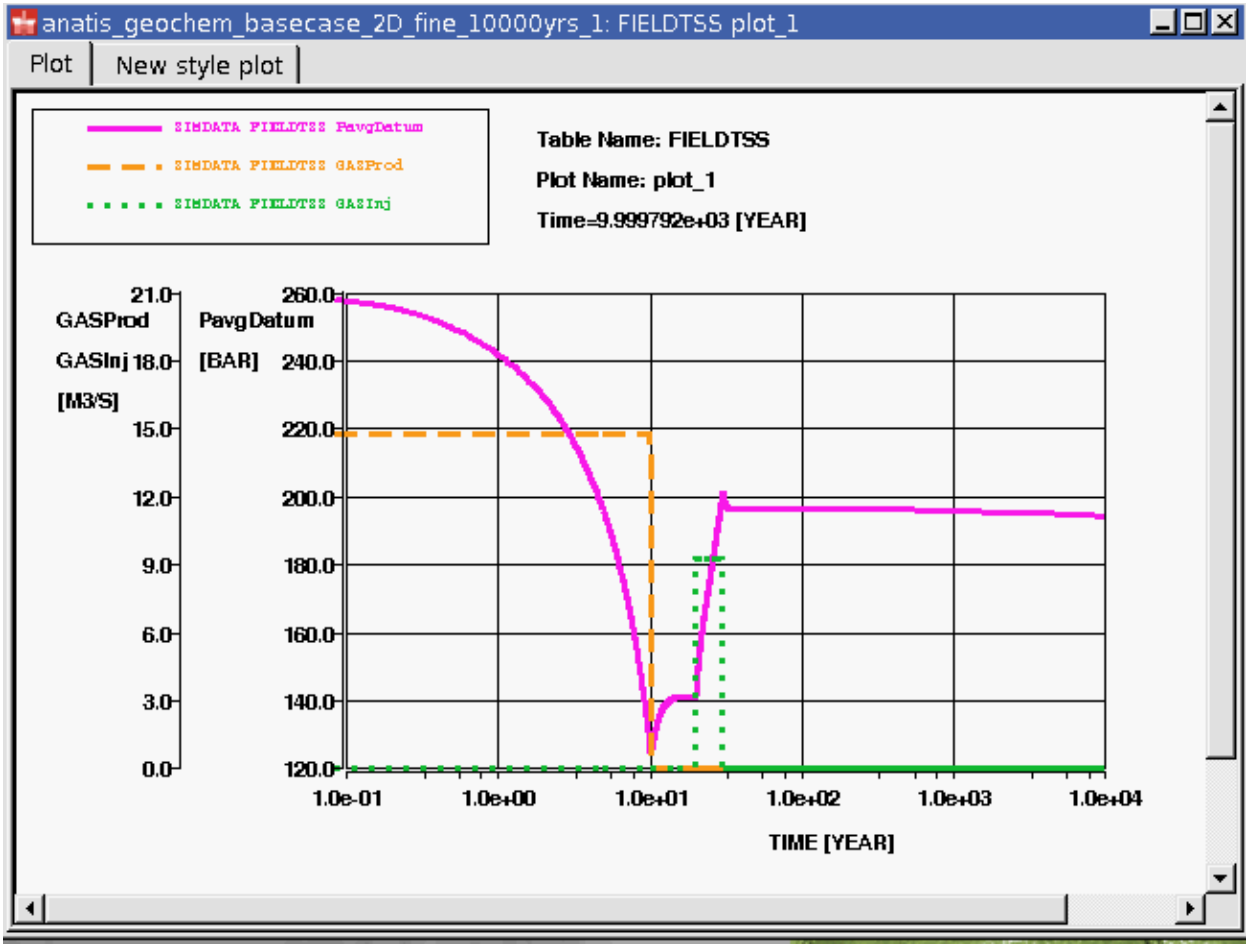

Figure 4-16: Average field pressure through time

Note: Average field pressure through time (purple line), responding to production (orange dashed line), CO_2 injection (green dotted line) and CO_2 dissolution during the post-injection period. No geochemical reaction case.

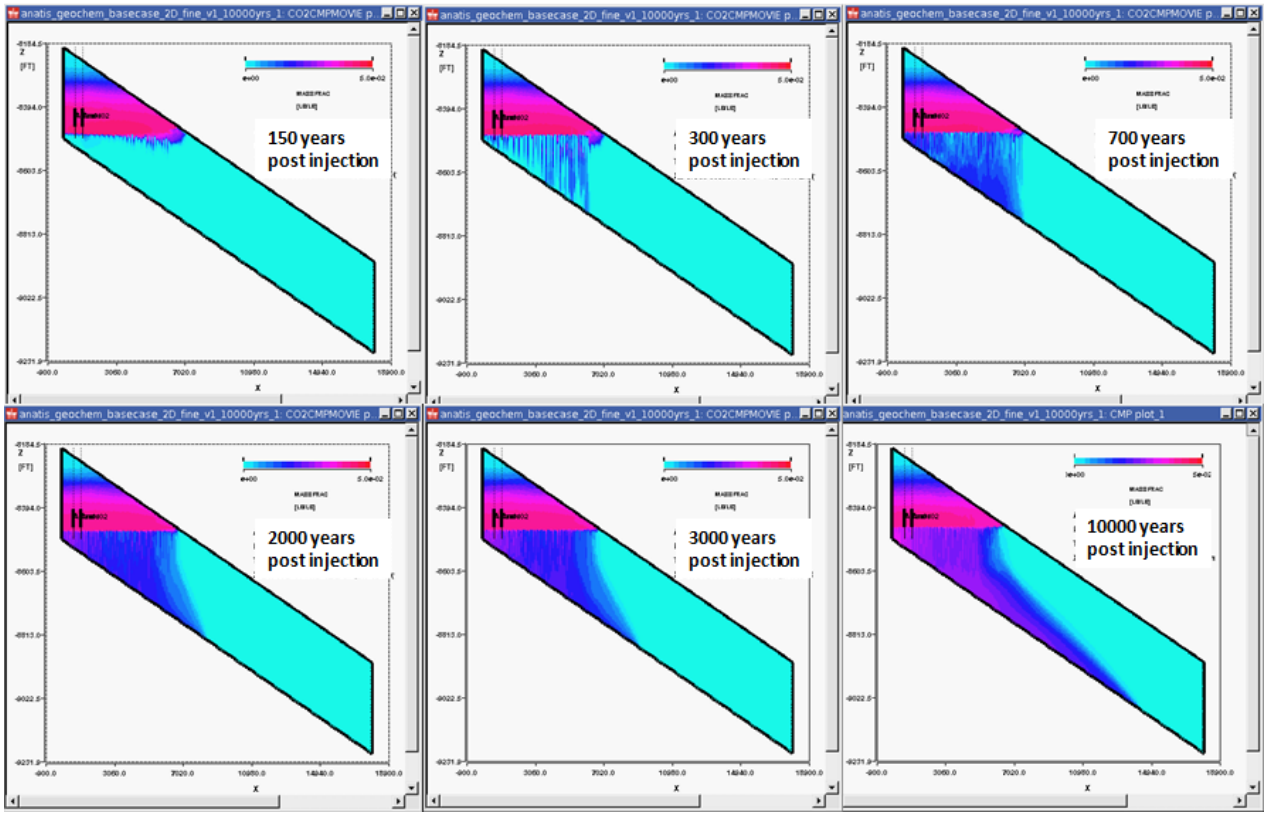

Figure 4-17: Dissolved CO_2 through time. No geochemical reaction case. Colour scale runs from 0 to 0.05.

The results with geochemistry (PHREEQC coupling) switched on are presented in Figure 4-18 through Figure 4-33.

Figure 4-18 shows that the gas cap shrinks over time post-injection. This is largely due to the geochemical reactions (300 years post-injection the gas water contact is shallower than in the model with only CO_2 dissolution i.e. without geochemical reactions, Figure 4-15). This is also reflected in the field pressure (Figure 4-19), where the post-injection pressures are lower than in the case without geochemical reactions (Figure 4-16). In the Anatis model the aquifer is weak, and it does not respond quickly enough to compensate for the pressure reduction due to the gas cap shrinkage.

The CO_2 fraction in the gas and water phase over time is given in Figure 4-20. It can be seen that a distinct compositional grading builds up in the gas cap post injection. This is primarily due to the CO_2 being injected low in the gas cap, followed by gravity stabilisation post-injection (the model without geochemical reactions shows a similar grading in the gas cap). This grading is reflected in the water composition in the gas cap (since the CO_2 fraction in the gas determines the CO_2 fugacity). Below the gas water contact fingers develop similar to the unreactive Anatis model, however these are not so clearly visible in the CO_2 fraction in the brine, because CO_2 is consumed within the fingers while the CO_2 source is at the top, therefore the CO_2 concentration decreases downwards in the fingers.

Figure 4-21 shows the pH through time. The pH is lowered (with respect to the original Goldeneye pH) in the gas cap and the brine fingers with increased CO_2 concentration. This is as expected. What is more interesting is that higher up in the gas cap the pH starts to increase after some time. This is caused by the CO_2 composition in this part of the gas cap going down (due to CO_2 consumption deeper in the gas cap), so that the brine gets out of equilibrium with respect to the carbonate minerals. The equilibrium is restored by a slight dissolution of the carbonate minerals. In this process H^+ is consumed, so the pH goes up. It should be noted that diffusive processes were not

incorporated in the Anatis models. With diffusion there will be a better vertical mixing between the hydrocarbon components and the CO_2 in the gas cap, and the effect of rising pH in this part of the gas cap will largely disappear.

The total dissolved solids (TDS, including bicarbonate) through time is presented in Figure 4-22. As in the batch model, within the gas plume the geochemical reactions (especially the 'early' one) lead to increased TDS. In Figure 4-23 this is split out over the main elements (master species) at the end of the simulation, from which it is clear that (as in the batch simulation) mainly K^+ and HCO_3^- cause the increased TDS. What is also clear in Figure 4-22 is that the increased TDS brine flows down in a convective process, and that the front of the fingers, as visible in the total salinity (and K^+), moves ahead of the CO_2 dissolution (Figure 4-20). In fact, the density difference is now dominated by the increased TDS rather than the dissolved CO_2, and the density difference is larger than in the model without geochemistry leading to the fingers reaching the base reservoir quicker than in the unreactive model (as can be seen by comparing Figure 4-17 and Figure 4-22). In the reactive model the brine that reaches the base reservoir and then flows along the base has increased TDS but with a pH similar to the original formation brine (since the carbonic acid has been spent). As a last comment on Figure 4-23, the increased Chlorine concentration at the gas water contact is not fully understood and might be a numerical artefact in the coupling due to a very local mixing at this contact (convective flow supplying fresh reservoir brine contacting the CO_2 rich region).

Figure 4-24 through to Figure 4-29 show the mineral evolution through time. Close to the gas water contact the speed of reactions is quicker than higher up in the gas cap due to the higher CO_2 concentrations in this area (Figure 4-20**)**. In this area the speed of the reactions is similar to that in the batch PHREEQC model. This can be verified by comparing Figure 4-29 and Figure 4-5. Higher up in the gas cap (and deeper down into the CO_2 rich brine fingers below the gas water contact) the reaction rate for all reactions is slower but the reaction path is still the same. Figure 4-28 shows the resulting porosity changes. Like in the batch PHREEQC model they are very small during the injection period, and post injection they build up to approximately -2% in the most reactive regions.

More detail on the convection is presented in Figure 4-30 through Figure 4-32. Figure 4-30 shows the phase densities at two snapshots in time. It should be noted that the gas phase density vertical trend is approximately reflected in the pressure trend (not shown), with the heaviest gas sitting at the base of the gas cap. However, at the gas water interface there is a sink of CO_2 (dissolution and then mineralisation) due to the convective flow in the water leg. Also CO_2 consumption in the gas cap itself is strongest at the base due to the highest CO_2 fugacities in that location (at least until the reactions higher up in the gas cap also kick off significantly). As a consequence CO_2 is consumed most strongly towards the base of the gas cap, making the gas lighter and thus creating a gravitational instability in the gas cap. On top of this CO_2 consumption will also lead to a local reduction in pressure, pulling gas volume towards it. The resulting convective flow patterns (at end of simulation) are shown in Figure 4-31, both in the water and in the gas. The water flow pattern highlights the well-known convection cells due to the water density contrast at the gas water contact. The gas convective pattern is much more complex than the water convective pattern because the CO_2 consumption process happens throughout the gas cap but at different rates. At the top of the gas cap there is a single clockwise convection pattern, presumably as a result of two processes: 1) the (unreactive) hydrocarbon gas at the top of the gas cap expanding due to the dropping field pressure, leading to overall a downward transport; 2) flow upwards (on the left) of relatively light gas due to CO_2 consumption further down in the gas cap and at the gas water contact. In Figure 4-32 the CO_2 mass flux (for water and gas phase combined) is presented. Note that the convergence/divergence of the mass flux can be either due to compressional effects or due to mineralisation (or dissolution). Again, it should be noted that diffusion has not been taken into account in the simulations, and a model with diffusion switched on probably has different convective patterns in the gas cap.

It should be stressed that for nearly every cell the reaction path in the Anatis model is the same as in the batch model, only the extent of the reaction path followed depends on the location of the grid cell with respect to the injected CO_2. Also the timescale of the reactions is similar to the timescale in the batch model (but somewhat slower in most of the gas plume due to reduced CO_2 concentrations). There seems to be only one exception: higher up in the gas cap, where the CO_2 concentration in the gas first increases and then decreases, eventually the pH goes up to values somewhat above initial Goldeneye pH.

The CO_2 fugacity (Figure 4-33) decreases somewhat over time within the gas plume. The reason is the reducing CO_2 composition in the gas phase as well as the reducing system pressure. The absolute value of the fugacity in the Anatis model, and also the gas density, is too low due to a too low pressure in the Anatis model at the start of injection (too weak aquifer). Therefore also the pressure trend post injection and impact on fugacity and gas density may be too strong in the model.

The CO_2 mineralisation in the Anatis reactive model is large, 59% at the end of simulation (amount of dissolved CO_2 is 2% at that stage). Once the 'late' reactions are completed (beyond the end of the simulation) this will be even larger, the upper limit coming from the simulations where instantaneous equilibrium is assumed (not presented in this report) which give a 76% mineralisation. This is high compared to the 39% in the batch PHREEQC model (run at 20% water saturation), the primary explanation being that the gas density in the Anatis model (Figure 4-30) is lower than what was assumed in the batch calculation (0.65 g/cm^3) so that there is less CO_2 mass in the system per rock volume. It illustrates that the predicted amount of CO_2 sequestration in the model is strongly dependent on the field pressure evolution and the amount of mixing with the hydrocarbon gas. It should be stressed once more that the model is geared towards high reactivity. Discount factors on the amount of mineralisation are covered in the Discussion section.

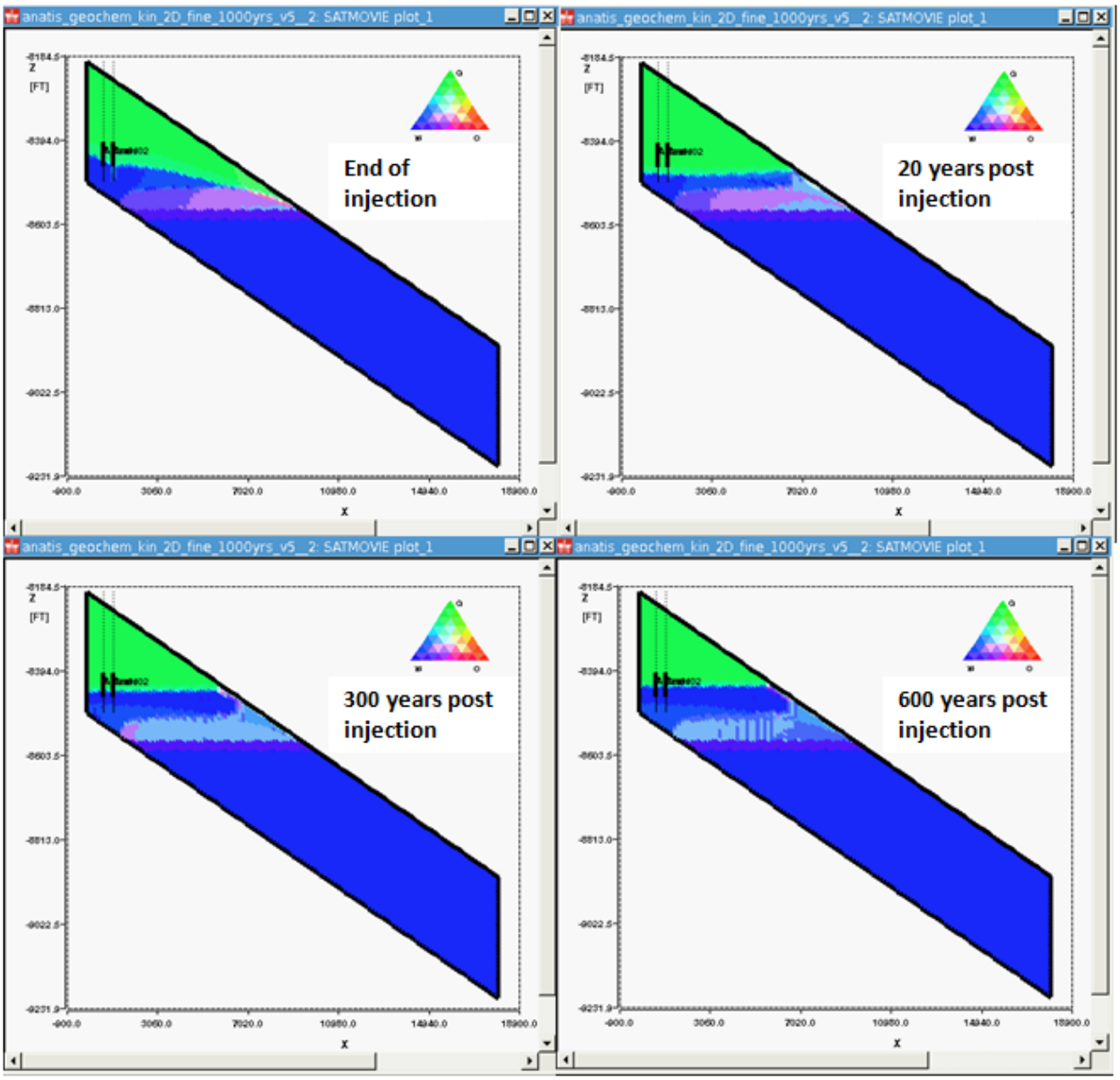

Figure 4-18: Saturation through time in the reactive Anatis model.

Note: Ternary colour scale with endpoints red (100% oil), blue (100% water) and green (100% gas).

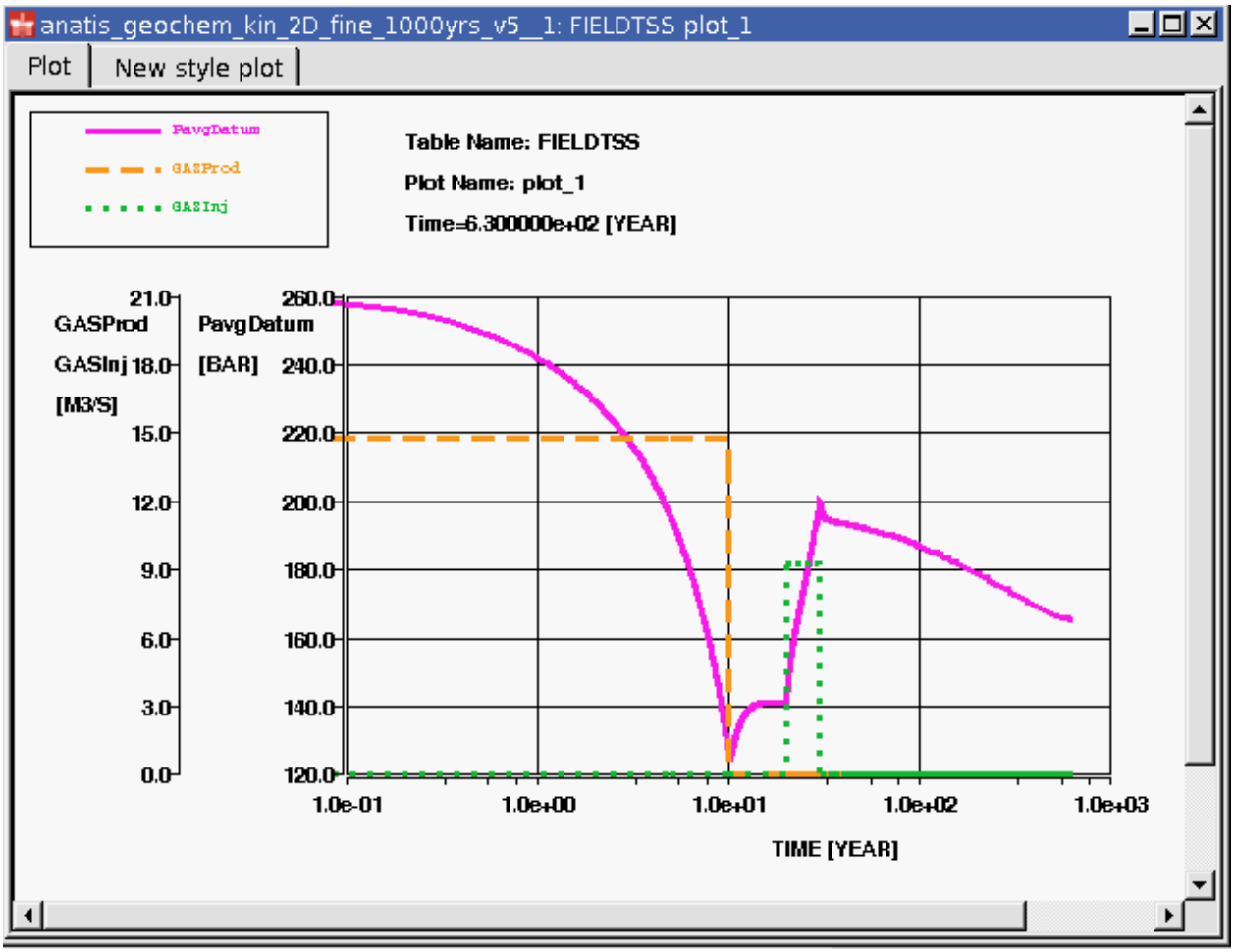

Figure 4-19: Average field pressure through time

Note: Average field pressure through time (purple line), responding to production (orange dashed line), CO_2 injection (green dotted line) and CO_2 dissolution and mineralisation during the post-injection period.

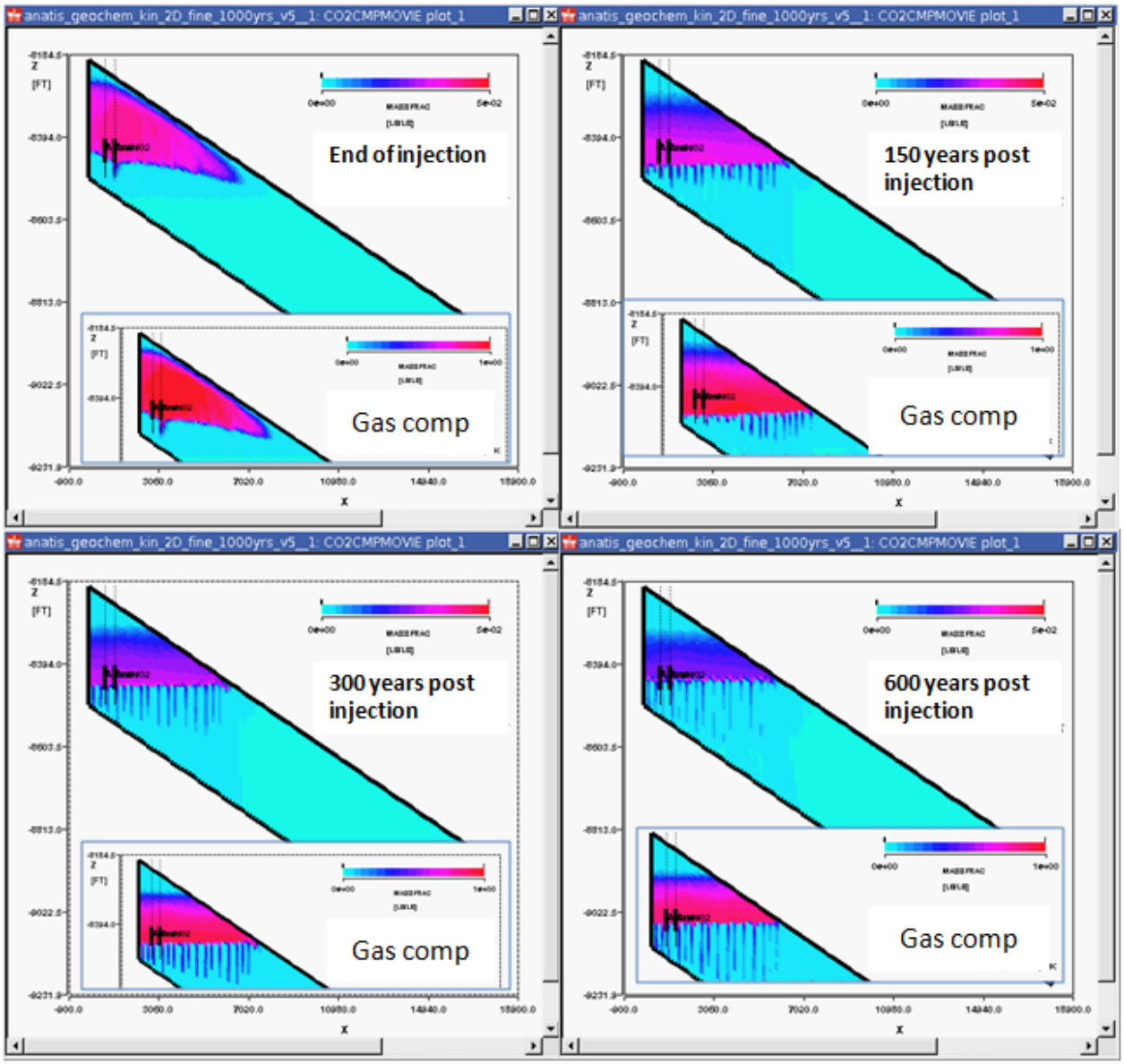

Figure 4-20: CO_2 composition through time, in water phase and (insert) in gas phase.

Note: The colour bar runs from 0 in to 0.05 in the water phase plots, and from 0 in to 1 in the gas phase plots. Note that the gas phase plots are truncated at the position of the original oil water contact, below which the gas saturation is zero and the gas composition is undefined. Above the original oil water contact there is a residual gas saturation and therefore the gas composition is defined.

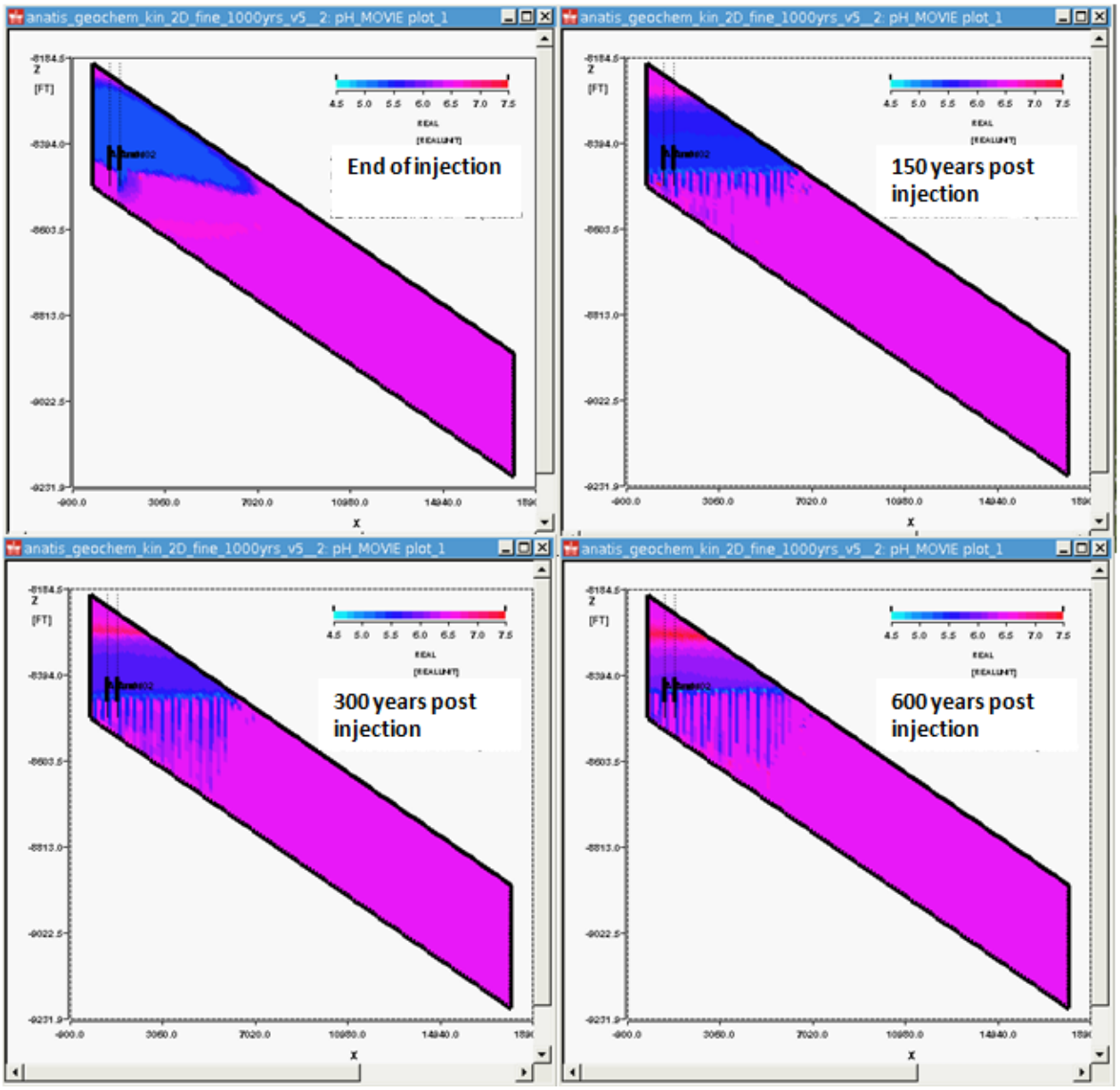

Figure 4-21: pH evolution through time. Colour scale runs from 4.0 to 7.5.

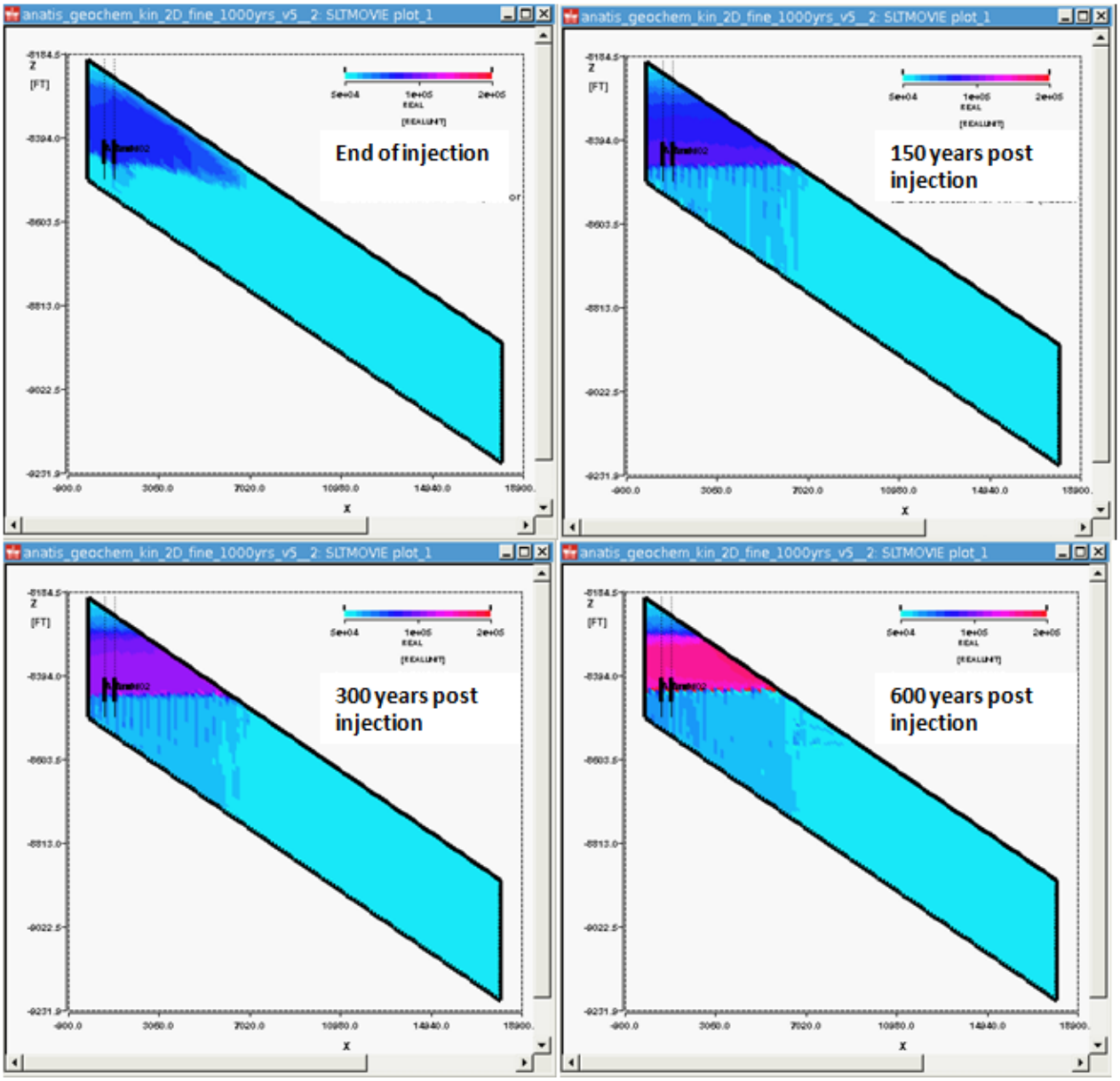

Figure 4-22: Brine total dissolved solids (TDS, including bicarbonate) evolution through time. Colour scale runs from 50,000 ppm to 150,000 ppm.

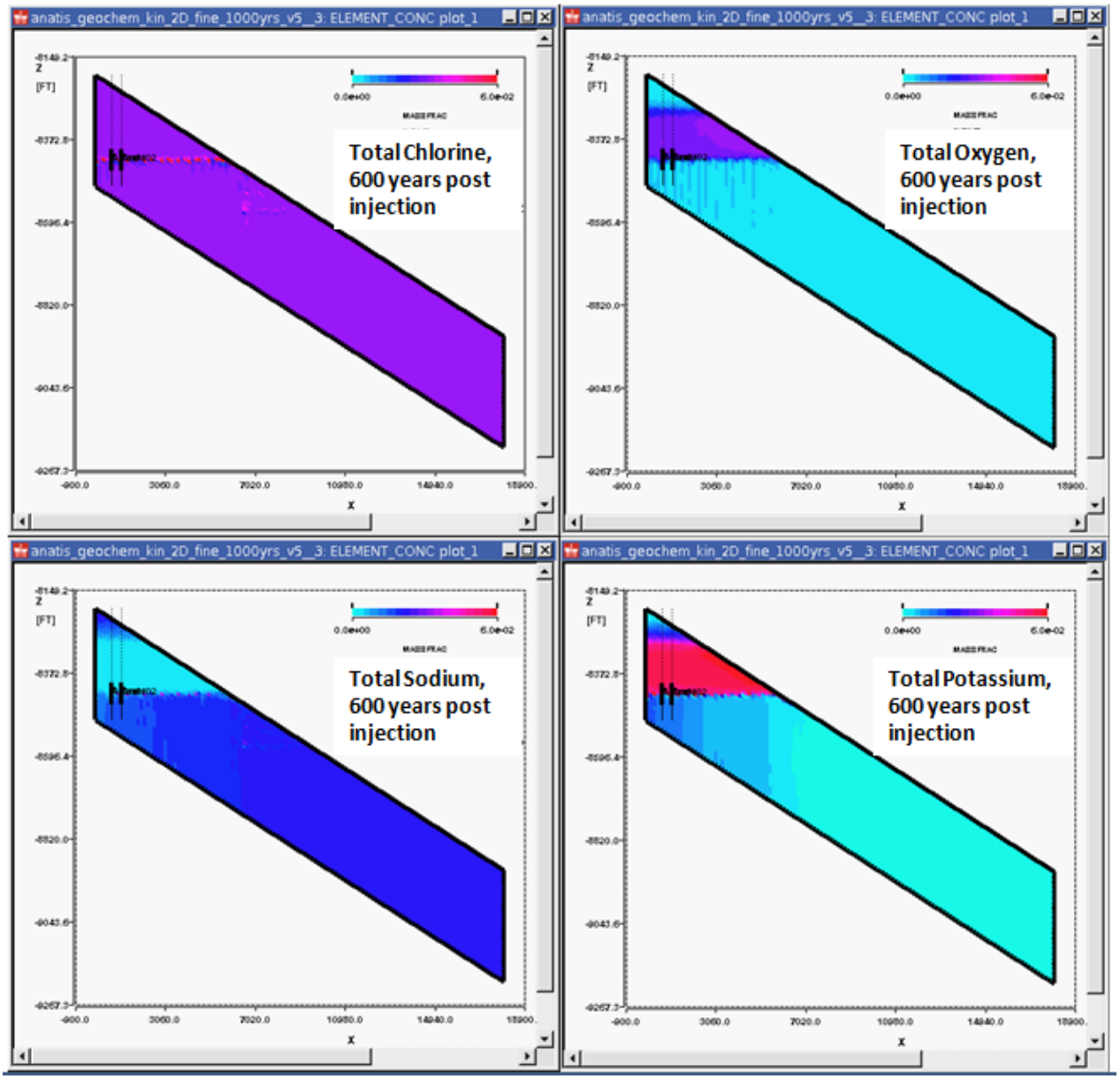

Figure 4-23: Main aqueous elements (master species) 600 years post injection (note Oxygen is part of bicarbonate). Colour scale runs from 0 mol/kgW to 0.05 mol/kgW.

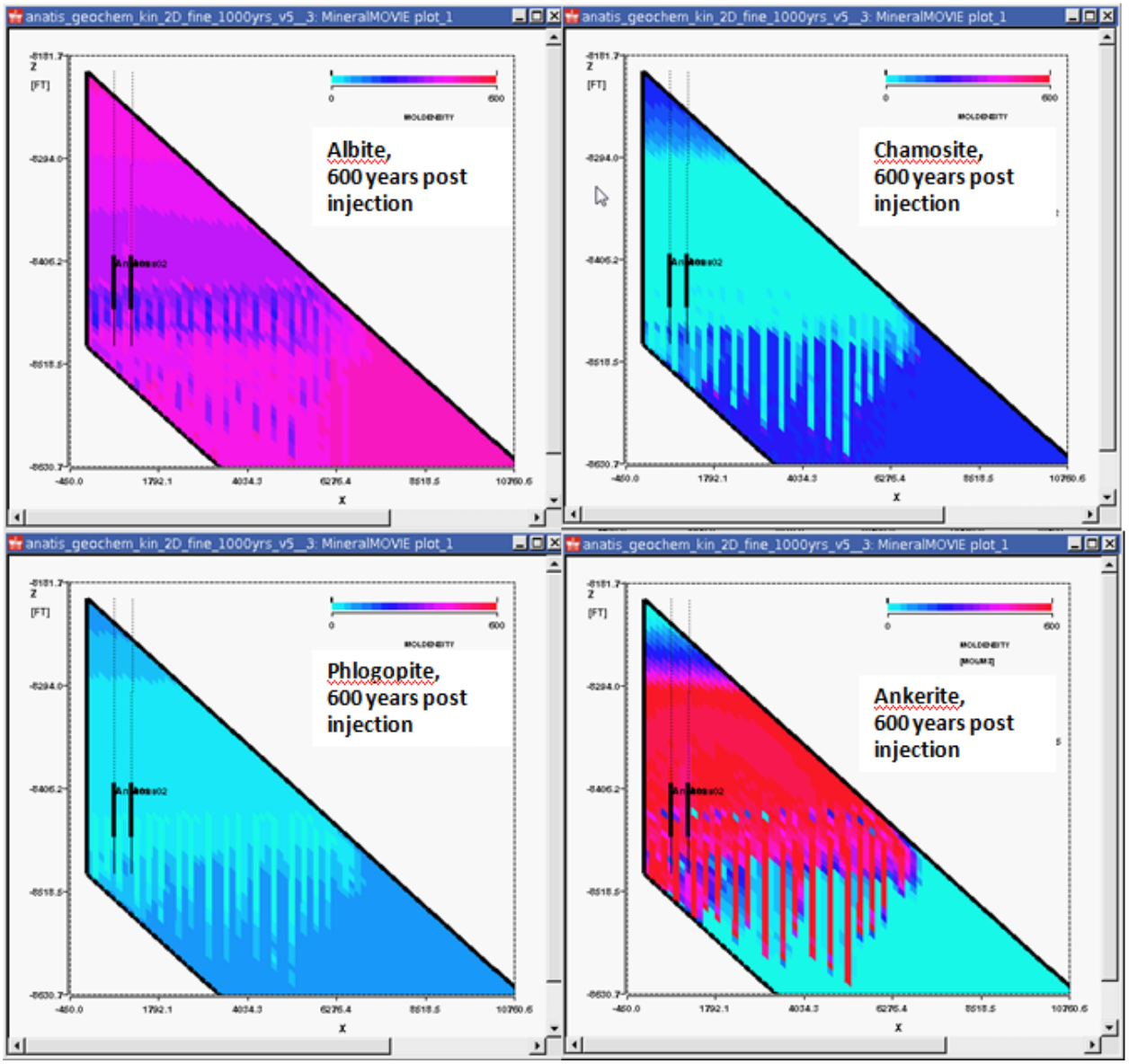

Figure 4-24: Mineral abundance 600 years post injection (albite, chamosite, phlogopite, ankerite). Colour scale runs from 0 mol/m³ to 600 mol/m³.

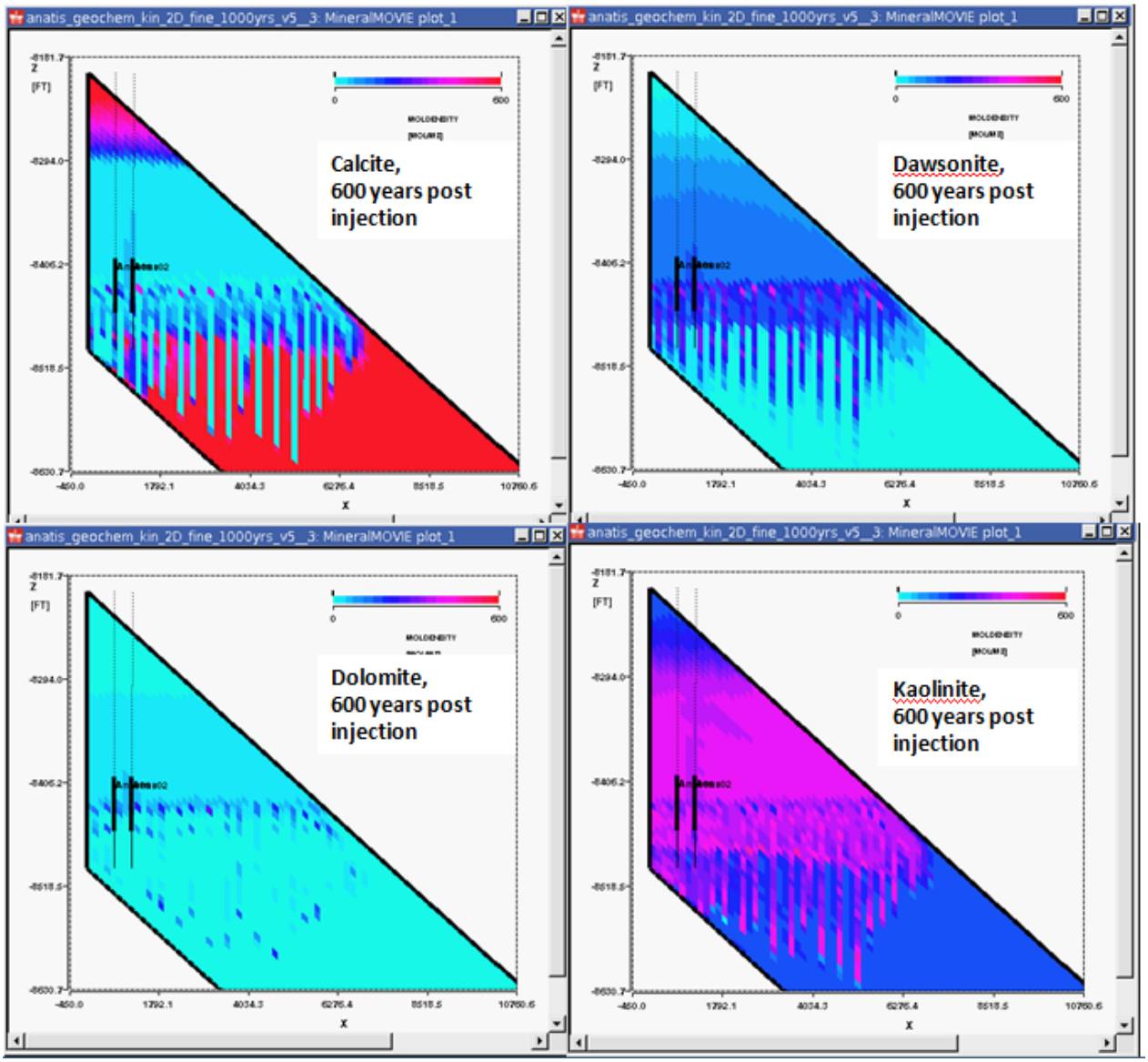

Figure 4-25: Mineral abundance 600 years post injection (calcite, dawsonite, dolomite, kaolinite). Colour scale runs from 0 mol/m³ to 600 mol/m³.

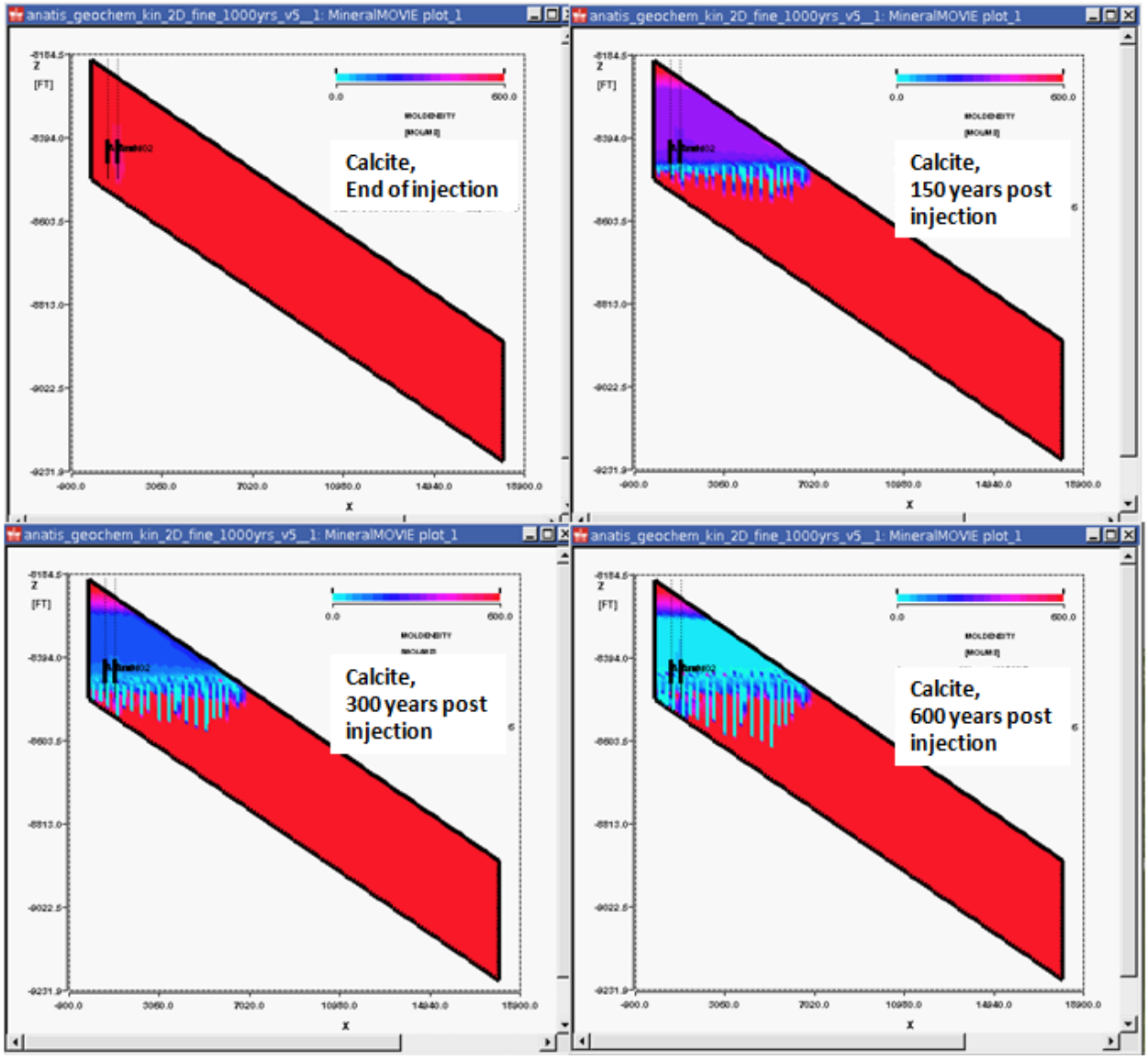

Figure 4-26: Calcite abundance evolution through time. Colour scale runs from 0 mol/m³ to 600 mol/m³.

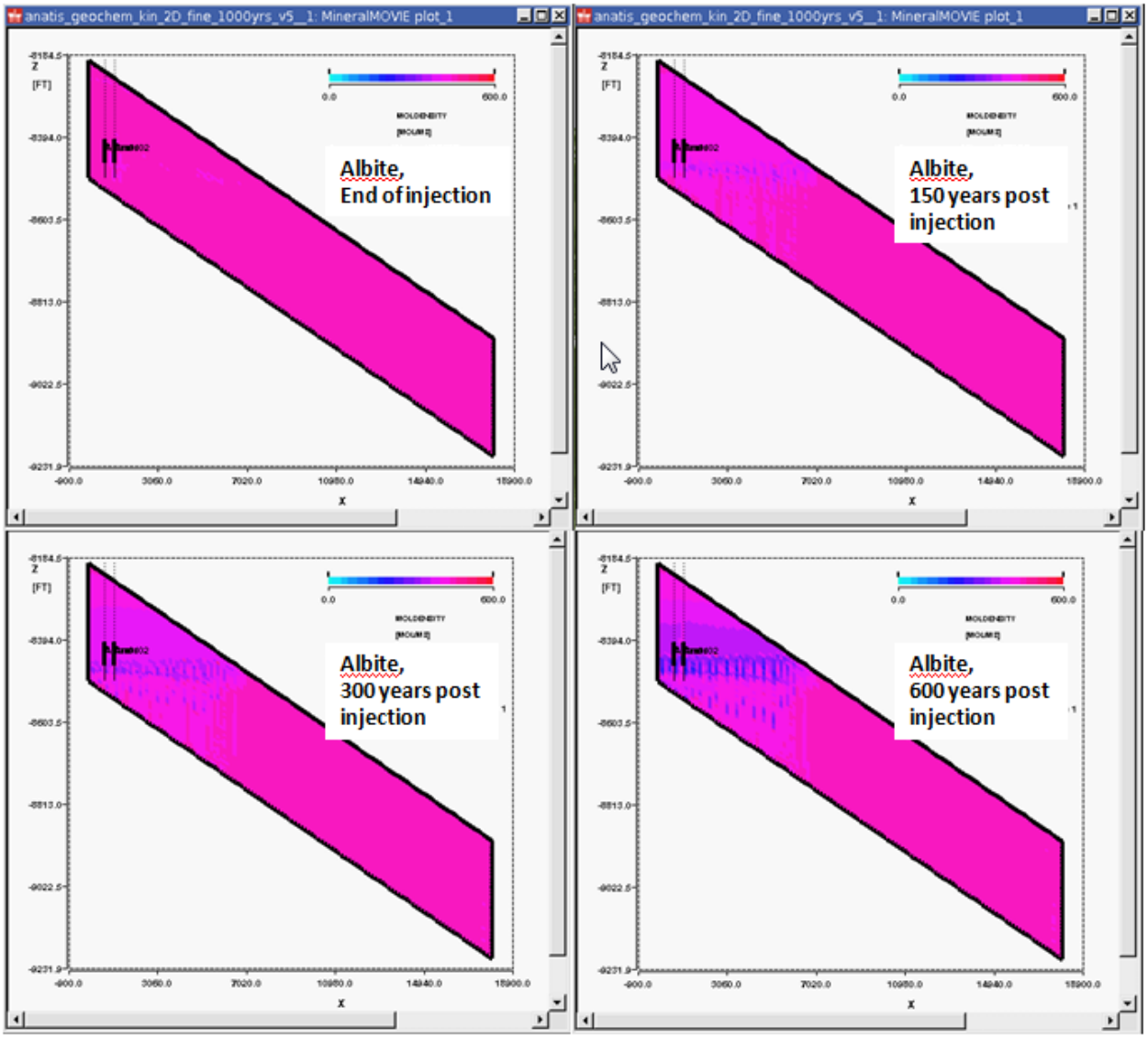

Figure 4-27: Albite abundance evolution through time. Colour scale runs from 0 mol/m³ to 600 mol/m³.

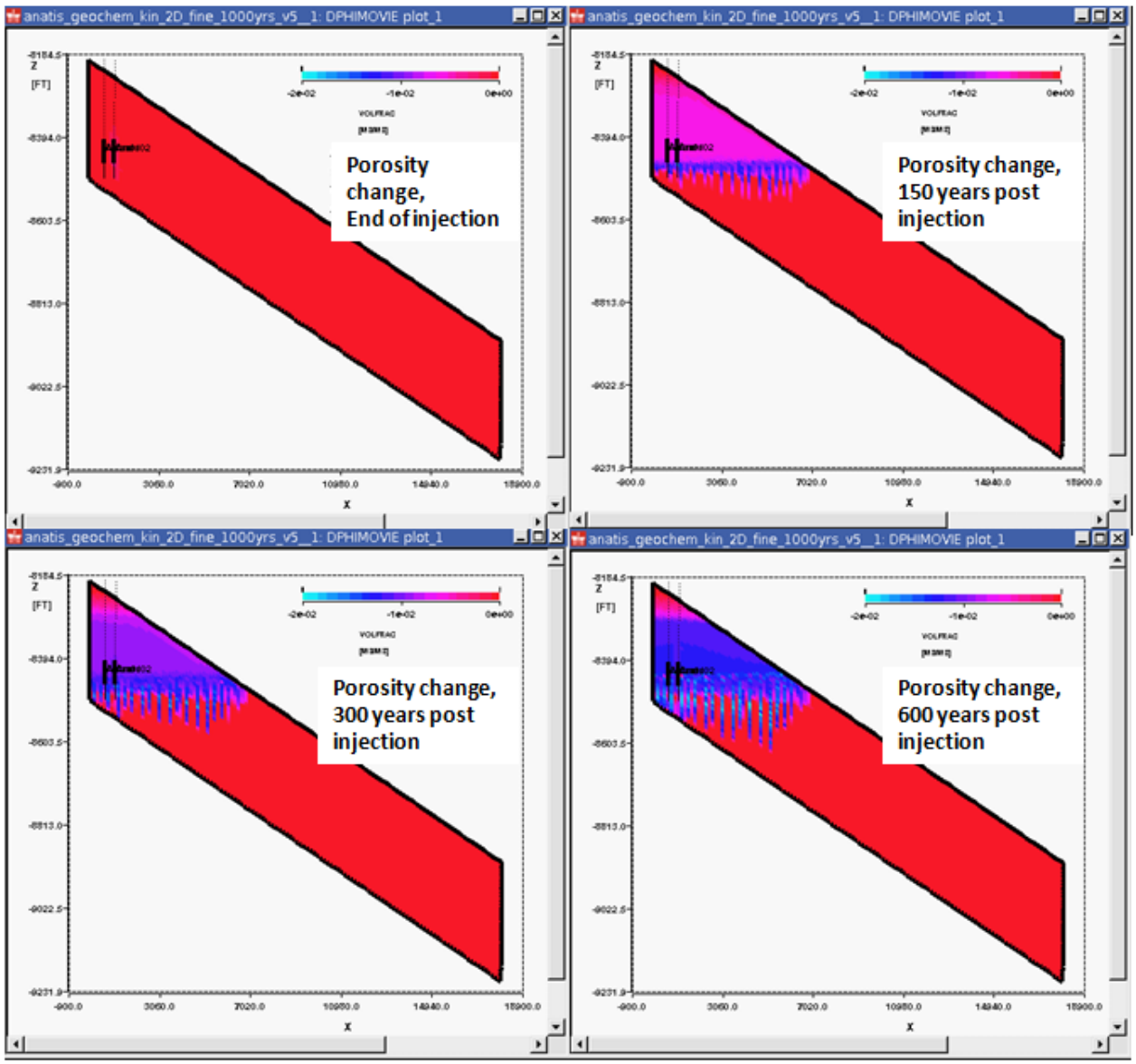

Figure 4-28: Porosity change through time. Colour scale runs from -0.02 to 0 (i.e. -2% to 0%).

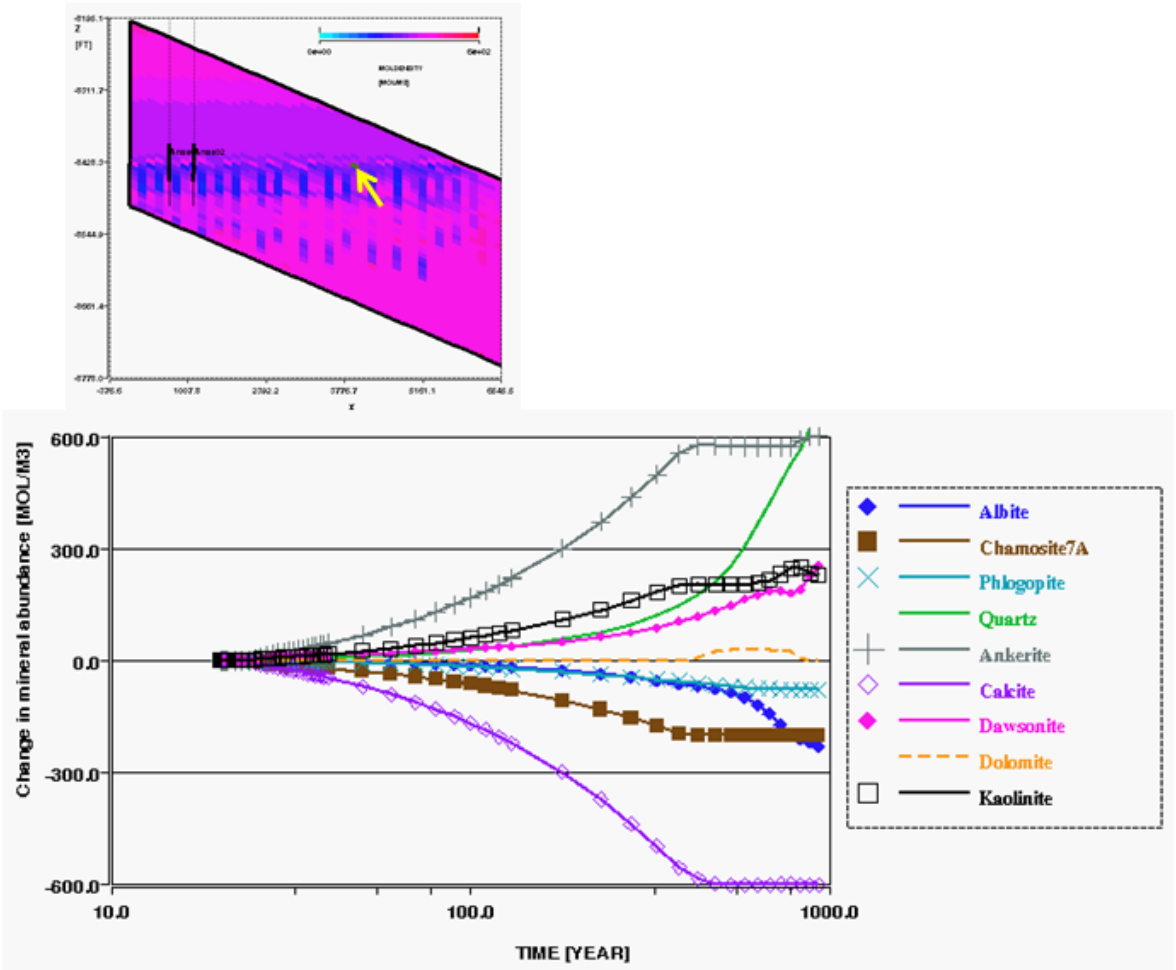

Figure 4-29: Mineral evolution in cell selected by yellow arrow

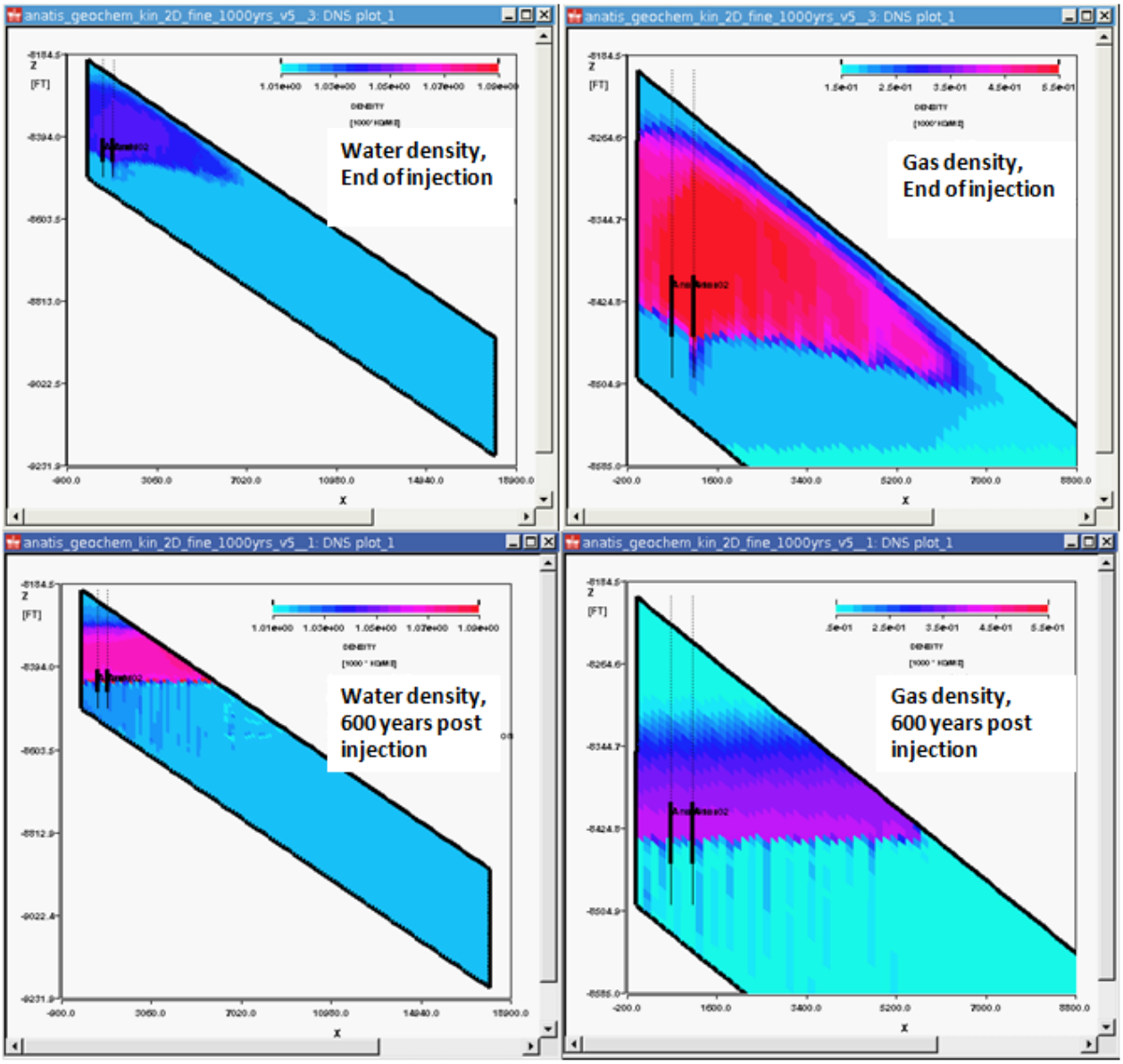

Figure 4-30: Phase densities at end of injection and 600 years post injection

Note: Colour scale runs from 1.01 g/cm^3 to 1.09 g/cm^3 for the water density and from 0.15 g/cm^3 to 0.55 g/cm^3 for the gas density.

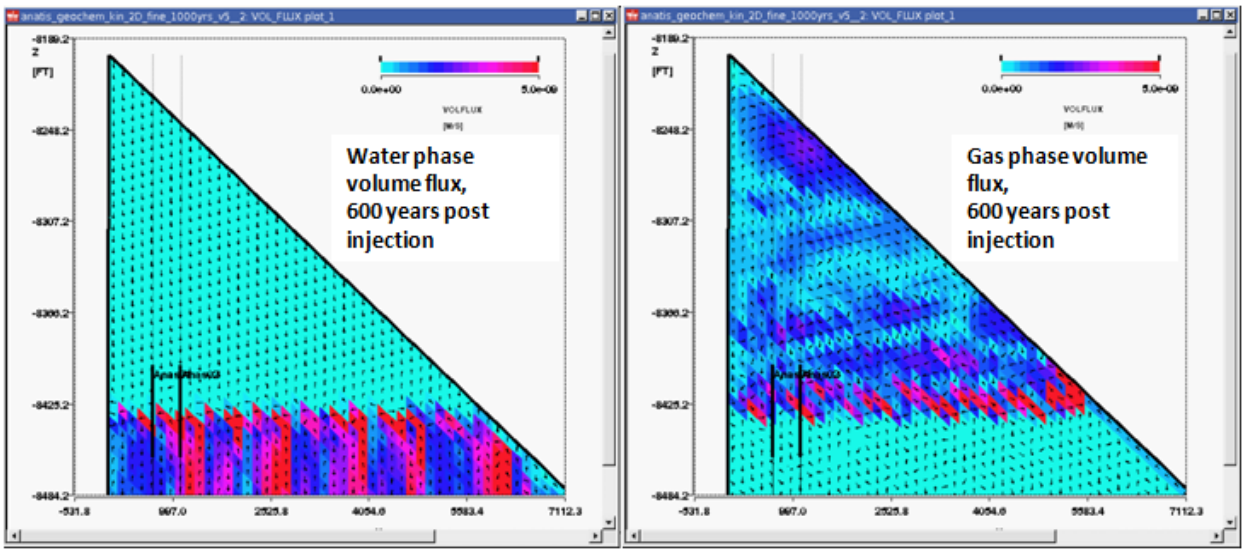

Figure 4-31: Phase volume fluxes 600 years post injection.

Note: Arrow indicates direction only, colour indicates magnitude. Colour scale runs from 0 m/s to 5e-9 m/s.

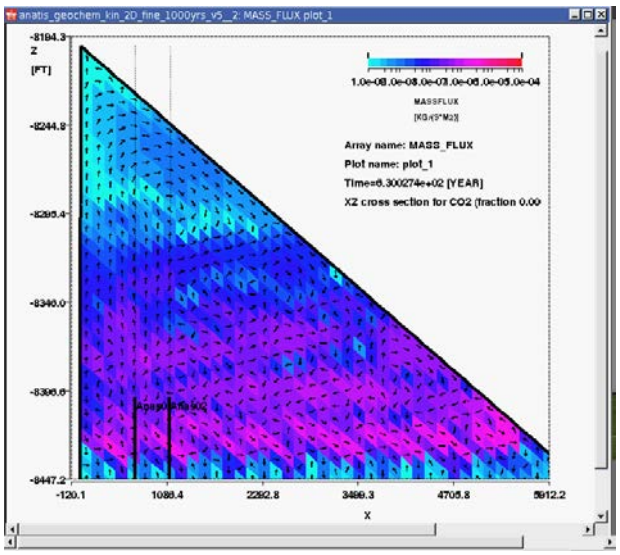

Figure 4-32: CO_2 mass flux 600 years post injection.

Note: Arrow indicates direction only, colour indicates magnitude. Colour scale (logarithmic) runs from 1e-9 kg/(m²s) to 1e-4 kg/(m²s).

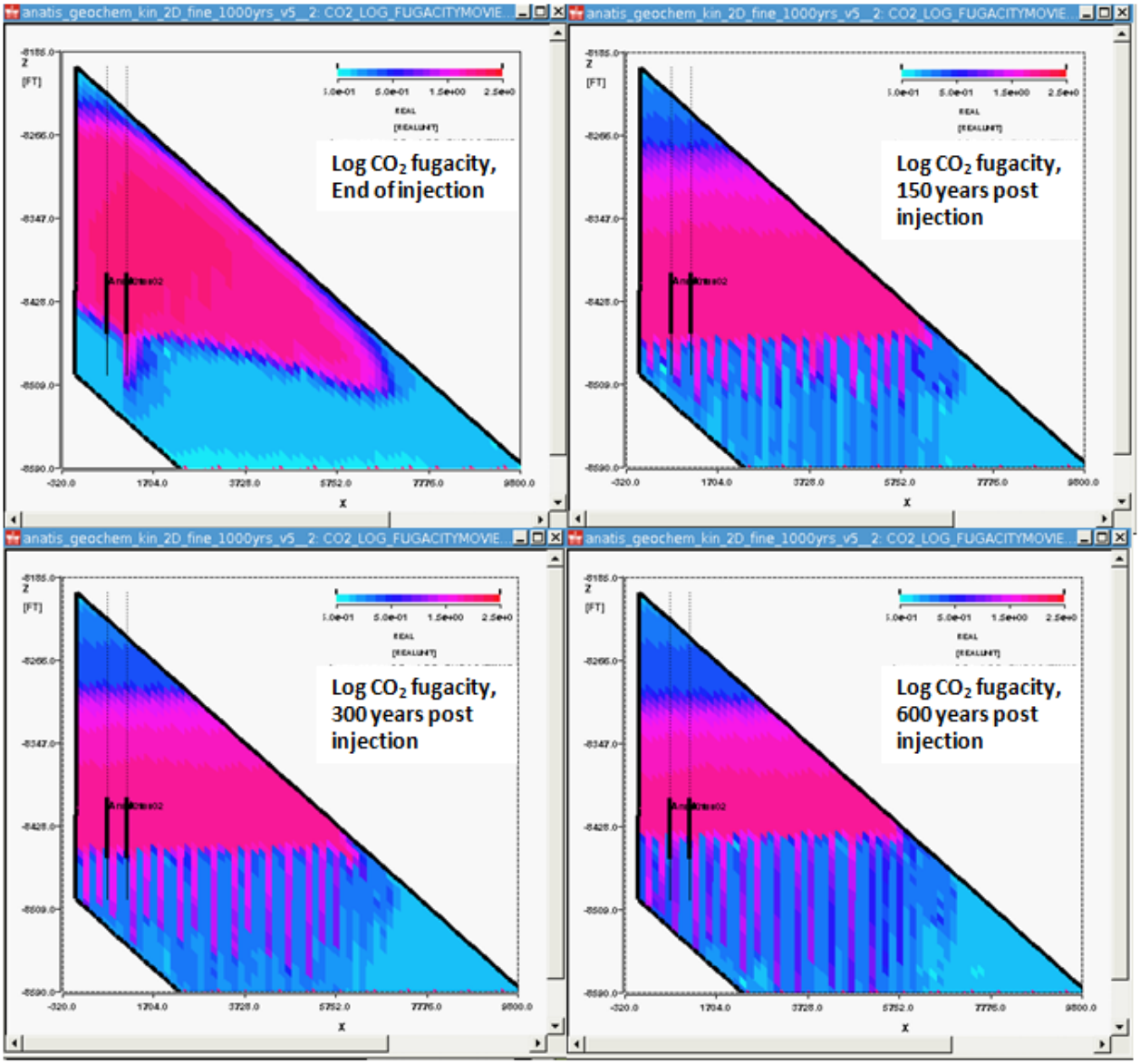

Figure 4-33: Evolution of log CO_2 fugacity.

Note: That the plots are truncated at the position of the original oil water contact, below which the gas saturation is zero and the CO_2 fugacity is not calculated. Above the original oil water contact there is a residual gas saturation and therefore the CO_2 fugacity is calculated. Colour scale runs from -0.5 to 2.5.

4.2.1. Potential for long term migration of geochemically altered formation brine toward the edge of the storage complex

From the results above, geochemical changes from CO_2 injection occur initially within the gas cap but on the very long term (after approximately 1,000 years) there is some lateral CO_2 migration in the water leg along the base reservoir. The CO_2 migration is most clearly seen in the nonreactive case because it was simulated forwards for a longer period, see e.g. Figure 4-17. For the reactive case, within the simulated period (600 years) only the onset of such lateral migration is visible, see Figure 4-20, albeit with much lower CO_2 concentration in the water (due to mineralisation of CO_2) and with nearly identical pH as original formation pH, see Figure 4-21. A recommendation from the external

review (British Geological Survey (BGS)/Heriot Watt University) conducted in May 2014 was to quantify the pH in the CO_2-rich tongue especially in the "no-reactivity" case, but with minimal geochemical fluid-rock interactions included. The true "no reactivity" scenario is not suitable for a realistic assessment of pH changes because the relatively low pH of the CO_2-saturated brine (without accounting for the interaction with minerals) will be buffered by calcite dissolution. The buffering by calcite dissolution is certain to happen for the following reasons:

- From laboratory experiments as well as oilfield experience (wellbore scaling) it is well known that equilibrium with calcite is reached quickly (typically within hours).
- From the petrographic analysis we know that in the Goldeneye reservoir (Captain sandstone) calcite is relatively abundant and spread homogeneously (from XRD it is detected in every sample analysed, see Table 3-1).
- Goldeneye specific experiments (30)[29] confirm that the calcite is well accessible to the pore fluids and that equilibrium with calcite is reached quickly. Therefore the scenario including calcite is much more realistic geochemically (in particular for pH predictions) than the pure "no reactivity" case.

Therefore a variation of the "no reactivity" scenario has been simulated, namely a scenario where only calcite dissolution (or precipitation) is allowed. Also the "high reactivity" scenario (i.e. the simulation with geochemistry included under fast kinetic rate assumptions, as described in the previous section) has been simulated forwards to 10,000 years in order to analyse further development of the lateral migration (including pH changes) in this case.

The spatial pH profile at various points in time up to 10,000 years are shown in Figure 4-34 for the Calcite-only scenario (top row) and in for the high reactivity scenario (bottom row). For the Calcite-only case also an additional simulation was done to study the sensitivity to diffusion, since this will smear out pH changes, using a relatively high value for the effective diffusion constant (D=2e-7 m^2/s and D=4e-9 m^2/s in the water phase). The results are shown in the middle row. Lateral migration distances (of the tip of the downdip tongue) are plotted in Figure 4-35.

From analytic estimates, diffusion leads to a typical length scale (over which smearing out occurs) that grows with the square root of time, namely as $\sqrt{(D*t)}$. After 10000 years this characteristic length scale is 35 m (120 ft) in the water phase and 250 m (800 ft) in the gas phase. Therefore on the model scale (300 ft reservoir thickness; 18,000 ft lateral extent, of which 7,500 ft is occupied by the gas cap) leads to significant redistribution in the vertical direction but not in the horizontal direction. Comparison of the top and middle row confirm this (not that the difference in lateral extent of the downdip finger after 10,000 years, which is larger than 120 ft, is caused by a secondary effect of diffusion: the vertical diffusion leads to a difference in the gravity head that pushes the downdip tongue).

The conclusion from these results is that lateral, downdip migration of geochemically altered brine is possible on the long term, but the pH of the brine will be only weakly acidic (pH slightly above 5) in the minimalistic geochemical scheme (only calcite dissolution) to 6.4 (which is equal to the original pH of the formation brine) in the 'high reactivity' case. Such weakly acidic pH is unlikely (21) to cause any problems (such as severe steel corrosion or cement dissolution) in any abandoned wells that might eventually be encountered. Moreover, the migration speed is very slow: from Figure 4-35, less than 9,000 ft (i.e. less than 3,000 m), relative to the edge of the gas cap, after 10,000 years, with little dependence on the geochemical scenario. Several effects are likely to slow this down even further:

- Geological heterogeneity. The model is homogeneous, while the Captain D sandstone is known to contain shale intervals. Additional simulations (not presented in this report) show

that introducing shale intervals (either explicitly or through introduction of a vertical to horizontal permeability ratio (kvkh) smaller than 1) cause severe slowdown.

- Captain C. The model incorporates Captain D. Below it is Captain C, which has much lower permeability (for which reason it was not incorporated in the model), but on long timescales it may act as a significant sink of the dense brine, thus slowing down (or even stopping) the lateral migration.
- Rugosity of the base reservoir. Rugosity will lead to pools of stagnant dense brine, thus slowing down the lateral migration.

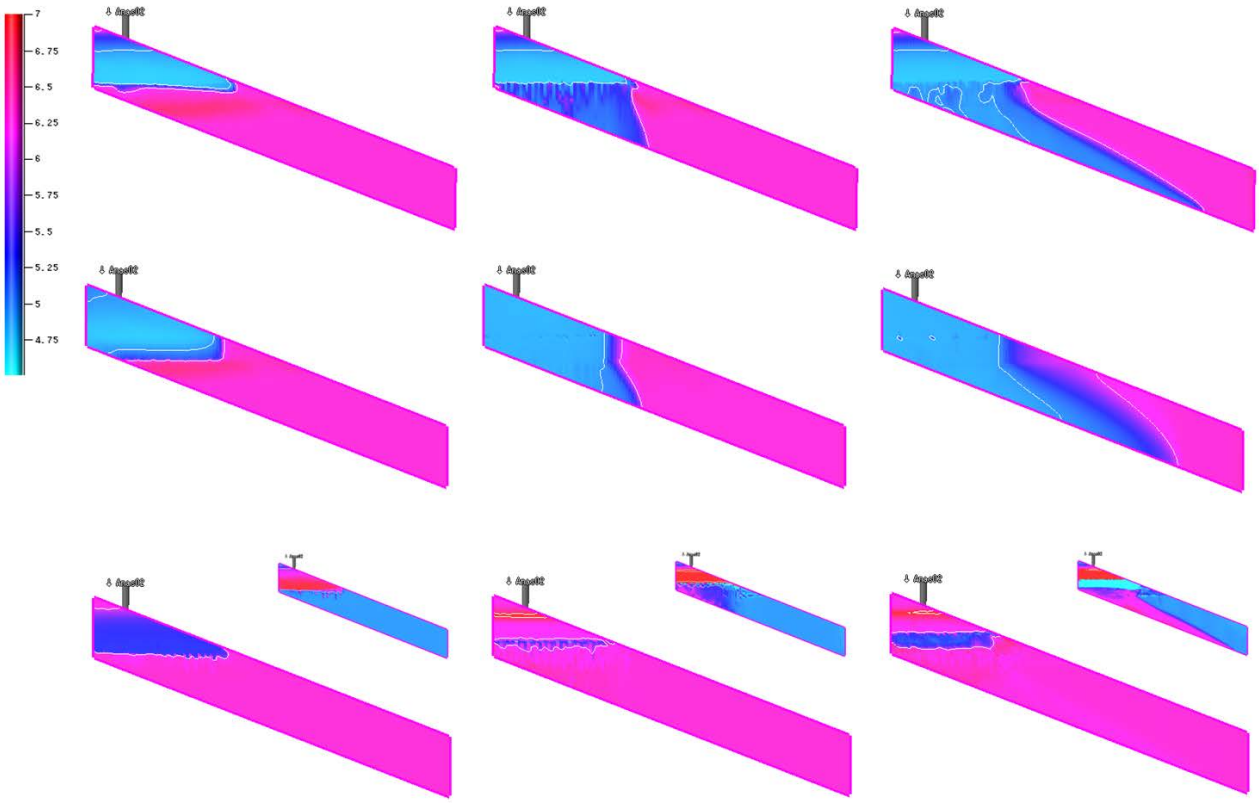

Figure 4-34: Evolution of pH in three scenarios

Note: Colour scale 4.5 to 7.0, contour lines at integer pH values (pH =5; 5; 7). From left to right: time. Left column: 80 years (50 years after end of injection). Middle column: 1,030 years (1,000 years after end of injection). Right column: 10,000 years. From top to bottom: the three scenarios. Top row: calcite only, no diffusion. Middle row: calcite only, with diffusion. Bottom row: high reactivity (this is the same simulation as underlying e.g. Figure 4-21 to Figure 4-33, with simulation period extended to 10,000 years). The insets in the bottom row show salinity in the third scenario (in order to show the lateral extent of the geochemically altered formation brine), colour scale 50,000 to 70,000 (ppm on mass basis), with contour lines still showing pH. The model dimension is the same as in . Figure 4-21 to Figure 4-33, i.e. 18,000 ft laterally and 300 ft reservoir thickness (dip angle 3 degrees, note that the vertical scale is exaggerated by a factor of 10).

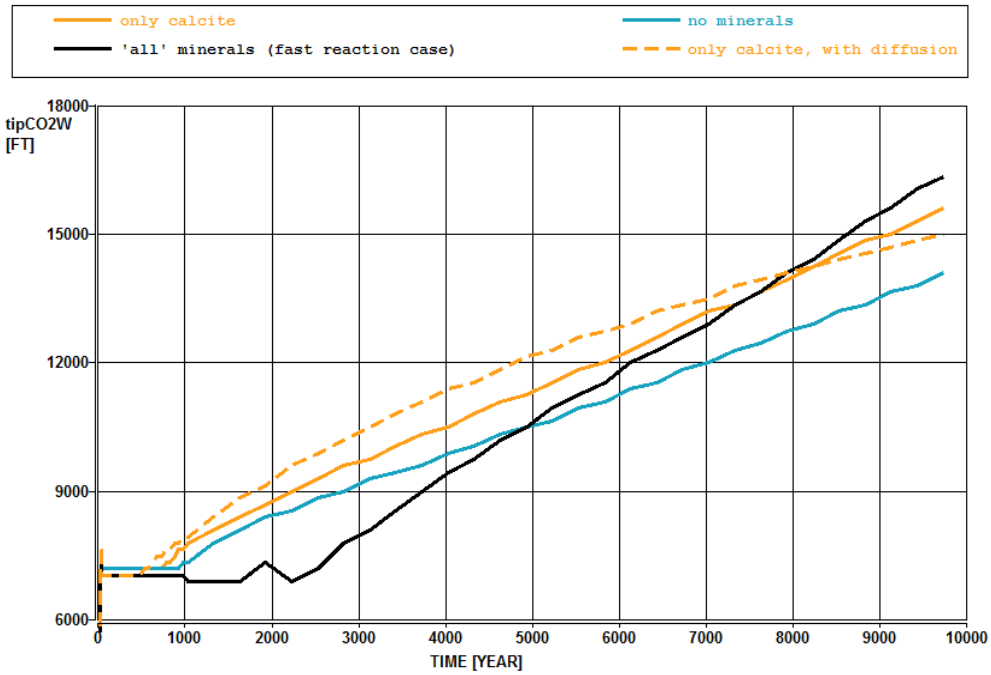

Figure 4-35: Extent of the downdip tongue (relative to model origin) as a function of time for the three cases shown in Figure 4-34

Note: Note the pure "no reactivity" scenario (blue line). The variation between the cases is explained by density variations in the downdip tongue and (for diffusive versus non-diffusive case) a difference in the vertical distribution of the CO_2. Note that all curves start at approx. 7,500 ft, which is the extent of the gas cap (relative to model origin).

4.3. Discussion

In this section the implications of the reservoir modelling results on injectivity and capacity (CO_2 mineralisation) are discussed. Implications on containment are in the domain of the caprock modelling (Section 5) and will be discussed there.

It should be stressed that the models (except some sensitivities) were run under maximum reactivity assumptions, in particular:

- Availability of all required primary minerals at close distance. In reality some of the primary minerals will be located some distance away from each other in the pore space, as indicated by the petrography (SEM images). Therefore a transport mechanism is required through the brine to mix the solutes coming from the various primary minerals. Especially in the gas plume (i.e. at low water saturation, so that the brine is poorly connected at the pore scale) this will be a (slow) diffusive process through the pore space. Moreover some minerals may be located in poorly accessible parts of the pore space. Additionally some of the primary minerals might be shielded by precipitation of the secondary minerals, thus slowing down the reactions.
- High effective surface areas leading to fast kinetic rates compared to most reactive transport modelling studies in the literature.
- For slower reaction rates the reactions might stop altogether because, due to dissolution of CO_2 and mixing due to convection flow, the CO_2 fugacity might become too small in most locations in the reservoir to drive the reactions. This is discussed in some more detail below.

Therefore the effects on injectivity and capacity are likely to be maximum possible effects in the models, with the real effects likely to be smaller.

4.3.1. Injectivity effects

Over all simulations the maximum effect on porosity over the injection period (10 years) is a reduction from 24.00% to 23.42%. The impact on permeability depends on the local sites in the pore scale network where dissolution versus precipitation occurs. Nevertheless due the high Goldeneye permeability (approximately 500 to 1,000 mD average) the impact on permeability is expected to be limited. For example, applying the Goldeneye Captain petrophysical k-phi relationship (approximately $k[mD]=10^{-2.93+24.72*phi}$ in the clean sandstone facies (22)) would give a permeability reduction from 1,000 mD to 720 mD. Since in this permeability range the well injectivity is dominated by tubing size, and not by permeability, the injectivity reduction due to such a permeability reduction will be negligible. Moreover, as already stressed above, this is under high reactivity assumptions. Therefore the risk of injectivity reduction due to geochemical interaction of CO_2 with the rock is estimated to be low. It should be remarked that the risk of injectivity reduction due to salt precipitation near the injector (dry-out effect) is also estimated to be low (see Appendix 2).

Since the calcite is mainly present as cement, the predicted calcite dissolution might reduce the rock strength. The main concern is that such weakening could reduce the maximum allowable injection pressures. For this reason a coreflood test was done to quantify the rock weakening. This test was run by flushing the sample with carbonated brine rather than with supercritical CO_2, and therefore addresses the worst case scenario where calcite is allowed to dissolve, but no carbonate phase is allowed to precipitate within the sample (while the modelling indicates that other carbonate minerals as well as kaolinite would precipitate). The results showed that even after total dissolution of the calcite there is no weakening (30). This might seem counter-intuitive, but as indicated in the experimental report (30) a likely explanation is that the reservoir material was already poorly consolidated, as confirmed by the very low cohesion of 3 MPa, so that removal of calcite cement has little 'room' for further loss of cohesion. Indeed, SEM analyisis (e.g. Fig. 4-8 in the experimental report (30)) shows that there is little to no cementation between the sand grains, and in particular it appears that the (secondary) calcite is pore filling rather than being part of the load-bearing rock framework. The (primary) calcite grains (i.e. skeletal fragments) may bear some of the load, but are encouragingpresent only in a very dispersed way (e.g. Fig. 4-7 in the experimental report (30)), so that it should be no surprise that their removal does not lead to significant rock weakening.

Note that in this experimental work (30) permeability was only measured before the experiment, so the permeability change due to the carbonate dissolution has not been quantified. The main question is whether there is any scope for permeability (injectivity) degradation from carbonate dissolution. Since the carbonate dissolution removes rock material, its primary effect would be permeability increase. However permeability decrease is conceivable if one of the following would occur in a significant way: 1) rock weakening leading to enhanced compaction; 2) fines production. The evidence from the experiment is that such effects do not occur: 1) the strain was measured during the experiment, and no enhanced compaction was measured; 2) fines were monitored in the effluent samples, and (prior to the triaxial failure test) no fines were detected. Only after triaxial failure, fines were detected.

4.3.2. Capacity effects ('fate of CO_2')

The amount of CO_2 mineralisation in the reactive models is high: 39% of injected CO_2 in the batch model (assuming a gas saturation of 80%, pure CO_2 with a density of 0.65g/cm^3)), corresponding to 49 kg per cubic metre of gross rock volume. For the 2D model it is 59% up to maximum 76%, although this would go down if the model were better pressure history matched. However this amount of mineralisation should be regarded as an upside because it is obtained under the high reactivity assumptions as listed above. Also it includes the effect of a significant formation of dawsonite that is only weakly supported by natural analogues. Without dawsonite formation the 39% reduces to 30%. An isotope study on natural analogues (20) suggests that the amount of mineralised CO_2 is lower, namely a maximum of 18% over the cases studied.

It is also interesting to compare to a 2D modelling study on Sleipner (18), which has similar mineralogy but lower temperature (37 °C) and lower pressure (100 bara). In the Sleipner batch models for the reservoir the mineralisation after 10,000 years is 13 kg/m^3 which is consistent with the value obtained for Goldeneye (49 kg/m^3) taking into account that in the Sleipner model less Chlorite and albite is present and the porosity is very high (42%). Also in the Sleipner model the reactions have not fully completed after 10,000 years, which is partly due to lower specific surface areas and partly due to the lower temperature (although the constants in the kinetic model are not temperature dependent, the equilibrium constants are temperature dependent and this leads to a larger undersaturation and therefore quicker dissolution of the relevant primary minerals on Goldeneye).

Interestingly in the Sleipner 2D model the CO_2 mineralisation is much lower than in the Sleipner batch models, namely only approximately 6% after 10,000 years (with the remainder, i.e. 94%, dissolved in water). This is not analysed in detail in the Sleipner paper, but presumably it is because of the fast convective mixing in combination with the slow geochemical kinetic rates: by the time the geochemical reactions kick off in the batch simulations, the CO_2 concentration is too low to kick them off in the 2D model. Indeed in the Sleipner 2D model the strongest mineralisation takes place in the top of the model (above a low permeability mudstone) where the CO_2 concentrations are the highest and the CO_2 residence times is the longest. In this area the CO_2 mineralisation goes up to a maximum of approximately 8 kg/m^3 (and in the mudstone to 20 kg/m^3).

In the (based on analogues perhaps more likely) scenario where the geochemical alterations are ignored, the 2D model indicates that after 10,000 years most (86%) of the injected CO_2 is still in the gaseous phase. This can be explained from the relatively thick gas cap plus the effect of the original oil rim which acts as a vertical baffle to water due to relative permeability effects.

The evolution of CO_2 trapping through time for the two cases discussed above (high reactivity case and no reactivity case) are shown in Figure 4-34 and Figure 4-35. To generate Figure 4-34 the high reactivity model was run forward to 10,000 years (for the other plots in this report it was run forward to 600 years). The plot confirms that (under the fast kinetics assumptions underlying the high reactivity case) most reactions have occurred already after 600 years, and that the rate of CO_2 mineralisation quickly slows down (note the logarithmic scale of the time axis in Figure 4-34 and Figure 4-35). After 10,000 years, 79% of the injected CO_2 has been mineralised (versus 59% after 600 years). In the no-reactivity case, by definition no CO_2 is mineralised, and the injected CO_2 slowly dissolves in the water due to the gravitationally driven CO_2 rich finger slowly sliding down along the base of the reservoir (Figure 4-17). Consequently the gas cap shrinks, so that the fraction of residually trapped CO_2 also slowly increases with time. In the high reactivity case, the mineralisation kinetics are relatively fast so that dissolved CO_2 quickly becomes mineralised relatively quickly; consequently there is no full development of a CO_2 rich finger sliding down the base of the reservoir (Figure 4-20).

Therefore the fraction of water-dissolved CO_2 is much lower than in the no-reactivity case. Also the fraction of residually trapped CO_2 is much lower than in the no reactivity case, because the mineralisation of CO_2 continuously extracts dissolved CO_2 from the water, which is then replenished by gaseous CO_2 dissolving into the water. Note that in both cases there is also some CO_2 dissolved in the oil rim, but this fraction is small because the relatively small volume of the oil rim.

Since these two cases probably represent end member cases, it is expected that the actual CO_2 fate plot lies somewhere between Figure 4-34 and Figure 4-35. From this it is clear that on the long term there is a large (but bounded) uncertainty around the fate of CO_2. This is due to the large uncertainty on geochemical input parameters (especially kinetic rate parameters). However this uncertainty has only little impact on the risk assessment of CO_2 storage in Goldeneye:

- On the injection timescale, the two end member cases still behave nearly the same. So the large spread has little to no impact on the assessment of the risk of injectivity reduction. Injectivity risks were already discussed above
- In both end members gaseous CO_2 remains present even after 10,000 years. So the non-containment risk, which is mostly attributed to CO_2 in the gaseous form (due to its highest mobility), is not much different between the two end member cases
- The risk of CO_2 escaping laterally within 10,000 years through migration in the brine phase (see section 4.2.1) is very low due to slow migration speeds. Moreover the main impact of such a migration would be through a reduced pH (eventually perhaps reaching an abandoned well), which in both end member cases is benign (pH of 5 to 6.4).

Note that the CO_2 fate plots are quite different from the schematic plot in Figure 1-1.

4.3.3. Comment on 'episodic' versus continuous injection

The (2D) modelling done, as described in section 4.2, assumes continuous CO_2 injection. In reality CO_2 will be injected will be done in an 'episodic' way, with average injection rate per well similar to what is assumed in section 4.2, however with frequent shutin and startup sequences. Since even in the high reactivity scenario the rock alterations predominantly occur on the post injection timescale, the precise injection profile should have only a very minor impact on the results. Having said this, for near wellbore phenomena (during the injection period) the episodic injection case is somewhat different from the continuous injection case, because in this area during shutin periods the water saturation may increase (driven by capillary and gravity forces), so that during the next injection period the water mobility is higher (compared to the continuous injection case). As a consequence the episodic injection case may lead to more sustained water mobility in the near wellbore area, perhaps leading to increased dissolution. However this water has already been in contact with the various water minerals, under high CO_2 partial pressure conditions, so it will be close to equilibrium with respect to rapidly dissolving minerals (e.g. calcite) and therefore will not have the capacity to dissolve more of such minerals in the near wellbore region. Moreover, from the experimental work (30) we have learned that even in an extreme dissolution case there is little to no impact on rock integrity and permeability. Therefore we conclude that the cyclic injection case, from a geochemical perspective, does not pose significant additional injectivity (nor containment) risks compared to the continuous injection case.

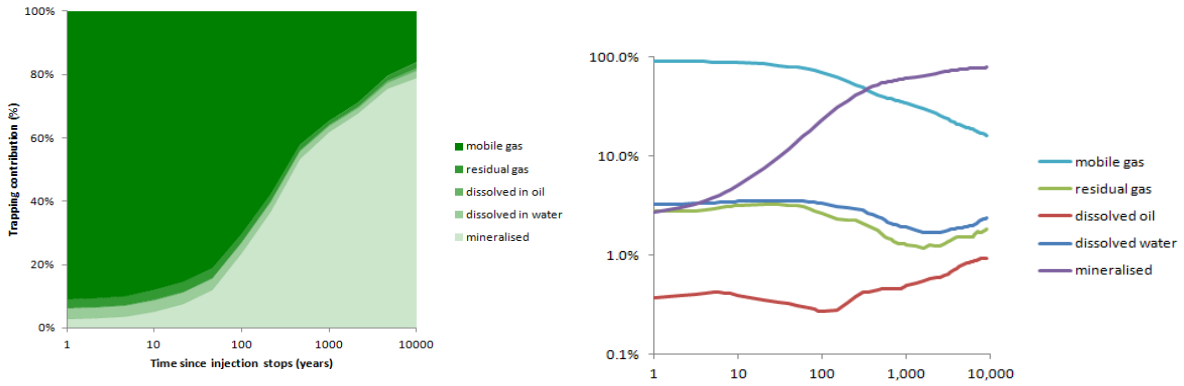

Figure 4-36: **CO_2 trapping mechanisms through time, high reactivity case. Left: linear vertical scale (stacked curves), right: logarithmic vertical scale (not stacked)**

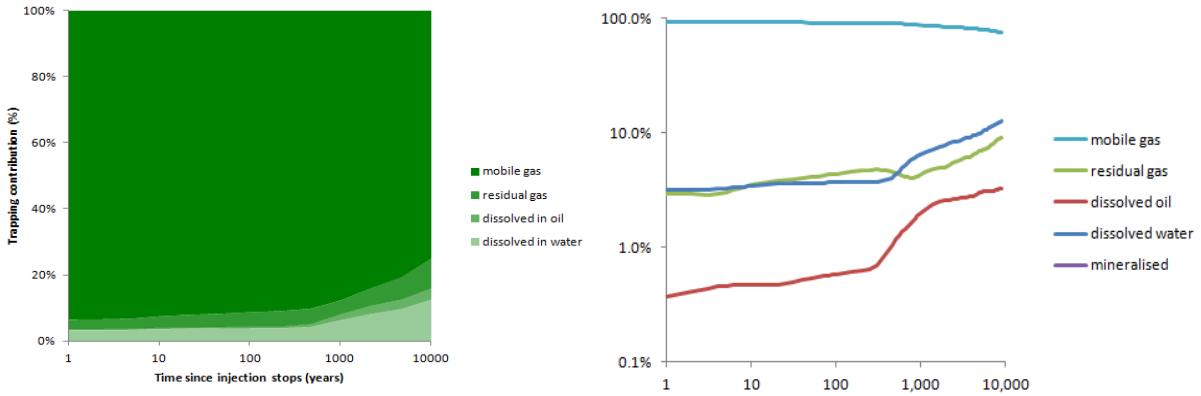

Figure 4-37: **CO_2 trapping mechanisms through time, no reactivity case. Left: linear vertical scale (stacked curves), right: logarithmic vertical scale (not stacked)**

5. Cap rock (Rødby) Reactivity

For the cap rock (Rødby) the modelling objective is to assess the implication of the CO_2–rock interaction on containment, i.e. to address the question whether the interaction could open up leak paths through the formation. For that reason the focus is on the most reactive scenarios (reaction rates, assumptions/boundary conditions on the models). As for the reservoir modelling the intention is to investigate the maximum effects, i.e. focus on the high reactivity case, since this would be the worst case for any geochemistry induced leak paths.

5.1. Batch models

5.1.1. Assumptions and initial conditions

The assumptions in the Rødby batch model are the same as for the reservoir batch model with the following exceptions.

A porosity of 11% has been assumed, based on petrophysical log data (22). The water saturation is assumed to be 100%. In the absence of a shale water analysis or salinity indication, the initial brine is assumed to be of lower salinity than the reservoir brine (35,000 mg/l instead of 54,000 mg/l), with all ions scaled back proportionally, since in some areas the salinity in shale formations is found to be close to seawater salinity. However a sensitivity was run to the higher brine salinity and this was found not to have an impact on the batch results. In early simulation runs the CO_2 fugacity was assumed to be the same as in the reservoir (which may only be true in the lower part of the cap rock). However in subsequent simulation runs no CO_2 fugacity was imposed on the initial brine (giving much lower carbonate concentration) because the imposed CO_2 fugacity on the initial brine was found not to have an impact on the batch model results, while for the 1D runs described later it stabilised the mineralogical changes ahead of the CO_2 front. The injection CO_2 fugacity was assumed to be the same as in the reservoir, i.e. log fugacity equal to 2.09 (in reality this will only be valid for the very lowermost part of the cap rock so it is a worst case assumption).

The mineralogy in the cap rock is somewhat different than in the reservoir in terms of volume fractions and also due to a poorer distinction between illite and smectite. Furthermore there is scope for much higher calcite abundances, especially higher up in the cap rock. Since calcite is very reactive to carbonic acid, a 'worst case' was assumed by setting the calcite volume percentage as high as 50%. Also the specific surface areas used for some of the minerals are different, based on XRD (the crystal sizes in the cap rock for these minerals being smaller). The mineralogical assumptions are summarised in Table 5-1. Note that a somewhat arbitrary assumption has been made on the relative abundance of illite and smectite (where the latter was also split out between smectite and montmorillonite). Therefore a sensitivity was run on this split. The reason for choosing a large proportion of montmorillonite, although not the base case, is the low specific gravity of montmorillonite, so that montmorillonite alteration into heavier minerals might lead to increased porosity despite the mineralisation of CO_2. The specific gravity of montmorillonite (like for some of the other minerals) is poorly defined since it depends on the precise make-up. In Table 5-1 a low case assumption was made. Since the focus is on the maximum reactivity case, the high case specific surface areas were used in all model runs.

Table 5-1: Caprock mineralogical parameters

				Based on Goldeneye petrography	Xu et al., Chem Geol 2010
Mineral Name	**Chemical Formula**	**specific gravity**	**Volume %**	**specific surface area (cm2/g)**	**specific surface area (cm2/g)**
Quartz	SiO2	2.65	7.58	256.70	9.80
Albite_low	NaAlSi3O8	2.62	1.82	595.40	9.80
K-Feldspar	KAlSi3O8	2.56	1.12	312.50	9.80
Kaolinite	Al2Si2O5(OH)4	2.60	2.41	38461.54	151.60
Illite	K0.6Mg0.25Al1.8Al0.5Si3.5O10(OH)2	2.90	15.58	538461.54	151.60
Smectite-low-Fe-Mg	Ca.02Na.15K.2Fe.29Fe.16Mg.9Al1.25Si3.75H2O12	2.41	7.79	538461.54	151.60
Montmor-Ca	Ca.165Mg.33Al1.67Si4O10(OH)2	2.15	7.79	538461.54	
Muscovite	KAl3Si3O10(OH)2	2.88	0.56	2207.00	
Phlogopite (for Biotite)	KAlMg3Si3O10(OH)2	2.90	0.56	2207.00	
Chamosite-7A	Fe2Al2SiO5(OH)4	3.13	3.37	10000.00	151.60
Calcite	CaCO3	2.71	50.20	738.01	9.80
Pyrite	FeS2	5.00	0.48	1197.60	12.90

5.1.2. Results

As in the reservoir case the model was run with all primary minerals and the full set of potential secondary minerals. The result is shown in Figure 5-1. The results are reminiscent of the reservoir batch results, with an 'early' and a 'late' reaction and a *relative* porosity decrease by 0.1 (i.e. from 11% to 10%). It is important to note that despite the high initial calcite abundance (50% by volume, corresponding to 111 mol/kgW) the reactivity (as reflected in the porosity change and CO_2 consumption) is not much stronger than in the reservoir case. The reason is that the calcite alteration stops once the other main ingredient (chamosite) is depleted.

The model was then simplified, to better understand the behaviour but also as preparation for the 1D model (where starting from near-exact equilibrium between the initial brine and selected set of primary minerals is essential in order to avoid any mineralogical changes ahead of the CO_2 front). The results are presented in Figure 5-2, with alternative illite/smectite choices in Figure 5-3 and Figure 5-4. The reactivity in all these cases (as expressed by amount of CO_2 consumed) is somewhat less than in Figure 5-1, and the 'early' reaction is somewhat delayed. However the main observation is that in all these cases the porosity is decreasing or (in the extreme case of only montmorillonite) constant, but never increasing.

As an additional check on the robustness of the result the sensitivity to the geochemical database was investigated (using the BRGM based one instead of the LLNL based one). For some minerals present in the LLNL database but not in the BRGM database, the closest matching mineral (in terms of formula) was used. The results, as shown in Figure 5-5, are somewhat (but not wildly) different. In both cases the same mineral specific gravities were used, nevertheless with the BRGM database this case gives a porosity decrease instead of constant porosity.

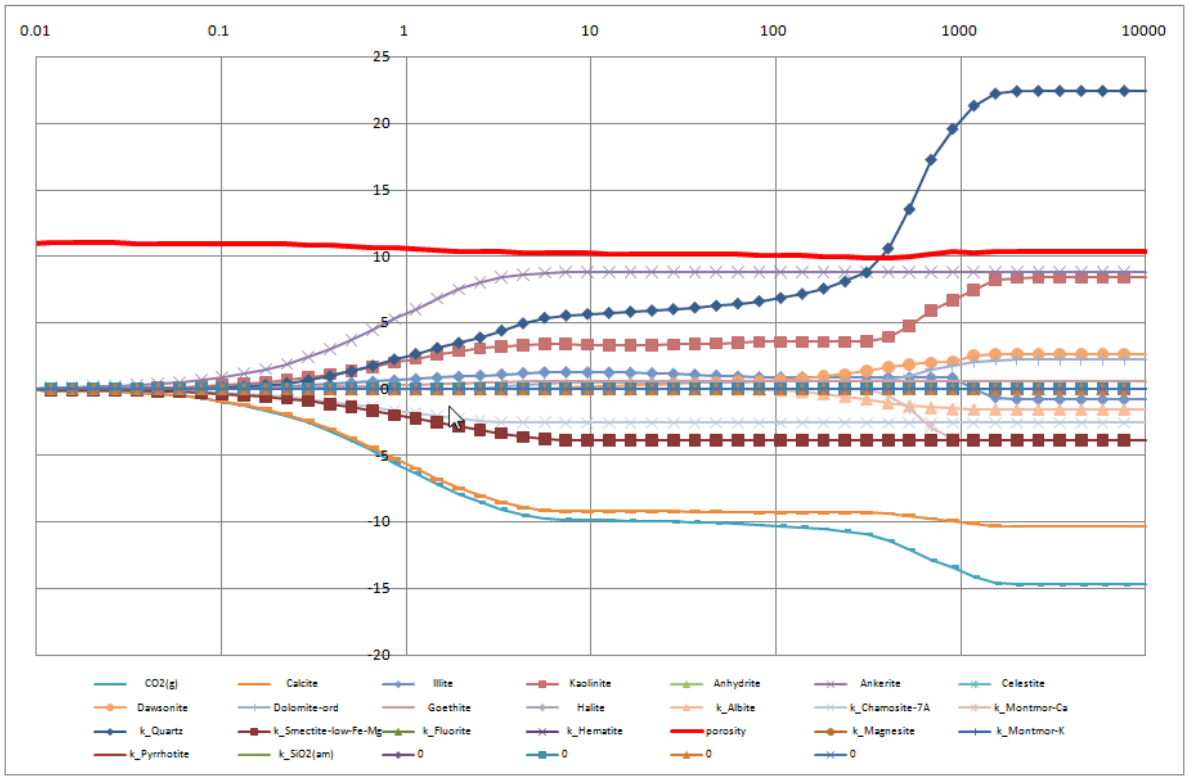

Figure 5-1: **Mineralogical changes in caprock (full set of minerals). The horizontal axis shows time (in years), the vertical axis changes in mineral abundance (in mol/kgW) and porosity (in %).**

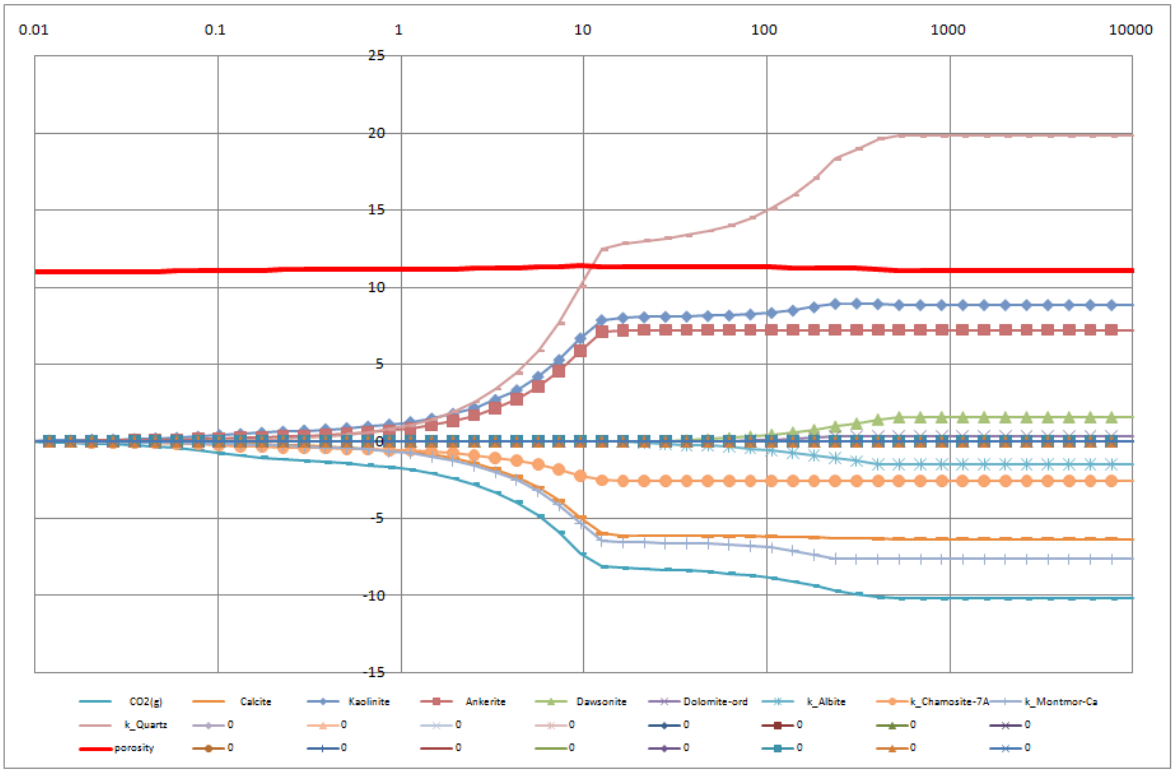

Figure 5-2: **Mineralogical changes in caprock (reduced set of minerals). The horizontal axis shows time (in years), the vertical axis changes in mineral abundance (in mol/kgW) and porosity (in %).**

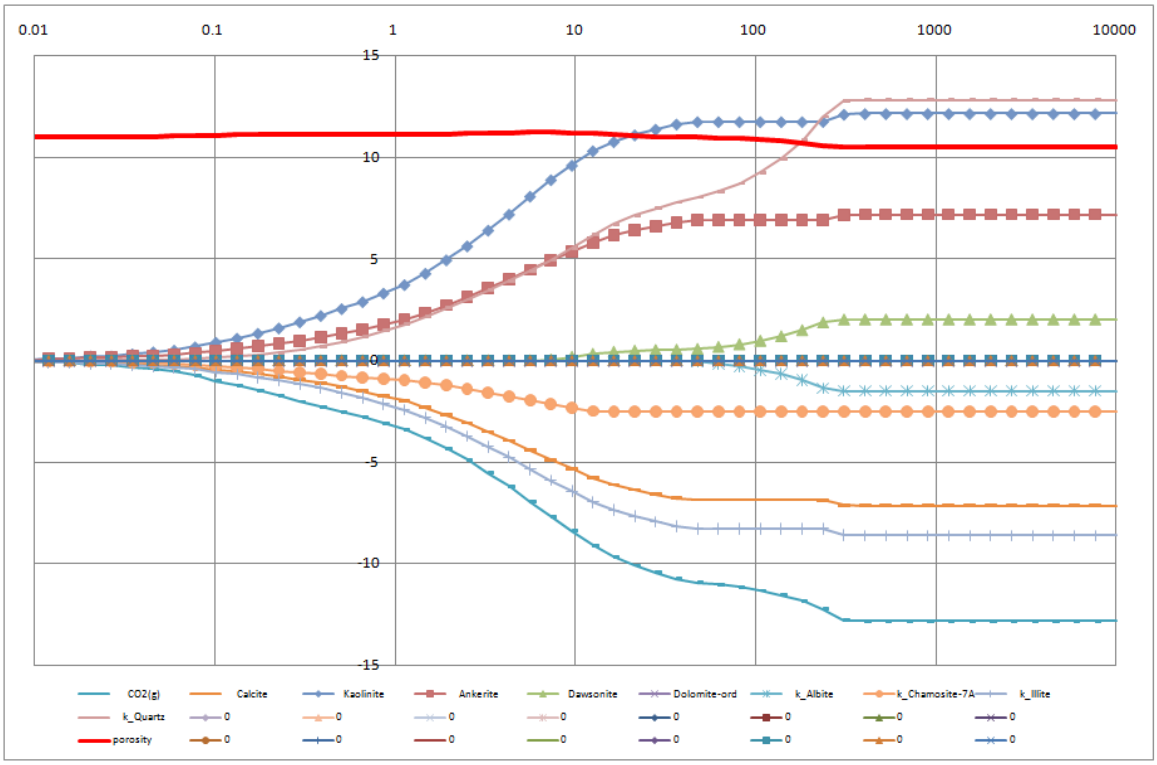

Figure 5-3: **Mineralogical changes in caprock (reduced set of minerals, illite variation). The horizontal axis shows time (in years), the vertical axis changes in mineral abundance (in mol/kgW) and porosity (in %).**

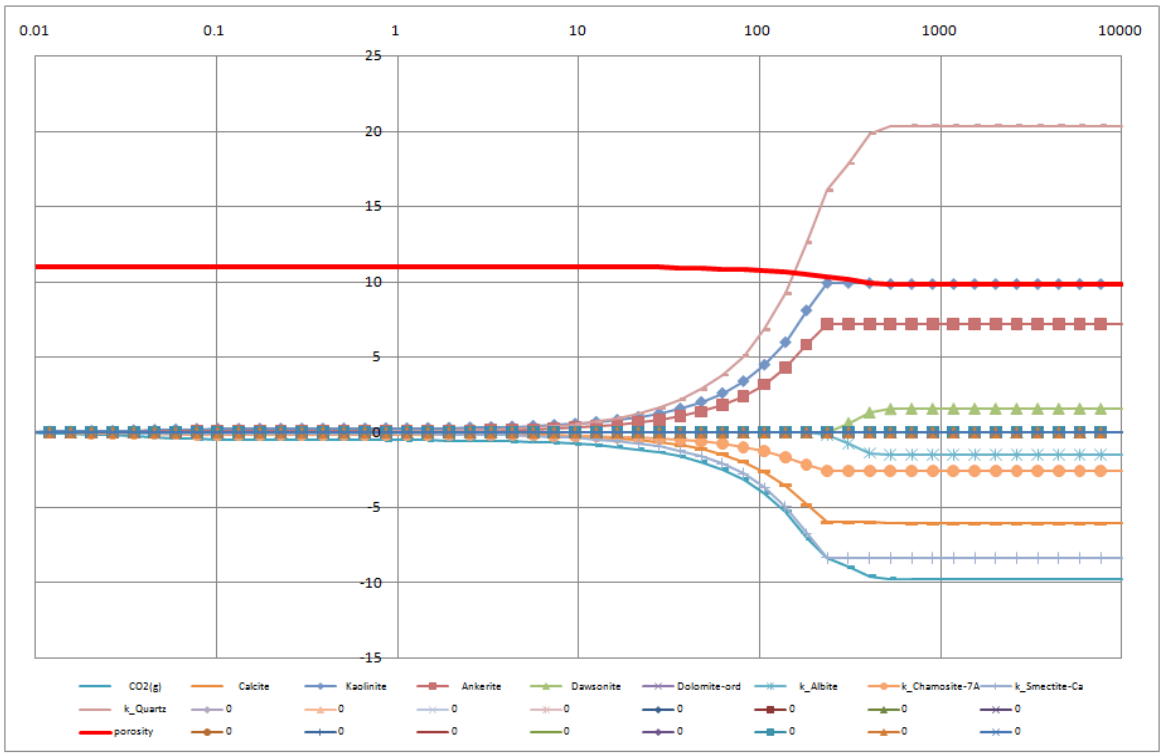

Figure 5-4: **Mineralogical changes in caprock (reduced set of minerals, smectite variation). The horizontal axis shows time (in years), the vertical axis changes in mineral abundance (in mol/kgW) and porosity (in %).**

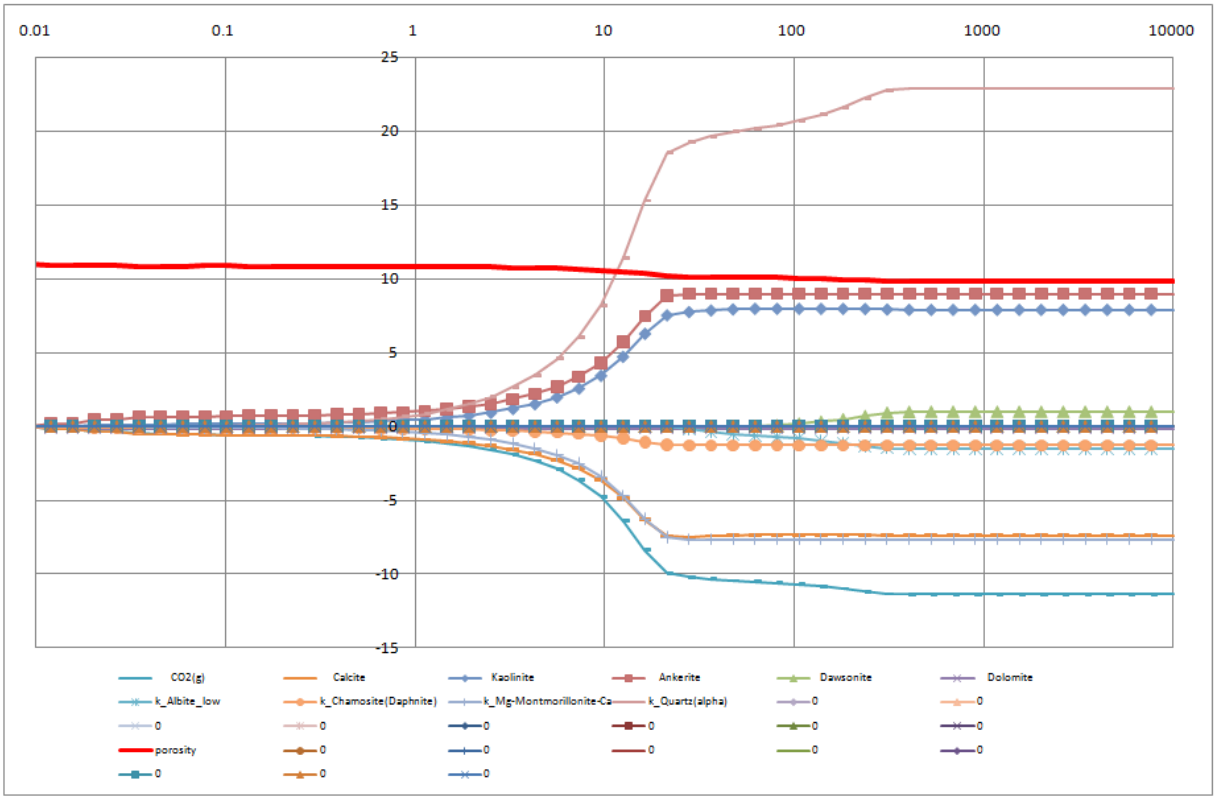

Figure 5-5: **Mineralogical changes in caprock (reduced set of minerals, BRGM-based database). The horizontal axis shows time (in years), the vertical axis changes in mineral abundance (in mol/kgW) and porosity (in %).**

5.2. Diffusion models for Rødby

5.2.1. Assumptions and initial conditions

Since the Rødby is a cap rock that has held back the hydrocarbon gas for millions of years with at most very low leakage rates, it is a very low permeability rock. Although the Rødby permeability has not been measured, it can be expected to have a permeability of 10^{-6} Darcy or (more likely) less based on lab measurements on analogues. This means that for CO_2 to enter the cap rock via convective transport, either in gaseous phase or dissolved in the formation brine, it will be a very slow process. How slow depends not only on the cap rock permeability but also on the pressure difference with the CO_2 at top reservoir. Since Goldeneye is a produced gas field, the reservoir pressure is below hydrostatic and therefore convective flow will be directed from the cap rock into the reservoir rather than the other way around. Only if the reservoir pressure gets back to its original (hydrostatic) pressure is there potential for CO_2 to enter the cap rock via convective flow, because the CO_2 phase is lighter than the formation brine (with a density difference of approximately 0.4 g/cm^3 and a gas cap thickness of approximately 100 m, this pressure difference would be approximately 4 bara). The range of pressure-history matched aquifer models predict that even in the strongest aquifer scenario, and taking into account the pressure up from 10 MT of injected CO_2, it will take very long (1000s of years) to reach hydrostatic pressures again. In other words, for the first 1000s of years the CO_2 cannot enter the cap rock via a convective process.

The other way for the CO_2 to enter the cap rock is by a diffusive process, via the water phase. This process does not require any permeability, only porosity. If the cap rock has a relatively high permeability (10^{-6} Darcy) then even the diffusion would be pushed back by a convective flow downward due to the cap rock dewatering due to the sub-hydrostatic reservoir pressure), however if the cap rock has much lower permeability then the diffusive movement upwards would be dominant over the convective movement downward. Therefore the worst case for CO_2 to move into the cap rock, at least for the first 1000s of years, is the case with only diffusion and no permeability. If at some point in time the reservoir reaches hydrostatic pressures, then in terms of CO_2 transport rates the 'high' permeability case (10^{-6} Darcy) would become dominant over the diffusion transport rates, however the estimated difference in transport rates is 'only' a factor of 10, so even at that stage the assumption of diffusion instead of convection is 'only' one order of magnitude off in terms of CO_2 influx into the cap rock. If the permeability is below 10^{-7} Darcy, the diffusive process would still be dominant over the convective process.

The key question for reactive transport modelling to address is to what extent the cap rock, and therefore the transport properties of the cap rock, could be affected as the CO_2 diffuses into it. In particular, could it open up leak pathways that would either make the diffusive process much faster or, more critically, could it vastly increase cap rock permeability so that if the reservoir pressure would ever come back to hydrostatic pressure (within approximately 4 bar) a significant convective flow of CO_2 out of the reservoir could develop.

To model the CO_2 reactivity with the cap rock during diffusive transport, a 1D diffusion model was created in PHREEQC. The following assumptions were made:

- Geochemistry (mineralogy, geochemical database, and brine) as in the simplified batch PHREEQC model (resulting in Figure 5-2).
- Multi component diffusion constants (23) as in the geochemical database, multiplied by a reduction factor. The reduction factor is generally expressed (24, 25) as the porosity divided by a tortuosity factor (larger than one). In this study we assumed the tortuosity factor to equal 1, which gives the highest diffusion coefficient and therefore represents a worst case for the rate of CO_2 diffusion into the cap rock. Based on petrophysical logs the cap rock porosity was estimated to be 11%. It should be noted that this is high compared to core measurements

on analogues, which typically have porosities of 5% or less. Nevertheless the 11% assumption was used in the modelling because it gives a higher diffusion constant and therefore, again, represents the worst case for the speed of the diffusive CO_2 front. It should be remarked that the multicomponent diffusion constants distinguish between the various aqueous species, and also carry a temperature dependence. For CO_2 at the Goldeneye temperature the diffusion coefficient is 5.9e-9 m^2/s, and for H^+ (which causes the dissolution of calcite) it is approximately 5 times higher.

- A cap rock thickness of 100 m was used, with 100 cells (i.e. cell length 1 m). A grid sensitivity was done to verify that this resolution is fine enough to support the conclusions. The simulation was run for 10,000 years.
- At the top of the grid cell stack (i.e. top of cap rock) no-flow boundary conditions were assumed. Note that these boundary conditions play an insignificant role because the CO_2 diffusion front does not reach the top of the cap rock within the 10,000 year forecast period.
- At the base of the cell stack two different boundary conditions were used (in two different simulation runs), representing significantly different spatial locations. The first boundary condition was a fixed aqueous solution, and represents a *location at the cap rock-reservoir interface with a high water saturation,* where the reservoir brine acts as a source and sink for the various ions needed or generated in the reactions in the cap rock, i.e. an open system. The brine composition in the reservoir will change over time, as illustrated by the 2D model results presented in Section 4.2. Therefore a worst case (maximum reactivity) assumption was used, namely the original reservoir brine equilibrated with the high fugacity (log fugacity 2.09) CO_2. This gives an acidic brine at the boundary (pH of 3.6) that furthermore is an extreme source/sink term for some of the major ions involved in the cap rock reactions (notably it has a lower Ca^{+2} concentration than the brine in the cap rock once calcite starts dissolving, and higher Mg^{+2} concentration than the brine in the cap rock once ankerite/dolomite starts forming). The second boundary condition assumed a closed system with respect to all aqueous species but still a fixed CO_2 log fugacity of 2.09. This represents a *location at the cap rock-reservoir interface with a low water saturation (i.e. in the CO_2 plume, and with low hydrocarbon fraction in the gas,* where reaction products (or ingredients) cannot be easily transported into (or out of) the reservoir.

5.2.2. Results

To check the diffusivity model a case without reactivity was run for the open boundary condition. In this case all aqueous species are allowed to diffuse into or out of the cap rock, but no mineral dissolution or precipitation is allowed. The results are shown in Figure 5-6. This figure shows that after 10,000 years CO_2 front (best read off from the fugacity) has progressed to approximately 50 m to 75 m into the cap rock. The point where the CO_2 has reached a large concentration (50% of the concentration at the inlet) is lagging behind the front, and has progressed to approximately 12 m, in line with the CO_2 diffusion constant D=5.9e-9 m^2 and the porosity of φ=11% (the characteristic length scale for diffusion being $\sqrt{(\varphi*D*t)}$). Moreover the figure shows that diffusion of the main ions has progressed to only approximately 8m (for the 50% level) in line with their smaller diffusion constants. Note that the pH (i.e. proton) front coincides with the CO_2 front, despite the diffusion coefficient for H^+ being 5 times as large as for CO_2, because the requirement of a charge balanced solution (i.e. it cannot travel faster than the HCO_3- front, which coincides with the CO_2 front).

The results with reactivity are presented in Figure 5-7 for the open boundary condition (high water saturation in reservoir), and for the closed boundary condition case (high gas saturation in reservoir) in Figure 5-8. In these cases the CO_2 front has only progressed 6 m to 8 m, this is because much of

the CO_2 is consumed in the mineralogical reactions (like in the batch simulations). Reading the Fig.s from right to left (corresponding to increasing exposure time to CO_2) one can see that the reaction path in the closed boundary condition case is nearly identical to that of the batch run, Figure 5-2 (note that in Figure 5-2 changes in mineral abundance are plotted, while in Figure 5-7 and Figure 5-8 absolute abundance is plotted). In the open boundary case the behaviour is also very similar to that of the closed boundary condition case, except for the first one or two meters, where there is an increased abundance of dawsonite and decreased abundance of kaolinite and ankerite. This is due to the fact that of Na^+ and other ions can diffuse into and out of the system. However in both cases there is hardly any porosity change, like in the batch case. For a (more likely) case with smectite or illite instead of montmorillonite a slight porosity decrease can be expected like in the batch runs (Figure 5-3 and Figure 5-4). Due to the very minor changes in porosity it is expected that the diffusion constant for CO_2 (and for all other aqueous species) is not affected by the mineralogy alteration, i.e. the model assumption of constant diffusion constants is reasonable.

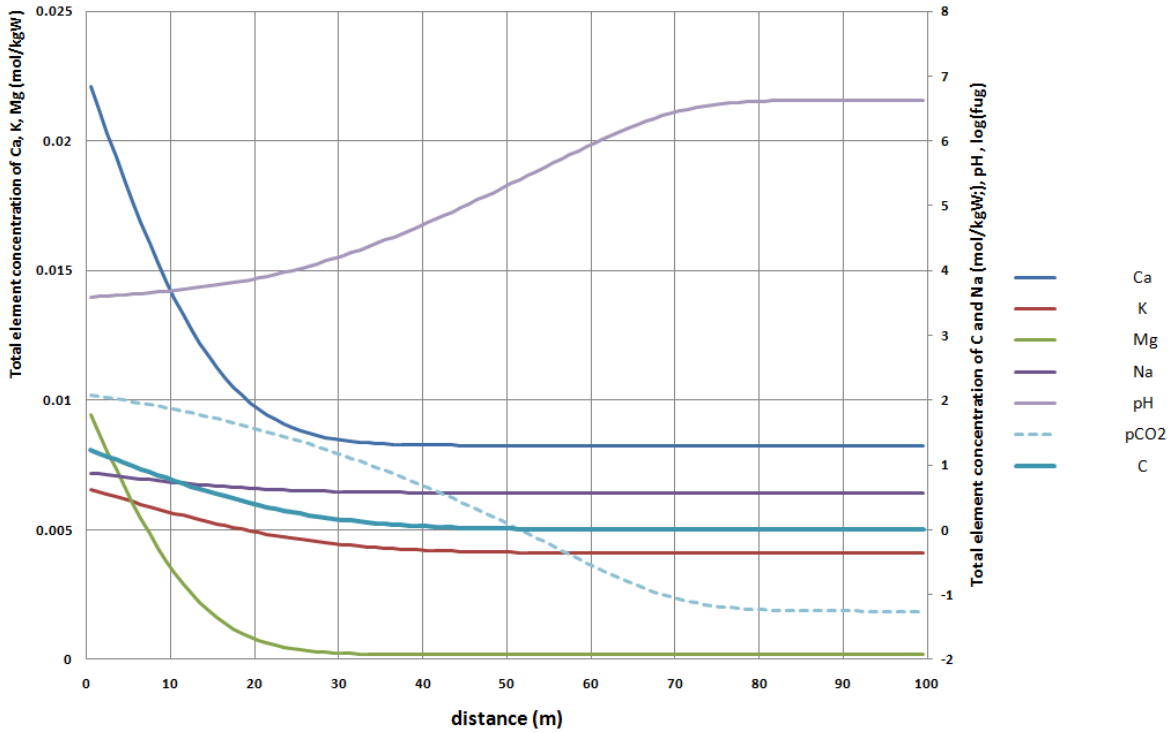

Figure 5-6: Log CO_2 fugacity, pH and main reactive total element concentrations versus distance, after 10,000 years, for the system without mineralogical alterations allowed

Note: That log CO_2 fugacity ('pCO_2' in the Fig.) increases with CO_2 concentration, so the CO_2 diffusion front can be obtained from pCO_2. Total element concentration of CO_2 (C) is also plotted.

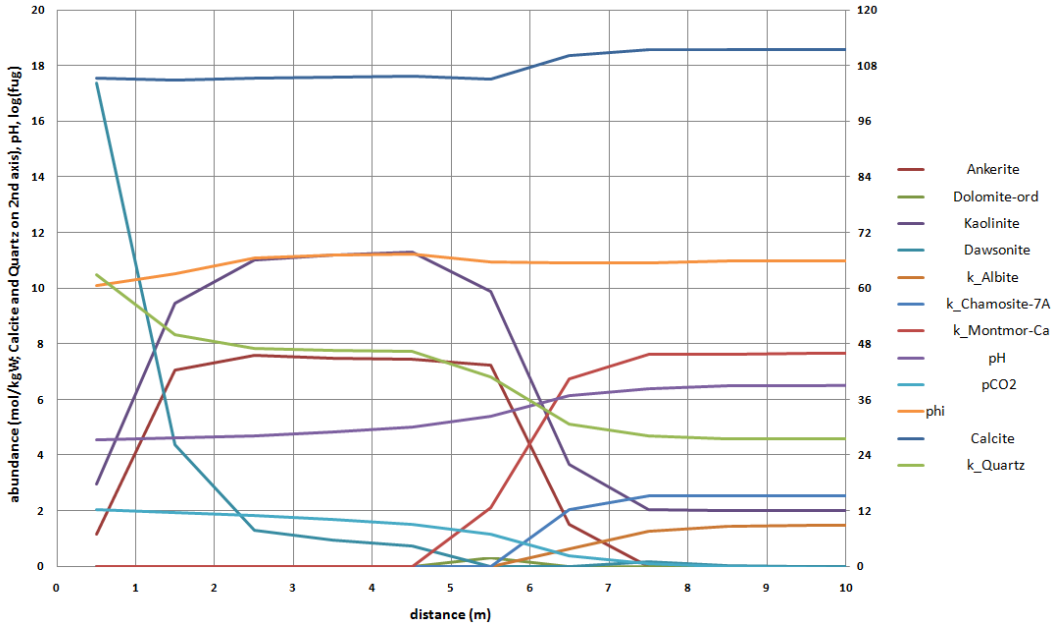

Figure 5-7: Mineral assemblage, porosity, log CO_2 fugacity and pH versus distance, after 10,000 years, for the reactive system with open boundary conditions for the ions.

Note: Calcite and quartz are on the second Y-axis. Only the first 10 m of cap rock is displayed, all curves are constant beyond that.

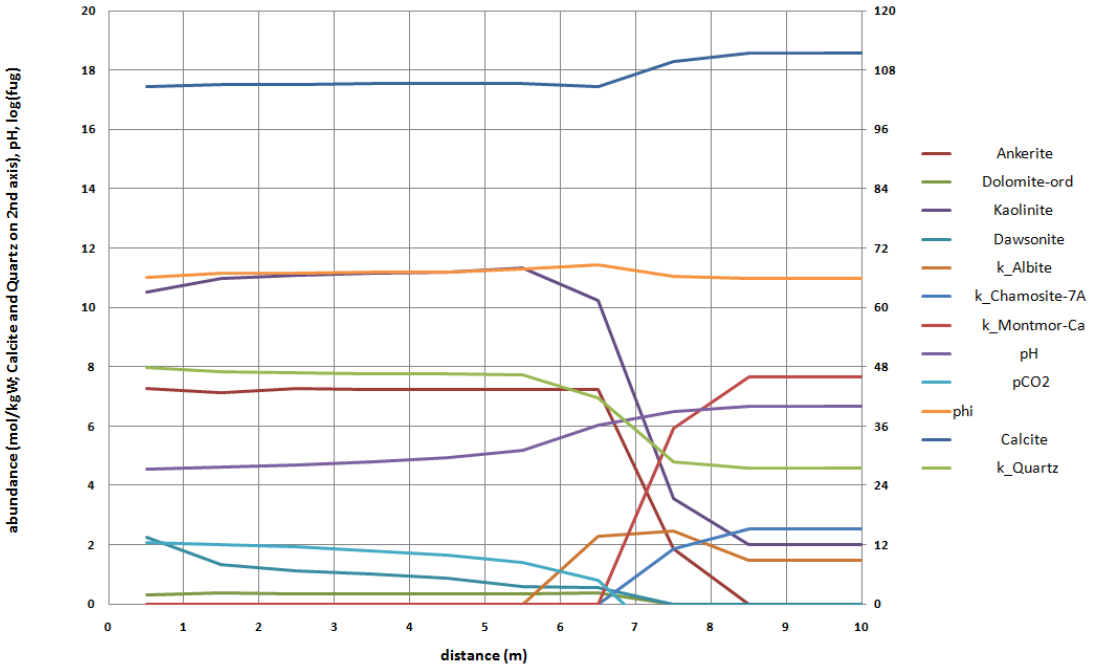

Figure 5-8: Mineral assemblage, porosity, log CO_2 fugacity and pH versus distance, after 10,000 years, for the reactive system with closed boundary conditions for the ions.

Note: Calcite and quartz are on the second Y-axis. Only the first 10 m of caprock is displayed, all curves are constant beyond that.

5.3. Diffusion models for faults

As mentioned in sections 2.1 and 3.1 there is indication for fault zones in the reservoir that are partially calcite-filled. Although there will be fractures (cemented joints/veins) associated with this fault zone, that can also be calcite filled, it is unlikely that the fractures would span across different mechanical zones (26). In other words, fractures in the reservoir are unlikely to extend into the Rødby, and vice versa. Also the fractures in Goldeneye are likely to be sparse, of limited vertical extent, and not connected. However, fault zones (with a throw) can extend through multiple zones. Their fill will be a reflection of the formations they run through plus surrounding formations ("shale gauge"), plus the potential of partial calcite filling. In parts of a fault zone running through the Rødby its mineralogy may be similar to that of the Rødby itself, which has been modelled already as presented in the previous section; in other parts there could be a much higher calcite percentage, potentially up to 100%. In terms of reactivity, a priori this is perceived as a risk for leakage, because calcite dissolves in carbonic acid. However, the dissolution will stop when the carbonic acid becomes saturated with respect to calcite, and at that stage the dissolution can only continue if the Ca^{++} (and HCO_3^-) ions are transported away, or if other minerals start precipitating. The transport away of ions will be difficult due to the low porosity and permeability in the fault zone in the Rødby. To determine how the rapid dissolution versus the slow transport and potential precipitation of other minerals balances out, a 1D reactive Transport model was constructed. In the below a vertically extended region in the fault plane with high calcite content is referred to as "calcite feature".

5.3.1. Assumptions and initial conditions

By the same reasoning as for the Rødby (Section 5.2), the model assumes a diffusive process for CO_2 to enter the calcite-filled feature. Although the fault zone will extend from the caprock into the reservoir, in the reservoir the permeability is much higher (due to lower shale contents), and it is assumed that the reservoir fluid (brine or gas) can enter the fault zone relatively easily in the reservoir. Therefore the selected boundary conditions are the same as for the 1D Rødby modelling (again two cases: closed and open with respect to dissolved ions). The only differences with the Rødby modelling are the mineral assemblage and the porosity. The primary mineral assemblage is assumed to be 100% calcite (the other end member is a mineral assemblage similar to the Rødby itself, which has been modelled already in the previous section). For secondary minerals two cases were simulated: 1) no secondary minerals allowed (this case focuses on calcite dissolution alone, and is likely to have the maximum porosity increase); 2) dolomite allowed to precipitate. The source of the required Mg^{++} ions is the reservoir brine, so the second case was only simulated with the open boundary conditions. Other secondary minerals are possible too, but since of the required ions Mg^{++} is the most abundant in the reservoir brine, only dolomite was considered.

For ease of comparison in most runs the porosity was assumed to be the same as in the Rødby model (11%). In reality, for a calcite filled feature the porosity is likely to be much lower. Literature (27) suggests a porosity as low as 0.01%. Therefore this case was simulated as well.

The calcite was assumed to be in instantaneous equilibrium with the brine. Sometimes this can lead to numerical artefacts when coupled to transport. Therefore a sensitivity run was performed with kinetics, but in this case no differences were observed.

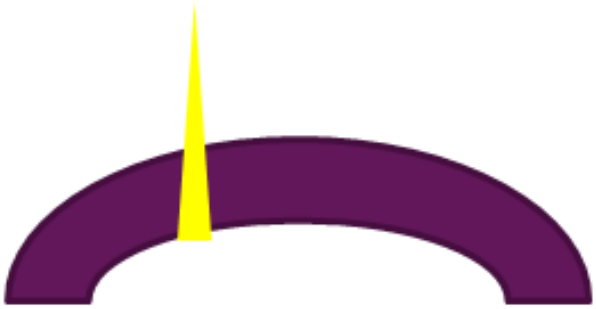

Figure 5-9: Schematic of a calcite-filled part (yellow) of a fault zone running through the Rødby (purple)

Note: The fault zone will continue downwards in the reservoir, but in the reservoir it may have much higher porosity and permeability due to the much lower shale contents. Therefore for the modelling it has been assumed that the reservoir fluids (gas or brine) can enter the fault zone within the reservoir section.

5.3.2. Results

Figure 5-10 shows the results (after 10,000 years) for the closed boundary conditions case (at 11% porosity). At the graph resolution there is no noticeable change in calcite abundance or porosity. On closer inspection there is a very slight change in the region in which CO_2 has diffused, namely a porosity increase from 11.00% to 11.04%, due to calcite dissolution of 0.1 mol/kgW out of the initial 222 mol/kgW. The reason simply is that at that stage the carbonated brine in the calcite feature is saturated with respect to calcite, and since the system is closed with respect to Ca^{++} ions further dissolution is not possible. Due to the only very small CO_2 consumption, the CO_2 diffusion front has progressed nearly as far as in the unreactive Rødby case (Figure 5-6).

Figure 5-11 shows the results for the open boundary conditions case (at 11% porosity, and no dolomite allowed to precipitate). The results are very similar to the closed boundary conditions case except in the first cell (0-1 m into the calcite feature) which (after 10,000 years) shows a porosity increase from 11% to 13% (see below for a short discussion on grid sensitivity). The implication of this is discussed in the next section.

Figure 5-12 shows the results for the open boundary conditions case with dolomite allowed to precipitate (at 11% porosity). The results (most importantly the porosity profile) are nearly identical to the one in Fig. 5-11 because only a limited amount of dolomite precipitates.

Figure 5-13 shows the results for the open boundary conditions case for the low (more realistic) porosity of 0.011% (and no dolomite allowed to precipitate). The CO_2 diffusion has progressed only by 2 m (as expected, factor $\sqrt{(11/0.011)}$ smaller), and the porosity increase again only occurs in the first cell which now is only 5 cm thick.

The fact that, for the open boundary conditions, only the first cell shows a significant porosity change (from 11% to 13% in the second case presented) suggests that the grid resolution is not quite fine enough. For that reason the model was re-run with a three times as fine grid. This model shows a porosity increase from 11% to 24% in the first cell (33 cm) and hardly any porosity increase in the second cell and beyond. So the average porosity increases over the first 100 cm is 4% (compared to

2% in the base model), but it happens over a narrower region. Therefore there is some grid dependency still, however extrapolating the grid sensitivity makes it plausible that on a very fine grid there would be complete dissolution on the boundary layer but there would be no porosity increase beyond a very thin interval (less than 33 cm after 10,000 years).

The question may be raised whether the assumption of a diffusive transport process (i.e. the absence of a much faster, convective transport process) would still be valid in this thin interval with significantly increased porosity. If this assumption would not be valid anymore, then the above model (with open boundary conditions) becomes invalid in this region, in which case further analysis would be required to test for the possibility of a 'runaway' scenario (rapid growth of the high porosity interval). This analysis is provided in the next section.

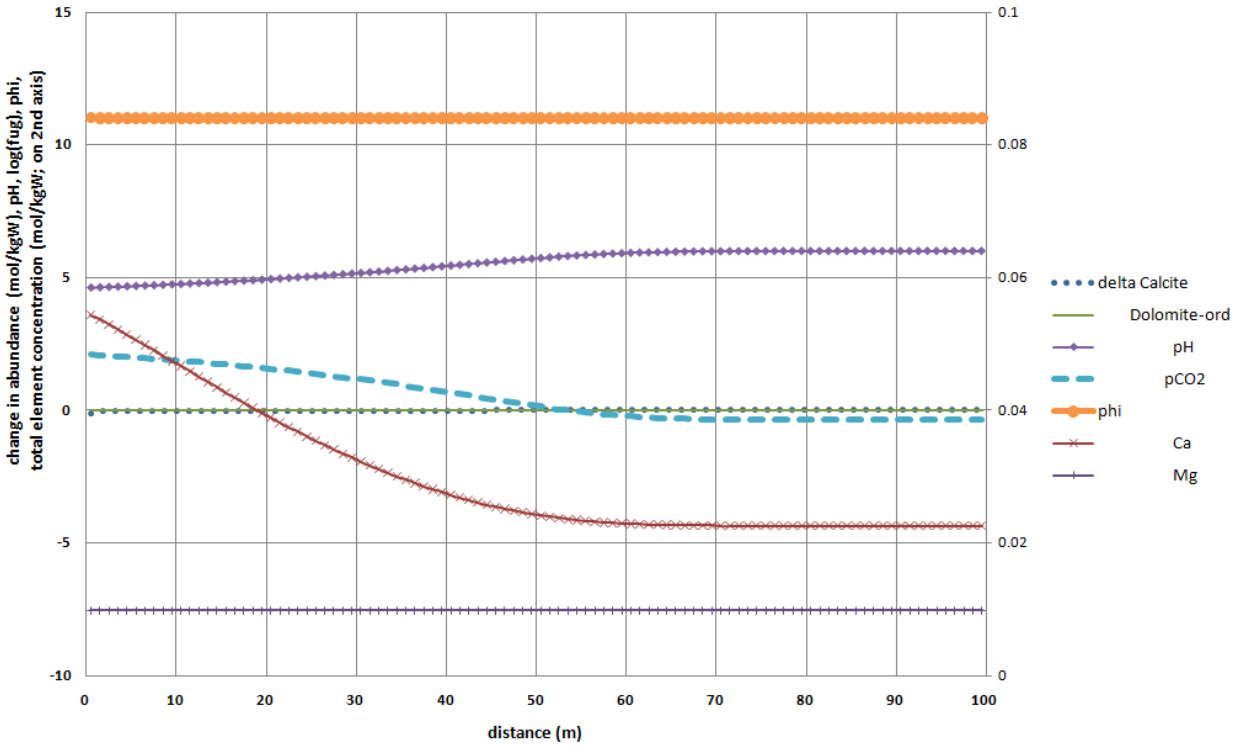

Figure 5-10: Mineralogical and brine changes into calcite feature after 10,000 years (closed boundary conditions). Element concentrations are on the second Y-axis. 11% porosity case

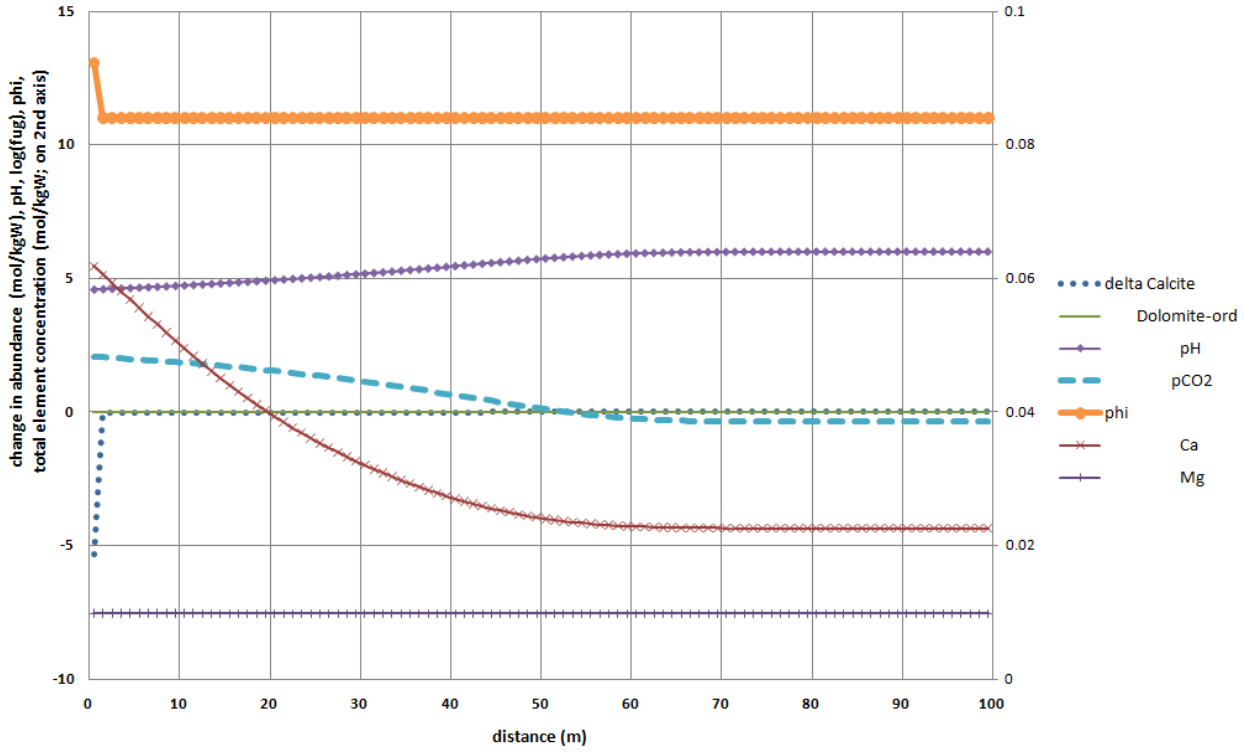

Figure 5-11: **Mineralogical and brine changes into calcite feature after 10,000 years (open boundary conditions, no dolomite allowed to precipitate). Element concentrations are on the second Y-axis. 11% porosity case**

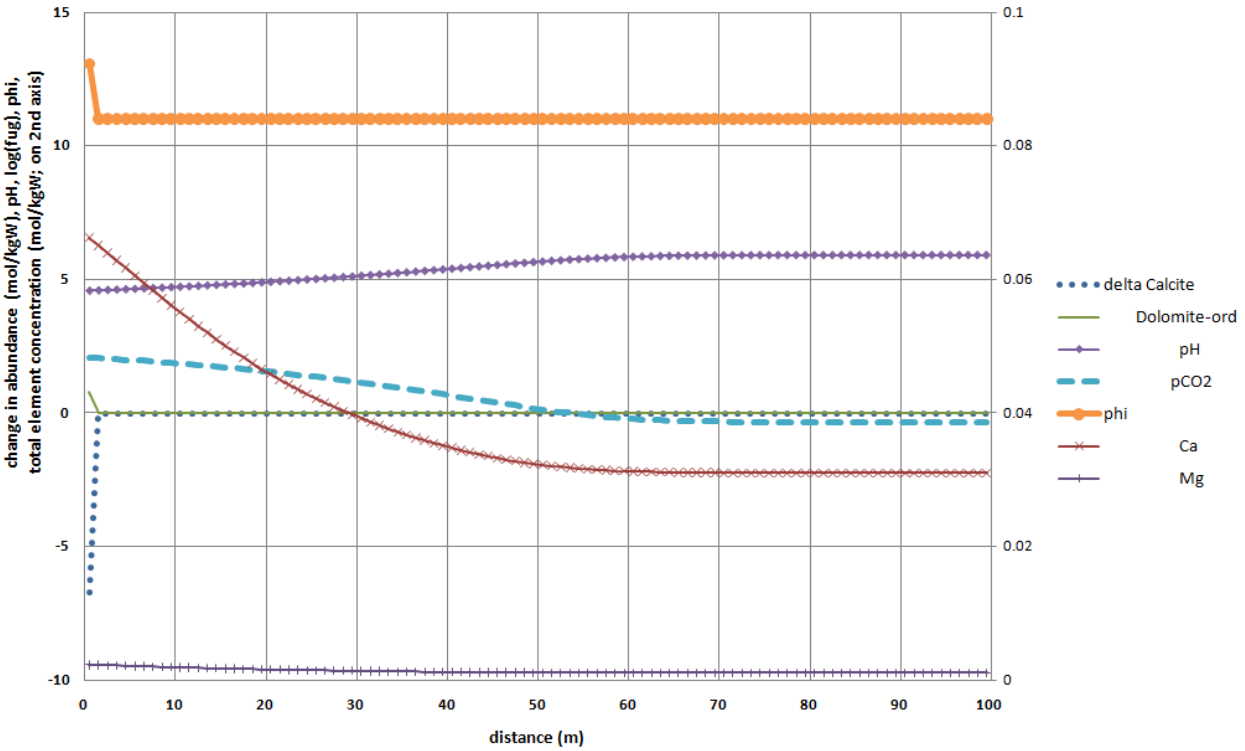

Figure 5-12: **Mineralogical and brine changes into calcite feature after 10,000 years (open boundary conditions, with dolomite allowed to precipitate). Element concentrations are on the second Y-axis. 11% porosity case**

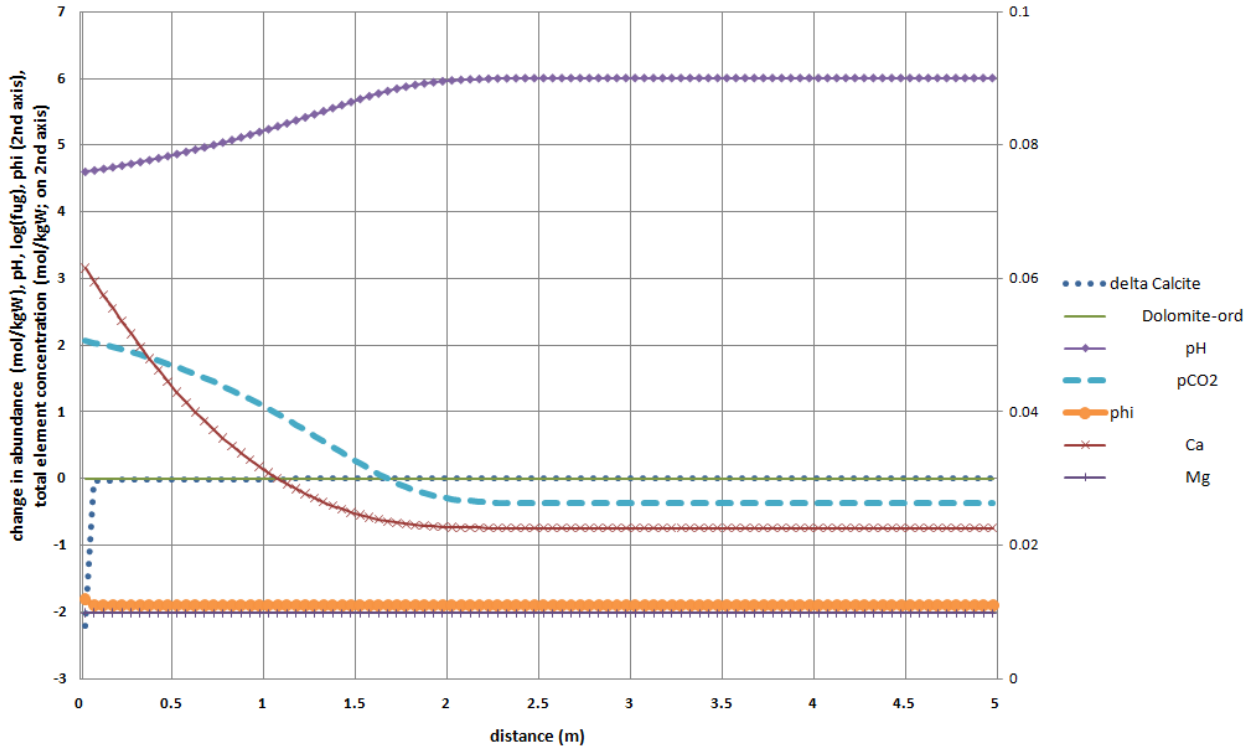

Figure 5-13: Mineralogical and brine changes into calcite feature after 10,000 years

Note: Low porosity (0.011%), open boundary conditions, no dolomite allowed to precipitate. Element concentrations and porosity are on the second Y-axis

5.4. Convective models for faults

In this section we investigate the case in which for some reason the dissolution of a calcite feature through the cap rock (as described in Section 5.3) would be controlled by a convective instead of a diffusive transport process. This is not the base case transport mechanism, but rather a worst case transport mechanism. Nevertheless it is difficult to rigorously exclude this case. Therefore it is important to provide an estimate of the maximum dissolution speed (i.e. minimal dissolution time) of such a calcite feature under this worst case assumption.

5.4.1. Rate constraints on calcite dissolution

The rate of calcite dissolution depends on two physio-chemical processes:

- Calcite dissolution per se. This process happens at a finite ('kinetic') rate if the calcite is thermodynamically unstable (i.e. if the surrounding brine is undersaturated with respect to calcite);
- The transport of dissolution products away from the calcite, and fresh supply of carbonated brine towards the calcite. The transport efficiency depends on the transport type (diffusion versus convection) and transport parameters (diffusion constants and concentration gradients in case of diffusion; concentrations, absolute and relative permeability, fluid viscosity and fluid pressure gradient in the case of convection).

The dominant transport process in the cap rock, and the speed of it, depends on the location in the reservoir. As will be shown in the subsections below, the transport process is different above and

below the (dynamic) gas water contact (i.e. regions 1 and 2 in Figure 5-14). The (dynamic) gas water contact is defined as the interface above which free gas exists (i.e. gas saturation larger than zero) and below which no free gas exists (gas saturation zero, i.e. 100% water saturation; however the water may contain dissolved CO_2).

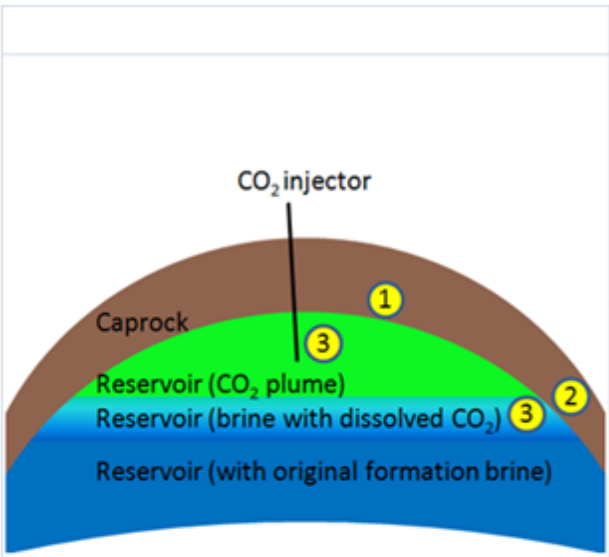

Region	Description
1	Caprock exposed to CO_2 plume
2	Caprock exposed to formation brine with dissolved CO_2
3	Reservoir within and close to CO_2 plume

Figure 5-14: Overview of the key regions of the reservoir and caprock exposed to CO_2

5.4.1.1. Chemical reactions

The following chemical reactions are relevant for calcite dissolution in the context of CO_2 injection:

CO_2 dissolution in the brine (forming carbonic acid, H_2CO_3):

$$CO_2(g) + H_2O \rightarrow H_2CO_3$$

Dissociation of carbonic acid (lowering the pH)

$$H_2CO_3 \rightarrow H^+ + HCO_3^-$$

Calcite dissolution:

$$CaCO_3 + H^+ \rightarrow Ca^{++} + HCO_3^-$$

5.4.1.2. Calcite dissolution with instantaneous transport of solutes

Before moving to the transport mechanisms, it is useful to estimate the time it would take to dissolve the entire calcite feature if it would be continuously exposed to 'fresh' (i.e. under-saturated with respect to calcite) carbonated brine. This is a theoretical case in which somehow the dissolution products (Ca^{++} and HCO_3^-) would be instantaneously removed from the brine, while there would be a constant supply of the reaction ingredient H^+ (such that the pH is kept constant through time).

The speed of the calcite dissolution process has been measured experimentally (essentially by putting a small piece of calcite in a large beaker of brine, and continuously stirring). The dissolution rate is temperature and pH dependent, and the rate equation (as function of pH and temperature), fitted to the experimental data, is reported in Palandri & Kharaka (28).

The temperature at the calcite feature can be assumed to be very close to the reservoir temperature (83°C). Near the injector, the temperature may be lower, but this temperature quickly reaches reservoir temperature over a relatively short distance away from the injector (order of 100 to 200 m), and also (post injection) over time the area around the injector will warm up to the initial reservoir temperature.

The dissolution rate becomes slower with increasing pH. The pH of the formation brine with dissolved CO_2 is 3.0 or higher without calcite (and 4.7 or higher after equilibrium with calcite, which is also present within the reservoir (see Section 3.1 or Table 4-1)). This was calculated using the thermodynamic electrolyte package OLI StreamAnalyzer (29). It was checked that PHREEQC gives the same values (i.e. 3.0 and 4.7). The above pH values are obtained under the following assumptions: temperature 83°C (Goldeneye reservoir temperature), pressure 250 bara (close to hydrostatic), a pure NaCl brine with salinity 55 g/l (Goldeneye salinity), and equilibrium with pure (100%) CO_2 gas at this pressure and temperature. For lower pressure, lower CO_2 contents or higher salinity, the pH will be somewhat higher (for lower temperature the sign of the pH change depends on the presence or absence of calcite). More importantly, for a brine containing already some alkalinity (as is the case for the Goldeneye brine, that is strongly NaCl dominated but does contain bicarbonate), the pH will be buffered to some extent, so that the pH after dissolution of injected CO_2 would be higher. Using Goldeneye alkalinity, the pH (after equilibrium with pure CO_2 at 83°C and 250 bara) becomes 4.0 (and 4.6 with calcite included). Therefore a pH of 3.0 is a pessimistic case.

At this temperature and pH, the calcite dissolution rate (per unit surface area of calcite) from Palandri & Kharaka (28) is 0.0013 mol/s/m^2 (at a pH of 4.7 this reduces to 0.000033 mol/s/m^2). Using a value of 2.71 g/cm^3 for calcite density and 100.0 g/mol for calcite mol weight, and a 70 m cap rock thickness, this gives a dissolution time of (46/α) year at pH=3.0 and (1820/α) year at pH=4.7, where α is the surface roughness factor of the calcite (i.e. effective surface area per geometric cross sectional area). From the SEM image (Figure 3-3), the surface roughness factor is larger than 1. Furthermore the calcite dissolution might increase the roughness.

Note that in the above it is implicitly assumed that the carbonic acid attacks only the calcite feature. However, in view of the presence of some calcite in the reservoir, it is likely that the carbonic acid would contact the calcite in the reservoir first, and would largely be spent before it reaches the calcite feature.

Nevertheless the calculation shows that under the (theoretical) assumption of instantaneous transport of solutes, a calcite feature in the cap rock is prone to complete dissolution within 1,000 years. Therefore further analysis (namely, of the transport mechanisms) is required to investigate if CO_2 can be stored in Goldeneye for (at least) 1,000 years without escaping through a calcite feature.

5.4.1.3. Transport considerations

In reality the solutes cannot be transported instantaneously. The transport of H^+ towards the calcite feature, and of Ca^{++} (and HCO_3^-) away from the calcite feature requires time. The time required to

transport a certain amount of these ions towards or away from the calcite feature depends on the transport process.

A schematic of the transport processes relevant for the dissolution of the calcite feature is provided in Figure 5-15. In this Fig. the Goldeneye reservoir is shown as green, the primary cap rock is shown as brown, and the calcite feature is shown as yellow. The schematic presents a snapshot in time at which the calcite feature has already been exposed to CO_2 for some time, with the source of CO_2 being either gaseous (or rather, supercritical) CO_2 or dissolved CO_2 in the reservoir brine, coming from CO_2 injection (not displayed in the schematic) in the reservoir.

The Goldeneye reservoir has good permeability (allowing for relatively quick convective transport, as well as diffusive transport), but it is assumed that the calcite feature (prior to dissolution) does not have significant permeability (i.e. it is not a leak path prior to CO_2 injection, in line with the fact that Goldeneye contained hydrocarbon gas for millions of years). However the calcite feature is expected to carry some (albeit low) connected porosity (see Section 5.3.1), in which diffusive transport is possible.

A number of different zones can be distinguished:

- Zone A is the part of the calcite feature not exposed to CO_2.
- Zone B is the part of the calcite feature into which H^+ (coming from the CO_2 and brine in the reservoir) has diffused. The vertical extent of zone B will grow over time. In this zone the H^+ will react with the calcite, forming Ca^{++} (and HCO_3^-), which will diffuse downwards.
- Zone C is the part of the calcite feature that has dissolved completely (assuming this happens at all; zone C might be absent in some cases as explained below). Note that between zone B and C there will be a transition zone in which some of the calcite has dissolved (increased porosity, but not yet 100% porosity). This is not displayed in the figure.
- Zone D is the part of the reservoir 'connected' to the calcite feature. Transport of calcite dissolution products, and supply of H^+ (or CO_2) need to go through this region.

It is crucial to understand the possible fluid contents in these zones:

- Zone A is 100% brine saturated, since (being part of the primary cap rock) no gas can enter due to the high capillary entry pressure.
- For the same reason zone B is also (nearly) 100% brine saturated.
- Zone C is either 100% brine saturated or 100% gas saturated (see below for explanation).
- Zone D can have any water saturation between irreducible water saturation and 100%. In terms of the (lateral) locations displayed in Figure 5-14, the water saturation will be 100% for a calcite feature at location 2, and much less than 100% at location 1.

A key observation is that region C, as soon as it would grow beyond microscopic dimension, will have zero entry pressure to gas (and vertical equilibrium can be established). This means that if the gas saturation in region D is not zero (even if it is very small), the top part of region C will be completely gas filled because the gas has lower density than the brine. Note that by 'gas' we mean any combination of CO_2 and original hydrocarbon gas forming a separate phase from the water (i.e. it could be supercritical CO_2 rather than gas).

If (the top part of) region C is gas-filled then it is possible to have a convective transport mechanism for CO_2 (in the gas phase) towards region B, however there is no convective transport mechanism possible to get the dissolution products (notably Ca^{++}) away from B (except perhaps in a very thin capillary water film on the edge of C, see below). The reason is that the Ca^{++} solubility in the gas is

practically zero. In other words, region C forms a boundary between the calcite and the reservoir that is open to CO_2 but closed to Ca^{++} (as well as to H^+ and HCO_3^-). It should be remarked that the very thin water film on the edge of C is expected to be static because the water sitting above C (i.e. in region B) is capillary trapped and therefore cannot drain down through the water film region C. The only viable mechanism to break the capillary trapping in region B is a volume increase in the brine in B (e.g. due to a pressure drop or due to the CO_2 dissolution), however such changes would lead to only a very small relative volume change and therefore to only very small cumulative volumes of expelled water (and therefore only very small transport rates). Therefore this effect has been ignored in the modelling of this case.

This case (open boundary conditions to gaseous CO_2, closed boundary conditions to aqueous species (Ca^{++}, H^+ and HCO_3^-) was modelled in Section 5.3.2, with results as shown in Figure 5-10. Essentially in this case the calcite dissolution is blocked. In region B a small amount of calcite dissolves, leading to a negligible porosity increase (from 11.00% to 11.04%, not visible on the scale of Figure 5-10), and then further dissolution stops because the brine is saturated with respect to calcite and the Ca^{++} is unlikely to be transported out. Region C stops growing once it is big enough for the gas phase to enter.

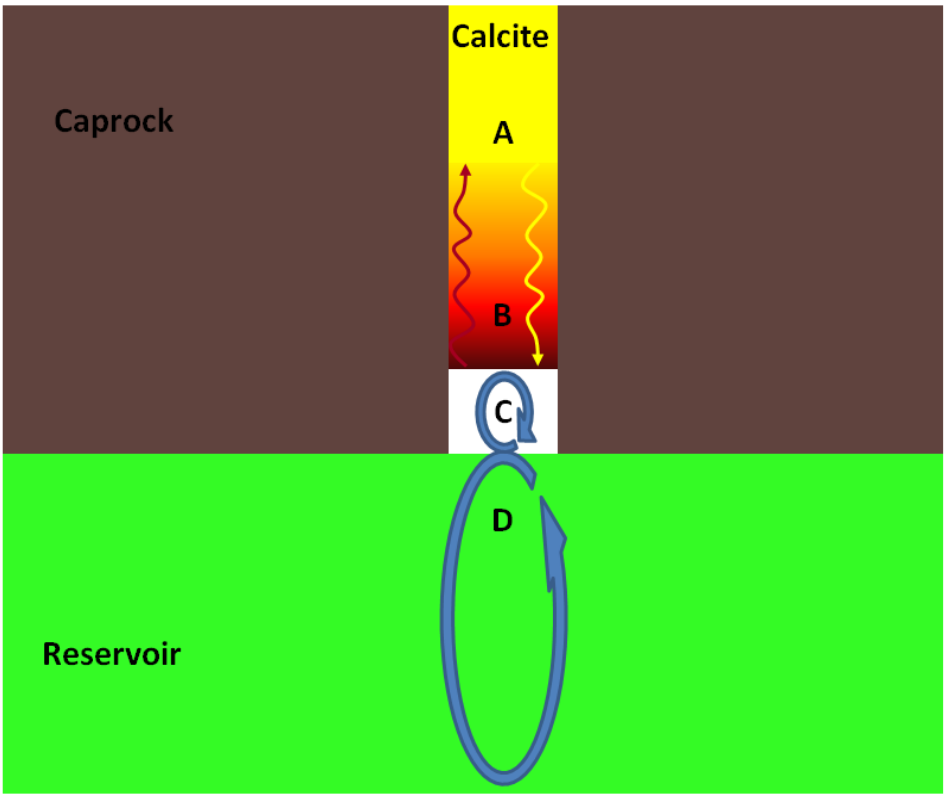

Figure 5-15: Schematic of transport mechanisms of Ca^{++} and CO_2 into and away from the calcite feature.

Note: A: uninvaded zone. B: diffusive zone (CO_2 (and H^+) diffusing upwards, Ca^{++} diffusing downwards). C: dissolved zone (either gas or brine filled, see main text). D: reservoir zone (mainly convective transport bringing CO_2 and H^+ towards zone C, and transporting Ca^{++} away from zone C.

The transport mechanisms in zones C and D depend on the phases present in the reservoir at the location of the calcite feature (only brine; or brine and gas). Zones A and B are fully brine saturated.

The other case to consider is the one where region D has zero gas saturation (i.e. 100% brine saturation). In this case it is still possible to have CO_2 (and therefore H^+) in the brine, because the CO_2 in the gas cap can dissolve in the brine which subsequently sinks down due to its slightly increased density, thus forming so-called convective cells. One of these cells is schematically drawn into Figure 5-15, as the blue arrow in the reservoir. In this case region C will be completely brine filled because (by definition of this case) there is no free gas at the base of it. Region C may develop its own convective cell (drawn in as the small blue arrow in Figure 5-15), because carbonated brine with dissolved calcite has somewhat higher density than carbonated brine without dissolved calcite. Since convective cells have a minimum intrinsic size (based on fluid viscosity and density gradient), this convective cell will only form once region C has grown large enough. However this minimum dimension is small for brine (less than cm scale, e.g., convective cells easily develop in simple experiments in a small water beaker that could be done at home). Once this convective cell has formed, the flow velocity in this cell is much larger than the velocity in the larger convective cell in the reservoir region, because region C is a cavity and therefore has nearly infinite 'permeability'. Therefore we assume that transport in region C is instantaneous (compared to transport in region D), i.e. that the overall transport rate of Ca^{++} (and H^+, etc.) is controlled only by the transport rate in region D. For completeness it is noted that in case no convective cell would develop in region C (e.g. very narrow or tortuous dissolution cavities), the transport through C would be diffusive and essentially the diffusive case with open boundary conditions (to all dissolved ions) applies (leading to a dissolution front of less than 33 cm in 10,000 years as described in Section 5.3.2 (see Figure 5-11 and the discussion above it).

The gravity driven convective flow pattern in the reservoir (region D) was studied in Section 4.2, by simulation of the full physics model in simplified reservoir geometry. The result (as visualised by the transport of dissolved CO_2) is shown in Figure 4-17. This model prediction will give one of the inputs (namely, convective flow velocity) into the calcite dissolution time estimate (that will follow at the end of this section). Note that the model geometry used is representative of the realistic geometry (15) on the flanks of Goldeneye (just below the gas water contact), as displayed in Figure 5-16.

It should be remarked that during injection there are also convective (or rather, advective) flow patterns (driven by the injection pressures). However these flow patterns only occur during a relatively short time period (namely, the injection period). More importantly they result in smaller cumulative volume flux in the water leg (and therefore smaller capacity for solutes transport) than the cumulative volume flux of the gravity driven convective flow pattern over a period of 10,000 years. Therefore these advective flow patterns have not been taken into account in the dissolution time estimates.

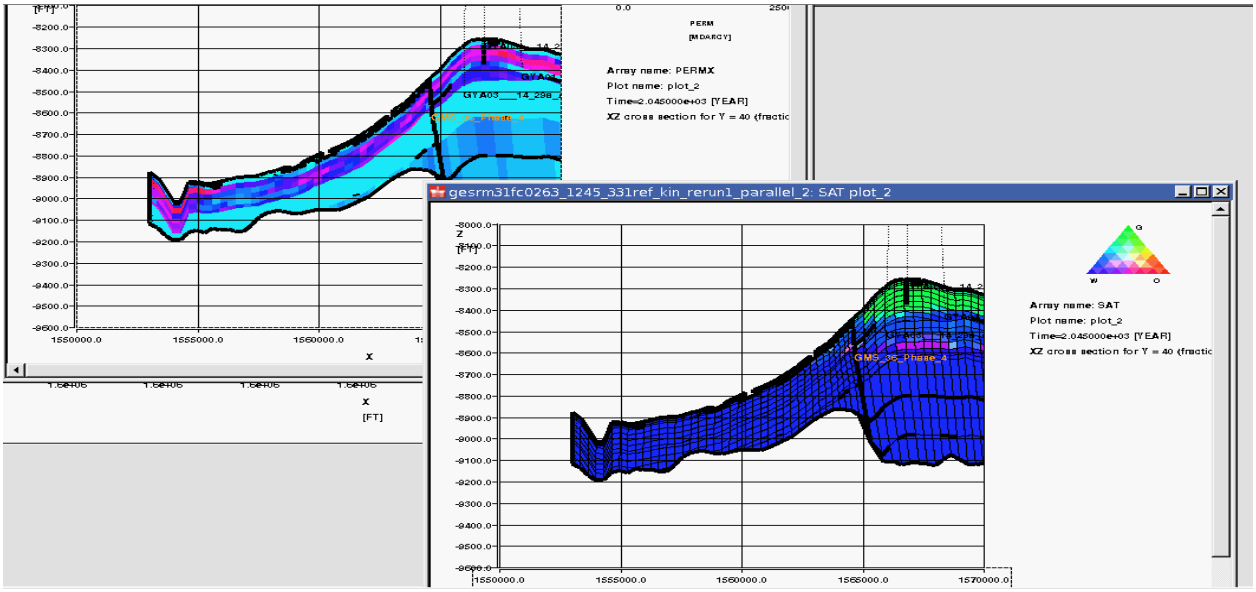

Figure 5-16: Representative cross section of the Goldeneye full field model (realistic Goldeneye geometry).

Note: Saturation shown in bottom right Fig. (gas in green, brine in blue), permeability shown in top left (colour scale runs from 0 mD (light blue) to 2,500 mD)

From Figure 4-17 it can be seen that initially (up to approximately 500 years post injection) a number of narrow vertically oriented convective cells develop. This carries dissolved CO_2 downwards, therefore this CO_2 is not contacting a calcite feature in the cap rock. After approximately 500 years the carbonated brine starts accumulating at base reservoir, and then forms a tongue sliding downwards. This tongue is part of a new, larger, convective flow cell. The situation is shown in larger detail in Figure 5-17, with the convective flow cell drawn in, and also a calcite feature drawn in. Due to volume conservation, a tongue of (relatively light) original (i.e. uncarbonated) formation brine is travelling along the top reservoir upwards, and the volume of this upwards tongue is the same as the volume of the downwards tongue.

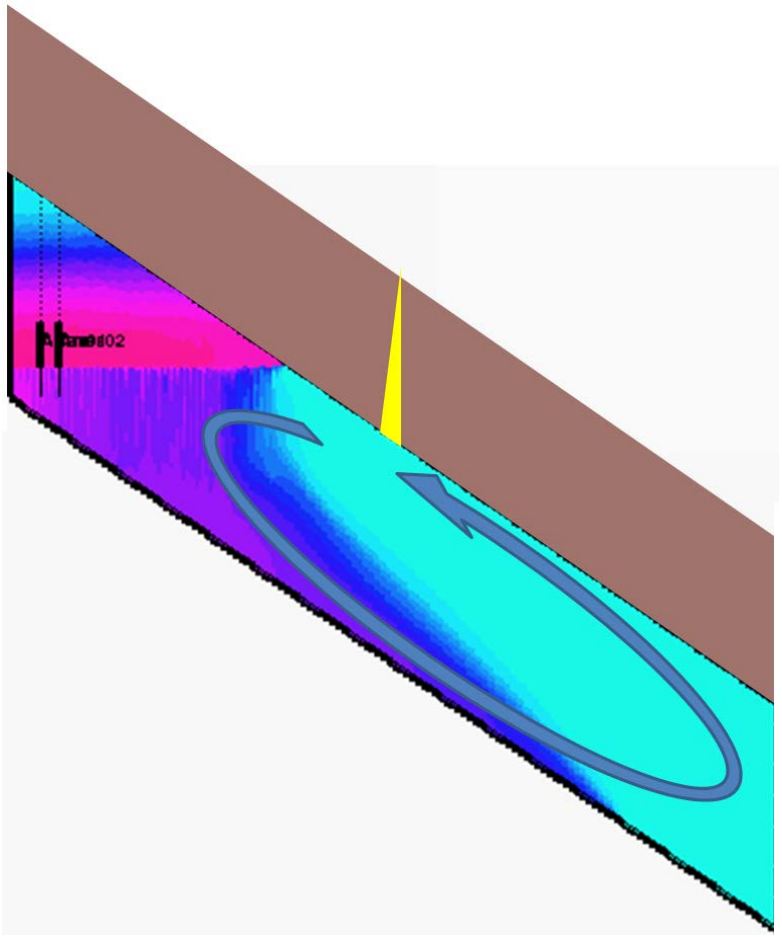

Figure 5-17: Convective flow cell (blue arrow) after development of the gravity tongue along base reservoir. Caprock (brown) with potential calcite feature (yellow) are drawn in. Colouring of the reservoir section represents dissolved CO_2 (same scale as in Fig. 4-17).

Note that the brine contacting the calcite feature is the brine in the upper tongue, which (in this model) is original formation brine (pH of 6.5) which (presumably) is in equilibrium with the calcite, so that no calcite would dissolve. However it should be noted that the model underlying Figure 4-17 and Figure 5-17 was run without diffusion. With diffusion, there is scope for some of the CO_2 in the downward tongue to diffuse into the upward tongue. On a timescale of 10,000 years this diffusive mixing can be expected to be significant (e.g., in the diffusion model underlying Figure 5-10 the diffusion distance is approximately 50 m; within the reservoir the diffusion can be expected to be somewhat faster due to the higher porosity). Therefore there is a source of H^+ at the base of the calcite feature.

The maximum amount of calcite that can be dissolved depends on the (cumulative) available brine that contacts the calcite over a period of time, because this brine needs to have the H^+ and Ca^{++} that is transported toward (or away from) the calcite feature. Therefore the estimate of the maximum amount of calcite that can dissolve (over a given time period) reduces to a relatively simple volumetric calculation:

$$\text{Amount}_{\text{dissolved calcite}} \leq \text{MIN}\left(\text{amount}_{\text{H+ transported towards calcite}}, \text{amount}_{\text{Ca++ transported away}}\right)$$

(inequality because spent acid still contains some H^+, and initial brine may already contain some Ca^{++});

$$amount_{H+\ transported\ towards\ calcite} \leq mass_{contacted\ H2O\ in\ reservoir} * molality_{H+};$$
$$amount_{Ca++\ transported\ away} \leq mass_{contacted\ H2O\ in\ reservoir} * molality_{Ca++};$$
$$molality_{H+} \leq 10^{-pH,min} / \gamma_{H+};$$
$$mass_{contacted\ H2O\ in\ reservoir} \leq H * v * t * dY * \varphi * \varrho_{brine}$$

where $amount_{dissolved\ calcite}$ (as well as $amount_{H+\ transported\ towards\ calcite}$ and $amount_{Ca++\ transported\ away}$) are in moles; $mass_{contacted\ H2O\ in\ reservoir}$ is the H_2O mass in the reservoir that (by convective and diffusive transport) is in (direct or indirect) contact with the calcite streak over the time period considered; $molality_{H+}$ is the (maximum) H^+ molality in the water leg (unit mol/kgW); $molality_{Ca++}$ is the (maximum) Ca^{++} molality in the water leg (unit mol/kgW); pH,min is the minimum pH in the reservoir region (in which $mass_{contacted\ H2O\ in\ reservoir}$ resides), and γ_{H+} is the H^+ activity coefficient at this pH; H is the reservoir thickness; v is the flow velocity in the reservoir; t is time (since start of tongue movement); φ is reservoir porosity; ϱ_{brine} is the brine density; and dY is some arbitrary distance in the direction perpendicular to the 2D cross section under consideration (i.e. perpendicular to the convective flow cell). The choice of dY is irrelevant for the final result.

The values for the various parameters from the Goldeneye geometry and geochemistry are:

pH,min = 3.0	*(conservative estimate)*;
$\gamma_{H+} \geq 0.74$	*(from OLI or PHREEQC)*;
$molality_{Ca++} \leq 0.036$ mol/kgW	*(from OLI or PHREEQC)*;
H = 300 ft	*(from box geometry, Figure 4-17)*;
v = 1 ft/year	*(from Figure 4-17, the tongue moves approx. 10,000 ft in10,000 year)*;
$\varphi = 0.24$	*(average Goldeneye reservoir porosity)*;
$\varrho_{brine} \geq 1000$ kg/m^3	*(1014 from OLI)*;

Note that in the place of maximum dip in the realistic reservoir geometry model (Figure 5-16), the dip is approximately 3 times as large as in the simplified model (leading to at most 3 times as high flow velocity), however the (effective) reservoir thickness (i.e. the thickness of the reservoir with sufficiently high permeability for significant convective flow to occur) is approximately 3 times as small as in the simplified model. Therefore the estimate of H*v in the realistic geometry model is approximately the same as in the simplified model.

Substituting the above values shows that (even at a pH as low as 3.0) the calcite dissolution rate is constrained by the transport of H^+ rather than the transport of Ca^{++}, and the maximum amount of dissolved calcite is:

$$amount_{dissolved\ calcite}[mol] \leq 9.0 * dY[m] * t[year]$$

To calculate the (minimum) time it requires to dissolve the calcite feature, we also need to estimate the amount of calcite in the feature:

$$amount_{calcite\ in\ feature}[mol] = h[m] * dX[m] * dY[m] * (1000 * \varrho_{calcite}[kg/m^3] / MW_{calcite}[g/mol])$$

where h is the height of the calcite feature; dX is the thickness (measured in the 2D plane) of the calcite feature; dY is the same distance (perpendicular to the 2D plane) as in the previous calculation; $\varrho_{calcite}$ is the calcite density; and $MW_{calcite}$ is the calcite molecular weight. The following values are reasonable for Goldeneye:

h = 70 m *(Goldeneye primary caprock thickness)*;
dX ≥ 1 m *(see below)*;
$\varrho_{calcite}$ = 2710 kg/m^3 *(from literature)*;
$MW_{calcite}$ = 100.1 g/mol *(from chemical formula)*;

The (minimum) value of the thickness of the calcite feature was estimated from the core photographs in Figure 2-3. In these photographs the length of each individual calcite interval is actually 3 m to 4 m, even for the intervals that seem to have been intersected at roughly a straight angle (as deduced from the angle of the calcite-sandstone interface). It is possible that in the cap rock, the calcite features are somewhat thinner. However for very thin features, it is unlikely that they would be continuous through the entire cap rock. Moreover, the convective flow loop in the reservoir is unlikely to be exactly perpendicular to the calcite feature, increasing the net thickness of the calcite feature as encountered by the flow. Finally (from Figure 2-3, and more generally from study of fault zones) it can be expected that there are multiple calcite features within a single fault zone, increasing the total calcite thickness encountered by the convective current. Therefore we consider 1 m as a conservative estimate for the minimum thickness of a calcite feature through the cap rock.

Using the above values gives

$amount_{calcite\ in\ feature}[mol] \geq 1.9 \cdot 10^6 * dY\ [m]$

Therefore the minimum time required to dissolve the entire calcite feature is

$t \geq (1.9 \cdot 10^6 * dY)/(9.0 * dY)$ year = 210,000 year

This value is conservative for two (related) reasons:

1. The assumed pH value of 3.0 is very low. As the carbonated brine contacts reservoir minerals it will be buffered to some extent. E.g. buffering by any calcite in the reservoir would raise the pH to 4.7, leading to a minimum dissolution time estimate of $10^{(4.7-3.0)} * 2.1 \cdot 10^5$ year = $1.1 \cdot 10^7$ year.
2. The reservoir itself contains some calcite. Using the average value from the petrography (3%, see Table 4-1), the amount of calcite in the reservoir region considered above (i.e. with gross rock volume H * v * t * dY) is $1.8 \cdot 10^8$ * dY[m] mol (i.e. much more than the $1.9 \cdot 10^6$ * dY[m] mol in the calcite feature). Presumably most of this would be contacted by the carbonated brine before contacting the calcite streak, so that all H^+ would be neutralised and the calcite feature would not dissolve at all.

Finally, it should be stressed once more that the above calculation applies to the water leg only. Therefore even if a calcite feature would completely dissolve at some point in time (from the above, after a minimum of 210,000 years), the dissolved feature would open a leak path through the cap rock only for carbonated brine, and not for gas. Furthermore, since the reservoir pressure at the end of CO_2 injection will still be sub hydrostatic and (in the water leg) can at most recharge to hydrostatic pressure, the flow rates through such a leak path would either be directed into the reservoir or it would be zero. Due to tectonic stress, a completely dissolved feature would not be completely open but partially closed. This would further reduce the mass exchange across the cap rock.

5.5. Discussion

The Rødby batch simulation results indicate that even if there is strong reactivity (large reactive surface areas of the relevant minerals) there is either no impact on porosity or (more likely) the porosity decreases somewhat (from 11% to 10%). Therefore it is unlikely that the diffusion of CO_2 into the cap rock will lead to an increase in the Rødby permeability.

The 1D Rødby diffusion simulations support the conclusions from the batch simulations. In the part of the cap rock that the CO_2 has contacted (via diffusion), 50 m to 75 m after 10,000 years, the mineralogical changes and resulting porosity change is nearly identical to that in the batch simulation.

1D diffusion simulations were also performed on the scenario of a calcite filled feature (within a fault zone) running through the Rødby. The most reactive case considered is the one with a high porosity (11%) calcite filled feature (fault) scenario with the open boundary conditions. This case allows ions to diffuse out of the feature into the reservoir, and is appropriate for a high water saturation in the reservoir i.e. for a fault zone entering the reservoir outside the CO_2 plume itself but inside a region where the water is saturated with dissolved CO_2. In this case the model predicts a porosity increase over a limited distance into the calcite feature. This increased porosity zone progresses into the calcite feature much more slowly than the CO_2 diffusion front. The fine grid sensitivity indicates that the front of significant porosity increase is less than 33 cm after 10,000 years, while the CO_2 diffusion front has progressed to approximately 70m at that stage. Even if one corrects for faster diffusion rates in the dissolved area (since the porosity has roughly doubled from 11% to 24% in the fine grid resolution, the expected increase in diffusion constant would be a factor of approximately two), this dissolution front will still lag very far behind the CO_2 diffusion front. Note that in the (more realistic) low case porosity (0.011%) the CO_2 diffusion front has only progressed 2 m after 10,000 years, and the front of porosity increase (in this case only from 0.011% to 0.012%) only by 5 cm (a finer grid simulation would presumably reduce this distance even further). The above cases all assume that the transport in the dissolved region would still be diffusion controlled. The case in which this assumption is dropped is discussed below.

In the calcite filled feature (fault) scenario with closed boundary conditions (no ions allowed to diffuse into the formation - appropriate for a low water saturation i.e. for a fault zone entering the reservoir within the CO_2 plume) there is no significant porosity increase because the calcite dissolution stops once the carbonated brine within the calcite feature is saturated with respect to calcite. In this case the porosity increases from 11.00% to 11.04%, since only 0.1 mol/kgW out of the initial 222 mol/kgW of calcite dissolves.

We also analysed what would happen in case the assumption of a diffusion controlled transport mechanism would not be valid anymore in the dissolved part of a calcite feature. In this case the following conclusions can be drawn:

- Calcite dissolution *with continuous supply of water under-saturated with respect to calcite* could dissolve calcite a feature through the caprock within 1,000 years.
- However the above scenario does not apply for Goldeneye. The rate of calcite dissolution is constrained by transport rates in the reservoir.
- For a calcite feature above the gas water contact (more precisely, above any region in the reservoir with nonzero gas saturation), dissolution of a calcite feature is most likely blocked as soon as a minor cavity forms. Therefore no leak path can form above the gas plume.
- For a calcite feature below the gas water contact (more precisely, within any region in the reservoir with zero gas saturation), dissolution of a calcite feature is unlikely because the reservoir brine contacting the calcite feature is probably saturated with calcite (due to the occurrence of approximately 3% calcite within the reservoir itself). Even if the brine contacting the calcite feature would be undersaturated with respect to calcite, it would take at

least 210,000 years to dissolve the entire feature. Moreover this could only lead to escape of brine with some dissolved CO_2, and not escape of gaseous (supercritical) CO_2.

The overall conclusion is that the potential calcite features through the cap rock will unlikely pose a risk to CCS in Goldeneye.

6. Conclusions

The main results from the work described in this report are:

- Mineralogical alterations in the cap rock, including in any calcite filled features (fault zones) through the cap rock, are unlikely to create leak paths. Therefore the risk of CO_2-rock reactivity on containment is low. For the Rødby itself the predicted mineral alterations do not lead to increased porosity, and therefore are unlikely to increase permeability.
- For a potential calcite feature running through the entire cap rock, the potential for complete dissolution cannot be rigorously ruled out, however the timescale for complete dissolution can be estimated to be more than 200,000 years even under worst case assumptions. Moreover this worst case is only viable below the gas water contact, so that such a leak path could only lead escape of brine (with some dissolved CO_2), and not escape of gaseous (supercritical) CO_2. In locations where the calcite is exposed to the CO_2 plume (i.e. above the gas water contact) there is no effective transport mechanism of dissolved calcite into the reservoir and consequently the predicted amount of calcite dissolution is extremely small.
- The predicted mineralogical alterations in the reservoir may have a limited impact on porosity during the injection period. Of all cases studied the largest reduction is from 24.00% to 23.42%. This is under fast reactivity assumptions. Since the reservoir permeability is high (approximately 500 m to 1,000 m Darcy) the well injectivity is dominated by tubing size rather than permeability, and therefore even a porosity change from 24.00% to 23.42% is unlikely to have a noticeable impact on injectivity.
- The predicted mineralogical alterations in the reservoir may lead to some, potentially even large, additional storage capacity due to mineral trapping. In view of data uncertainties and comparison to natural analogue studies a large mineralisation component should be viewed as an upside rather than as the base case. It is also worthwhile mentioning that the dissolution storage of CO_2 is predicted to be low (14% of injected CO_2 after 10,000 years) in a 2D representation of Goldeneye.
- Downdip, lateral movement, of CO_2-rich or geochemically reacted formation brine is possible. However this movement is very slow (less than 3,000 m in 10,000 years, based on the 2D representation, with factors such as geological heterogeneity likely to slow this down further). Moreover the pH of this laterally migrating brine is expected to be benign, ranging from pH=5 in case of little reactivity with the reservoir (only buffering by calcite), to pH=6.4 (which equals the original formation brine pH) under the fast reactivity assumption.

With the current state of technology it is not possible for reactive transport models to predict changes in rock mechanical properties. This is due to the absence of reliable correlations. However it is important to know if rock weakening could occur as this could have a negative impact on injectivity or containment integrity. Therefore coreflood experiments were performed on Goldeneye reservoir samples. In the samples the sandstone grains were cemented mainly by calcite and quartz. The results showed that even after total dissolution of the calcite there is no weakening (30).

Although the conclusion on containment is robust under all sensitivities considered in the model it would be beneficial to verify some of the assumptions in experiments (notably permeability, capillary entry pressure, diffusion rates, and changes in all of these due to dissolution by carbonated brine). This would require fresh caprock samples – potentially costing tens of millions of pounds to acquire – since the existing caprock samples are not suitable for reliable measurements of transport properties because they have dried out.

7. References – Bibliography

1. Shell (2013). Conceptual CWI design report, PCCS-05-PT-ZW-7180-00002 (Chapter 5), Key Knowledge Deliverable 11.093.
2. IPCC - Intergovernmental Panel on Climate Change, 2005. In: Metz, B., Davidson, O., de Coninck, H.C., Loos, M., Meyer, L.A. (Eds.), Special Report on Carbon Dioxide Capture and Storage. Cambridge University Press, Cambridge, UK and New York, NY, USA.
3. Shell 2013. Goldeneye Static Model (Field) Report, PCCS-05-PT-ZG-0580-00004, Key Knowledge Deliverable 11.108.
4. Parkhurst, D. L., and C. A. J. Appelo (1999). User's guide to PHREEQC (version 2)—A computer program for speciation, batch-reaction, one dimensional transport, and inverse geochemical modeling. U. S. Geological Survey Water-Resource Investigation Report 99-4259, 312 p. (http://wwwbrr.cr.usgs.gov/projects/GWC_coupled/phreeqc/index.html).
5. Chadwick, A., et al. (2008). Best Practice for the Storage of CO_2 in saline aquifers - observations and guidelines from the SACS and CO2STORE projects. Nottingham, UK, British Geological Survey, British Geological Survey Occasional Publication, 14 (http://nora.nerc.ac.uk/view/programme/DRSREI.html)
6. Class, H., et al. (2009). A benchmark study on problems related to CO_2 storage in geologic formations, Comput Geosci DOI 10.1007/s10596-009-9146-x
7. Wolery, T.J., and Daveler, S.A. (1992). EQ6, A computer program for reaction path modeling of aqueous geochemical systems: theoretical manual, user's guide, and related documentation (version 7.0): Lawrence Livermore National Laboratory, report no. UCRL-MA-110662 PT IV.
8. Xu, T., et al. (2006). TOUGHREACT User's Guide: A Simulation Program for Non-isothermal Multiphase Reactive Geochemical Transport in Variably Saturated Geologic Media. Earth Sciences Division, Lawrence Berkeley National Laboratory, University of California, LBNL-55460
9. James L. Palandri & Yousif K. Kharaka (2004). A Compilation of Rate Parameters of Water-Mineral Interaction Kinetics for Application to Geochemical Modeling. U.S. G. S. Open File Report 2004-1068 (http://pubs.usgs.gov/of/2004/1068/).
10. Xu, T., et al. (2010). Reactive transport modeling to study changes in water chemistry induced by CO_2 injection at the Frio-I Brine Pilot, Chem. Geol. (2010), doi:10.1016/j.chemgeo.2010.01.006
11. Blanc P. (2008). Thermoddem: Selection de proprieties thermodynamiques pour les principales especes aqueuses et minerals porteuses de fer, BRGM/RP-56587-FR (http://thermoddem.brgm.fr)
12. CoreLab 2010. A detailed Petrographic & Mineralogical Study of 34 Core Chip and Plug Trim Samples, Reservoir Geology 100411
13. The Expro Group (2004), Fluid Analysis Report - PVT Gas Condensate Study Goldeneye / GYA-02S1 (14/29a-A4Z)
14. Peterhead CCS Project Basis for Design documentation:
    Basis for Design Part II - Design Basis and Design Requirements, PCCS-00-PT-AA-7704-00002;
    Basis for Design Part IV - Design Dossiers, PCCS-00-PT-AA-7704-00004.
    Both the above documents are part of Key Knowledge Deliverable 11.003

15. Shell (2013). FFM Dynamic Model Report, PCCS-05-PT-ZR-3323-00002, Key Knowledge Deliverable 11.122
16. Watson, M.N. et al. (2004), The Ladbroke Grove-Katnook carbon dioxide natural laboratory : A recent CO_2 accumulation in a lithic sandstone reservoir. Energy 2004. **29**(9-10): p.1457-1466
17. Watson, M. et al. (2006), An integrated petrological and geochemical approach to predicting long term CO_2-induced diagenesis in geosequestration. Eighth International Conference on Greenhouse Gas Control Technologies (GHGT-8), 2006, Trondheim, Norway
18. Audigane, P. et al (2007), Two-dimensional reactive transport modeling of CO_2 injection in a saline aquifer at the Sleipner site, North Sea. American Journal of Science, Vol. 307, September 2007.
19. A. Riaz, M. Hesse, H. A. Tchelepi & F. M. Orr (2006) "Onset of convection in a gravitationally unstable diffusive boundary layer in porous media". J. Fluid Mech., vol. 548, pp. 87–111.
20. Gilfillan, S.M.V., et al (2009), Solubility trapping in formation water as dominant CO_2 sink in natural gas fields, Nature Vol 458, 2 April 2009.
21. Eric MacKay (external review team, Heriot Watt University), private communication, 28th May 2014
22. Shell 2013. Goldeneye Petrophysical Modelling Report, PCCS-00-PT-ZP-9032-00001, Key Knowledge Deliverable 11.111.
23. Appelo, C.A.J., et al. (2010), Multicomponent diffusion of a suite of tracers (HTO, Cl, Br, I, Na, Sr, Cs) in a single sample of Opalinus Clay. Geochimica et Cosmochimica Acta 74 (2010) 1201–1219.
24. Van Loon et al. (2007). Appl. Geochem. 22, 2536
25. Shen, L. et al. (2007). Critical review of the impact of tortuosity on diffusion. Chemical Engineering Science, 2007. 62(14): p. 3748-3755
26. Micarelli, L., and Benedicto, A. (2008), Normal fault terminations in limestones from the SE-Basin(France): implications for fluid flow. From: WIBBERLEY, C. A. J., KURZ, W., IMBER, J., HOLDSWORTH, R. E. & COLLETTINI, C. (eds) The Internal Structure of Fault Zones: Implications for Mechanical and Fluid-Flow Properties. 299, 123–138.
27. Lockman, D.F., et al. (1997), A systematic technique for describing and quantifying fractures in core. Pacific section of American Association of Petroleum Geologists (AAPG).
28. L. Palandri & Yousif K. Kharaka (2004). A Compilation of Rate Parameters of Water-Mineral Interaction Kinetics for Application to Geochemical Modeling. U.S. G. S. Open File Report 2004-1068 (http://pubs.usgs.gov/of/2004/1068/).
29. OLI StreamAnalyzer 3.1.6 OLI systems, http://www.olisystems.com/
30. Shell 2013. Report On Results of Lab Experiments (Geo-Mechanical Investigation): Chemo-mechanical response of Captain Sandstone to CO_2 injection, PCCS-05-PT-ZP-9018-00001, Key Knowledge Deliverable 11.112.
31. O. Hansen et al, "Snøhvit: The history of injecting and storing 1 Mt CO_2 in the fluvial Tubåen Fm", Energy Procedia 37 (2013) 3565 – 3573.

8. Glossary of terms

Term	Definition
0D	Zero Dimensional (no spatial variability)
1D	One Dimensional
2D	Two Dimensional
3D	Three Dimensional
Al	Aluminium
Ba	Barium
BET	Brunauer–Emmett–Teller procedure
Bg	Formation Volume Factor (Gas)
BGS	British Geological Survey
Bo	Formation Volume Factor (Oil)
BRGM	Bureau de Recherches Géologiques et Minières
Ca	Calcium
CCGT	Combined cycle gas turbine
CCS	Carbon Capture & Storage
CO_2	Carbon Dioxide
EDX	Energy-dispersive X-ray spectroscopy
EOS	Equation of State
Fe	Iron
H_2CO_3	Carbonic acid
H_2O	Water
H_2S	Hydrogen Sulphide
HCO_3^-	Bicarbonate
HSE	Health, Safety, Environment
IPCC	Intergovernmental Panel on Climate Change
K	Potassium
kgW	Kilogram of water (pure H_2O)
Li	Lithium
LLNL	Lawrence Livermore National Laboratory
MEG	Mono-Ethylene Glycol
Mg	Magnesium
MT	Megatons (106 kg)
N_2	Nitrogen
Na	Sodium
NDMA	N-Nitrosodimethylamine
OSBL	OutSide Battery Limit
P	Phosphorus
ppm	Parts per Million (by mass)
ppmv	Parts per Million (by volume)
PVT	Pressure, Volume, Temperature

SEM	Scanning Electron Microscopy
Si	Silicon
Sr	Strontium
SRB	Sulphate Reducing Bacteria
TDS	Total Dissolved Solids
TS	Thin Section
XRD	X-Ray Diffraction

9. Glossary of Unit Conversions

For the provision of the SI metric conversion factor as applicable to all imperial units in the Key Knowledge Deliverable.

Table 8-1: Unit Conversion Table

Function	Unit - Imperial to SI Metric conversion Factor
Length	1 Foot = 0.3048m Metres 1 Inch = 2.54cm Centimetres 1 Inch = 254mm millimetres
Pressure	1 Psia = 0.0690 Bara
Temperature	1°F Fahrenheit = -17.22°C Centigrade
Weight	1lb Pound = 0.45kg Kilogram

APPENDIX 1. Kinetic rate formula

The below example shows the kinetic rate formula used for dissolution and precipitation. The formula is the same for every mineral, but the rate constants vary from mineral to mineral.

```
# Source: Palandri & Kharaka (2004)
# The following parameters are specified in KINETICS for each kinetic mineral in the system
#    PARM(1): initial reactive surface area (m2/kgw) - History matching parameter if M0 > 0
#      PARM(2): used when M0 = 0, (Nucleation) param for history matching (cannot be negative)
#    PARM(3): exponent for M/M0 for surface area correction (=1 if no data)
#    PARM(4): when M0 > 0, rate constant ratio (K_precipitation / K_dissolution),
#           (=1 if no data)

# k25(a,n,b): Rate constant k at 25oC, pH = 0, mole m-2 s-1.
# Ea(a,n,b):  Arrhenius activation energy E, kJ mole-1.
# n(a,b):     Reaction order n with respect to H+ (apart from carbonates and sulfides).
#           (a) = acid mechanism (H+)
#           (n) = neutral mechanism
#           (b) = base mechanism (OH-), apart from carbonates (HCO3-)
# Note: for sulfide, other mechanisms (Fe+3 and O2)
#       for carbonates, followed Xu et al (2010)
Chamosite-7A
-start
10 k25a =       7.76247E-12
20 k25n =       3.01995E-13
30 k25b =       0
40 Eaa =        88000
50 Ean =        88000
60 Eab =        0
70 na =         0.5
80 nb =         0
90  SatIndex = SI("Chamosite-7A")
100 SatRatio = SR("Chamosite-7A")
110 R = 8.314472 # (gas constant J/mol/Kelvin)
120 REM If SI too small, then No dissolution nor precipitation
130 IF (SatIndex > -1e-15) AND ( SatIndex < 1e-15) THEN GOTO 900
140 IF (M = 0) AND (SatIndex < PARM(2)) THEN GOTO 900
160 t = 1    # surface area correction factor
170 IF (M0 > 0) AND (M > 0) THEN t = (M / M0)^PARM(4)
200 REM acid mechanism
210     IF (k25a > 0) THEN KTa = k25a * EXP((-Eaa/R) * (1/TK - 1/298.15)) * ACT("H+")^na
220 REM neutral mechanism
230   IF (k25n>0) THEN KTn = k25n * EXP((-Ean/R) * (1/TK - 1/298.15))
240 REM base mechanism
250     IF (k25b > 0) THEN KTb = k25b * EXP((-Eab/R) * (1/TK - 1/298.15)) * ACT("H+")^nb
```

```
300 REM Dissolution
310   moles = PARM(1) * t * (KTa+KTn+KTb) * (1 - SatRatio) * TIME
320 IF (SatIndex > 0) THEN GOTO 400
330   REM Do not dissolve more than what is available
340   IF (moles > M) THEN moles = M
350   GOTO 900
400 REM Precipitation when M0 > 0
410 IF (M0 = 0) THEN GOTO 500
420   moles = moles * PARM(5)
430   GOTO 600
500 REM Precipitation when M0 = 0 (secondary mineral)
520   surfArea = 1.0e-5  # default nucleation surface area
530   IF (M > 0) THEN surfArea = M * PARM(3)
540   moles = surfArea * (KTa+KTn+KTb)* PARM(5) * (1 - SatRatio) * TIME
600 REM Do not precipitate more than the elements in solution
610   maxMol = TOT("Si")
620   IF (maxMol > TOT("Al")/2) THEN maxMol =TOT("Al")/2
670   IF (maxMol > TOT("Fe")/2) THEN maxMol =TOT("Fe")/2
690   IF (maxMol < -moles) THEN moles = -maxMol
900 SAVE moles
-end
```

APPENDIX 2. Dry-out zone

CO_2 injection can lead to the formation of a so-called dry-out zone near the injector due to the slight solubility of water into the CO_2 -rich phase if the injection stream is dry. When a large number of pore volumes of dry CO_2 have been in contact with the water (i.e. close to the injector) all water will have evaporated. Since the salt dissolved in the water is not soluble in the CO_2 stream it will stay behind and (upon complete dry-out) deposit as solid salt. In theory this can lead to a reduction of absolute permeability in the near-wellbore zone, and might lead to a reduction in injectivity. A straightforward calculation and comparison to operational CCS projects, presented in the next two paragraphs, shows that for Goldeneye the risk of injectivity reduction due to this dry-out effect is low.

The Goldeneye water chemistry has a TDS concentration of around 56,000 mg/l. The Goldeneye water is a NaCl dominated brine (Na plus Cl concentration is 54,000 mg/l). Even with full deposition of salt in situ the total salt deposited is only 56 gram for every liter of formation water, almost completely as halite (solid NaCl). Since the specific gravity of halite is 2.17 g/cm^3 this corresponds to 26 cm^3 of solids for every liter of formation water. Even if the pore space would be completely filled by formation water (i.e. 100% water saturation) this would lead to a relative porosity reduction of only 26/1000. Given the average porosity of 24% in the main reservoir sands (Captain D) this would reduce porosity from 24% to 23.4%. However around the injectors the water saturation is much lower, namely very close to original connate water saturation i.e. only approximately 5-10% (with the exception of some water thief zones that developed during the production phase and caused water breakthrough in the producers). Therefore in most of the dry-out zone the relative porosity reduction is only [0.05-0.10]*26/1000 = [1-3]/1000, and therefore the porosity only reduces from 24% to [23.94-23.97]%. This is a very small reduction. Even if much of the salt deposition would occur in the pore throats (which have a relatively large diameter in Captain D due to its high permeability) it is not expected to have a measurable effect on permeability and therefore injectivity is expected to be unaffected by the buildup of the dry-out zone.

From field experience perspective, CO_2 injection is ongoing in Sleipner in Norway and in In Salah in Algeria. These operations have a higher likelihood than Goldeneye to exhibit injectivity decline due to the buildup of a dry-out zone. This is for two reasons: 1) they have a higher value of the product (salinity * water saturation), primarily due to the higher (100%) initial water saturation (injection into saline aquifer rather than depleted gas field), and therefore more salt is available for deposition; 2) they have similar (Sleipner) or much lower (In Salah) permeability and therefore (even for the same amount of salt deposition per unit of pore volume) similar or higher risk of deposition in the pore throats leading to permeability reduction. However no injectivity decline (besides decline due to pressure up of the formation) has been reported for these operations during their injection period since start-up (14 and 6 years, respectively). The only CO_2 injection project for which injectivity decline has been reported is the Snøhvit project in Norway (31). In the Snøhvit case a near-wellbore injectivity problem was experienced shortly after start-up of CO_2 injection in 2008. The problem was solved after weekly injection of seawater with MEG for some time. However to the best of our knowledge there is not a good understanding of the cause of the problem (nor through which mechanism remediation solved this). Salt precipitation is mentioned (e.g. Hansen et al (31)) but other possibilities cannot be excluded because no specific data gathering was attempted. Note that later on in the Snøhvit operation (2011) a severe injectivity problem due to compartmentalisation was identified. This could only be solved by abandoning the well in the original storage formation (Tubåen) and reperforating in a shallower formation. However a compartmentalisation problem is very different from a near-wellbore problem such as dry-out, and these two types of problems should not be mixed up and could be diagnosed using pressure transient analysis (near wellbore versus far field effects).

Taking all evidence into account, for Goldeneye the risk of injectivity impairment due to salt deposition in the dry-out zone is estimated to be low.

In fact, without the dry-out effect, i.e. no water vaporizing into the gas phase, the gas relative permeability near the injector will be at water saturation 5% to 10%, occupying a greater amount of pore space compared to the case where the drying-out zone is developed. Therefore, in the simulation models, where the dry-out zone is not considered, the gas mobility nearby injectors (thus injectivity) may be under-estimated.

APPENDIX 3. Reservoir souring

Hydrogen sulphide (H_2S) is a colourless, highly toxic, corrosive gas. It dissolves readily in both water and hydrocarbons. H_2S can occur naturally as a component of hydrocarbon accumulations or their associated water, often associated with the presence of carbonates, anhydrites or volcanic sediments. It can also be generated by reservoir development processes (such as water injection, thermal recovery methods), either from microbiological activity or thermochemical processes – collectively known as "reservoir souring". For this reason Shell has embedded the prediction of initial H_2S levels as well as changes in H_2S levels due to reservoir development processes into its internal standards.

For Goldeneye no further fluid production is planned, so that any generated H_2S would normally be contained within the reservoir, however it is still relevant to understand the souring potential, e.g. in view of the well integrity assessment of abandoned wells.

The two known reservoir souring mechanisms are

1. Microbiological souring
2. Abiotic chemical souring

In the first mechanism, sulphate reducing bacteria (SRB) convert sulphate (SO_4^{2-}) into H_2S. This is controlled by the presence of bacteria, the concentration of sulphate, and the presence of hydrocarbons (which together with the sulphate form the nutrients for the SRB), as well as reservoir temperature and water salinity. Due to the low sulphate concentration in the Goldeneye formation water (see Table 3-4) the probability of this process to occur is negligible, as long as no new continuous source of sulphate is introduced to the reservoir (e.g., through water injection).

The second mechanism (typically either by chemical reduction of sulphate by hydrocarbons, or by breakdown of organo-sulphur compounds in the oil) generally requires temperatures well above the Goldeneye reservoir temperature, and therefore is not a viable mechanism.

Note that the absence of H_2S in the Goldeneye hydrocarbons (e.g. Table 3-5) supports the above assessment. Furthermore, H_2S levels were monitored during the gas production phase. Approximately once a month gas samples were taken from the Goldeneye slug catcher at the gas processing plant at St Fergus, and analysed for H_2S (with good measurement accuracy down to 0.5 ppm). H_2S contents were always found to be below 0.5 ppm.

CO_2 injection is unlikely to increase the souring potential because:

1. The CO_2 injection does not increase the reservoir temperature (around the injector it actually lowers the reservoir temperature).
2. The CO_2 injection is unlikely to increase the sulphate concentration in the formation water.

The reason for the second point is that the low amounts of sulphate in the concentration water could only increase through dissolution of reservoir minerals. However no sulphate containing minerals were observed in the petrographic study (Table 3-1. and Table 3-2) with the possible exception of gypsum (which was observed in XRD but not in SEM or thin sections). However as mentioned in the core petrographic study report (12) the small amount of gypsum observed in XRD could have been caused by sample handling/storage and/or preparation. The occurrence of gypsum (or, more likely, anhydrite) in the reservoir is very unlikely because the measured calcium and sulphate concentrations (Table 3-4) show that the formation water is highly undersaturated with respect to anhydrite and gypsum. On the other hand, the measured barium and sulphate concentrations are consistent with barite solubility at Goldeneye pressure and temperature conditions, thus indicating that some barite may be present in the reservoir (although not observed in the petrographic analysis).

Even if barite is present in the reservoir, CO_2 injection is unlikely to lead to increased dissolution of barite because, at low to neutral pH, barite solubility is nearly independent of pH.

In conclusion, the probability of reservoir souring during CO_2 injection (as well as post CO_2 injection) in Goldeneye is negligible.